Ricardo José
Coelho de Figueiredo

Técnicas e Métricas Multi-Tom para Caracterização de Linearidade de Sistemas RF Não-Lineares Dinâmicos

Multi-Tone Linearity Characterization Techniques and Metrics for Nonlinear Dynamic RF Systems

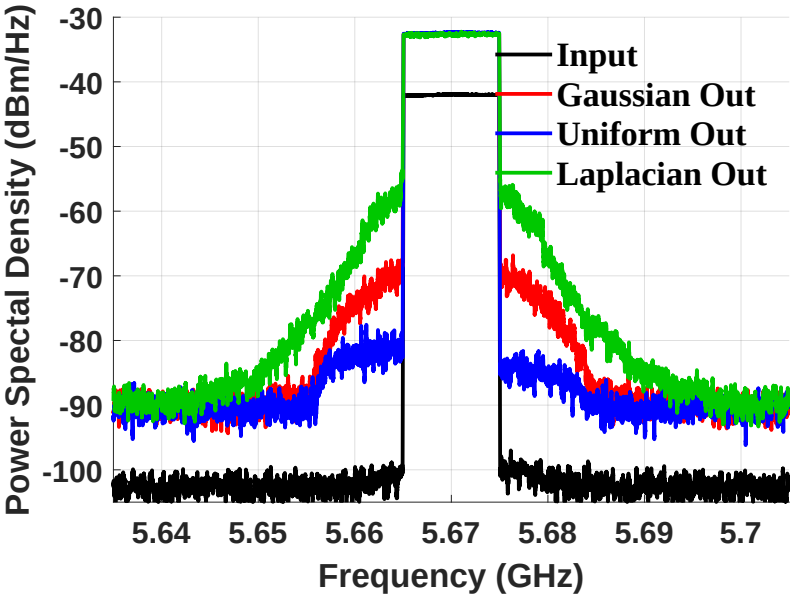

Ricardo José
Coelho de Figueiredo

Técnicas e Métricas Multi-Tom para Caracterização de Linearidade de Sistemas RF Não-Lineares Dinâmicos

Multi-Tone Linearity Characterization Techniques and Metrics for Nonlinear Dynamic RF Systems

Tese apresentada à Universidade de Aveiro para cumprimento dos requisitos necessários à obtenção do grau de Doutor em Engenharia Eletrotécnica, realizada sob a orientação científica do Prof. Dr. Nuno Miguel Gonçalves Borges de Carvalho, Professor Catedrático do Departamento de Electrónica, Telecomunicações e Informática da Universidade de Aveiro.

Apoio financeiro da Fundação para a Ciência e Tecnologia (FCT) e da União Europeia através do Fundo Social Europeu (FSE) e do Programa Operacional Regional do Centro no âmbito da bolsa de doutoramento ref: SFRH/BD/146935/2019.

Ao José, à Maria, à Raquel, ao Gustavo, ao Lourenço, e aos que vierem.

o júri / the jury

presidente / president	Doutor José Fernando Ferreira Mendes, Professor Catedrático da Universidade de Aveiro.
vogais / examiners committee	Doutora Dominique Schreurs, Professora Catedrática, Ku Leuven;
	Doutor Anding Zhu, Professor, University College Dublin;
	Doutor Nuno Miguel Gonçalves Borges de Carvalho, Professor Catedrático, Universidade de Aveiro (orientador);
	Doutor José Angel Garcia Garcia, Professor Titular, Universidad de Cantabria;
	Doutor Telmo Reis Cunha, Professor Associado, Universidade de Aveiro.

Agradecimentos / Acknowledgement

Em primeiro lugar, agradeço aos meus pais, por me ensinarem a importância da disciplina e do espírito de sacrifício, e por valorizarem o ensino e a ciência. Vocês ajudaram-me a contruir-me e são os impulsionadores primários daquilo que consegui alcançar.

Agradeço ao meu orientador, Prof. Nuno Borges Carvalho, por me ter acolhido, por todas as oportunidades que me deu, e pela liberdade e confiança que depositou no meu trabalho. Não creio que encontrasse igual disponibilidade e abertura de espírito noutro lugar.

Agradeço à Universidade de Aveiro, ao Departamento de Eletrónica, Telecomunicações e Informática, e ao Instituto de Telecomunicações por me terem facultado os meios e ambiente necessários para desenvolver este trabalho doutoral. Bem como aos trabalhadores destas instituições que de algum modo me ajudaram, nomeadamente ao Hugo Mostardinha, e ao Paulo Gonçalves por me terem ajudado em vários aspetos técnicos.

Agradeço à Fundação para a Ciência e Tecnologia por ter financiado o meu trabalho através de uma bolsa de doutoramento.

Agradeço a todos os colegas do programa doutoral e do Instituto de Telecomunicações pela jornada que vivemos juntos.

Agradeço a todos os os meu amigos, por todos os convívios e tertúlias, e pela força que sempre me deram para completar este percurso.

Por fim, agradeço à Raquel, a mulher da minha vida, e aos meus filhos Gustavo e Lourenço, pela vivência do quotidiano, e pelo futuro que construímos dia a dia. São o meu porto seguro. Fazem-me muito feliz. Amo-vos.

Obrigado!

Palavras-Chave Caracterização de Linearidade, Multi-tom, Dinâmica Não Linear, Razão de Potência de Ruído Varrida, Métrica de Linearidade Esperada.

Resumo A linearidade quantifica quanto um sistema diverge do funcionamento linear ideal. Infelizmente, a capacidade técnica para caracterizar linearidade é incompleta. Medir dinâmica não linear e relacionar métricas de linearidade medidas com sinais de teste diferentes sempre foi um problema. À medida que as tecnologias de telecomunicação transcendem os limites do hardware de rádio frequência ao ocuparem bandas mais largas, ao se moverem para frequências portadoras mais elevadas, e ao usarem sinais modulados cada vez mais deversificados, o tempo para ultrapassar estas limitações de caracterização de linearidade fica curto. Este trabalho aborda ambos problemas. Ele explica como os efeitos de dinâmica não linear se manifestam sob excitação banda-larga, apresentando uma técnica para os medir: a razão de potência de ruído varrida. E define uma plataforma para comparar linearidade quando diferentes sinais de teste são usados. Esta plataforma consiste numa clara compreensão de como o sistema sob teste e o sinal de teste influenciam a métrica de linearidade esperada, independentemente do sistema e do sinal, permitindo uma avaliação de linearidade despercebida.

Keywords Linearity Characterization, Multi-tone, Nonlinear Dynamics, Swept Noise Power Ratio, Expected Linearity Metric.

Abstract Linearity quantifies how much a system drifts from the ideal linear operation. Unfortunatelly, the technical ability to characterize linearity is incomplete. Measuring nonlinear dynamics, and relating linearity metrics measured with different test signals has always been a problem. As telecommunication technologies transcend the limits of radio frequency hardware by occupying broader bandwidths, moving to higher carrier frequencies, and using a more deversified set of modulated signals, the time to overcome these linearity characterization limitations runs short. This work addresses both problems. It explains how nonlinear dynamic effects manifest under broadband excitation, presenting a technique to measure them: swept noise power ratio. And defines a framework to compare linearity when using different signals. This framework consists of a clear understanding of how the system under test and the test signal influence linearity metrics, and of the expected linearity metric, a linearity metric definition that, regardless of the system and signal, enables a seamless linearity evaluation.

Table of Contents

List of Figures

List of Tables

List of Acronyms

5G	Fifth Generation
ACPR	Adjacent-Channel Power Ratio
AM	Amplitude Modulation
AWGN	Additive White Gaussian Noise
CCPR	Co-Channel Power Ratio
CDMA	Code Devision Multiple Access
CW	Continuous Wave
DAC	Digital to Analog Converter
DC	Direct Current
ELM	Expected Linearity Metric
EVM	Error Vector Magnitude
IMD	Intermodulation Distortion
IMR	Intermodulation Ratio
IP_3	Third-Order Intercept Point
LTE	Long Term Evolution
MIMO	Multiple Input Multiple Output
MMIC	Monolitic Microwave Integrated Circuit
NIST	National Institute of Standard and Technology
NPR	Noise Power Ratio
OTA	Over the Air
PA	Power Amplifier
PAPR	Peak-to-Average Power Ratio
PDF	Probability Density Function
PM	Phase Modulation
PSD	Power Spectral Density
RF	Radio Frequency
SNDR	Signal to Noise Distortion Ratio
SNR	Signal-to-Noise Ratio
SUT	System Under Test
VSA	Vector Signal Analyser
VSG	Vector Signal Generator

Document Outline

This document is organized in four chapters.

Chapter 1 introduces the fundamentals of multi-tone linearity characterization, explains the motives to keep on researching it, presents the state of the art, defines the work objectives, and clarifies some assumptions made in this work.

Chapter 2 explains how to detect nonlinear dynamics under broadband excitation using static reference IMD profiles, evidences the limitations of classical approaches to nonlinear dynamic characterization, and presents a novel characterization technique: swept NPR.

Chapter 3 defines linearity test signal standards to guarantee consistent linearity metric measurements, and presents the ELM framework, that enables the comparison of RF system linearity performance under different test signal excitation.

Chapter 4 concludes, making a critical overview of this work major contributions, limitations, and future work possibilities.

Chapter 1

Introduction

1.1 Background

RF communication systems are designed to exchange information using the radio electric spectrum. But real systems are not ideal, they distort and filter input information. In other words, their output response is a nonlinear dynamic function of the input information.

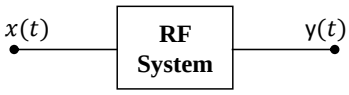

Figure 1.1: Generic RF system diagram block.

The output response of a nonlinear dynamic system, $y(t)$, is composed of a linear function, $f_{lin}[\cdot]$, and a nonlinear function, $f_{nlin}[\cdot]$, of the input information signal, $x(t)$:

$$y(t) = f_{lin}[x(t)] + f_{nlin}[x(t)] \tag{1.1}$$

The nonlinear function is further decomposed into a correlated, and uncorrelated response:

$$f_{nlin}[x(t)] = f_{nlin_{corr}}[x(t)] + f_{nlin_{uncorr}}[x(t)] \tag{1.2}$$

The correlated response contains some input information, whereas the uncorrelated response, despite being imposed by the input signal, contains no information.
The linearity level is the linear to nonlinear response ratio at the system output response.

$$\text{Linearity Level} \propto \frac{f_{lin}[x(t)]}{f_{nlin}[x(t)]} \tag{1.3}$$

RF system linearity characterization consists of exciting the system with a test signal, measuring the output response, separating the linear and nonlinear responses, and assessing the linearity level. Since the nonlinear response produces novel spectral components at the system output around DC, and around all carrier harmonic frequencies, and the linear response only filters the input signal spectrum, as shown in Fig. 1.2, the RF system linearity characterization is performed in the frequency domain, being mostly concerned with in-band distortion around the carrier frequency, i.e. adjacent-channel and co-channel distortion. The characterization goal is to determine what spectral components are generated from input to

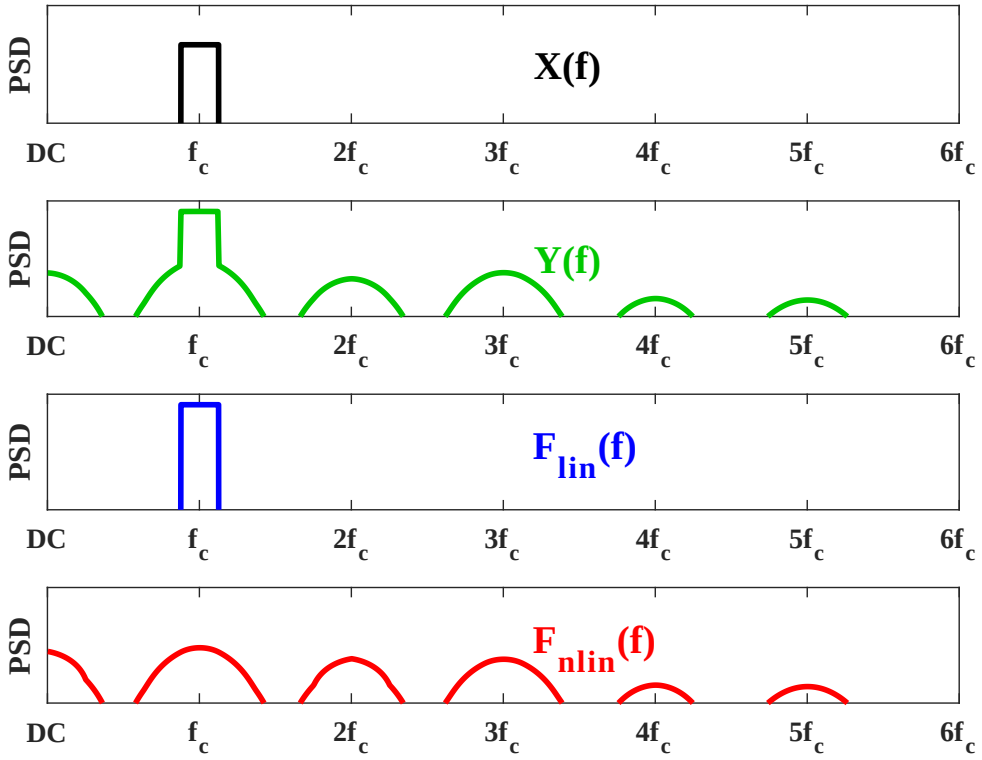

Figure 1.2: Spectral decomposition of the nonlinear dynamic RF system response.

output, what are their magnitude and phase, what is their relation to the linear response, and if they manifest dynamic behavior.

There are four major aspects of RF system linearity characterization: instrumentation, techniques, metrics, and test signals.

1.1.1 Linearity instrumentation

Linearity instrumentation is the development of hardware to perform RF system linearity characterization, i.e. hardware capable of generating/measuring test signals with desired temporal amplitude statistics, and spectral magnitude and phase. Thankfully, modern Vector Signal Generator (VSG), and Vector Signal Analyser (VSA) equipment is capable of performing the signal generation/measurement tasks required for general purpose RF sytem linearity characterization, therefore, for most applications, there is no need to develop tailored hardware, like there was in the past [7, 8].

1.1.2 Linearity characterization techniques

Linearity characterization techniques are methods to configure RF instruments in experimental setups to measure the linear, and the nonlinear RF system response. Most modern

techniques use some variation of the experimental setup schematized in Fig. 1.3. In this setup, the VSG generates the test signal, and the VSA measures the output response.

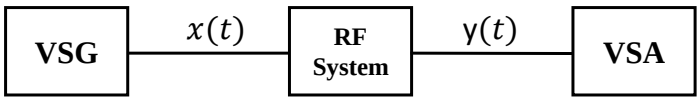

Figure 1.3: RF system linearity characterization experimental setup.

As stated, the interest nonlinear response in RF system linearity characterization is the in-band nonlinear response, that includes both co-channel, and adjacent-channel distortion. Measuring the adjacent channel portion of the nonlinear response is straightforward, it is directly observed from the output response spectrum, as shown in Fig. 1.4. The complex aspect of linearity characterization techniques is the measurement of co-channel distortion, whose spectrum overlaps the linear system response. In fact, RF system linearity characterization techniques can be grouped based on the method they use to measure co-channel distortion. The most relevant are notch based, correlation based, and feed-forward based techniques.

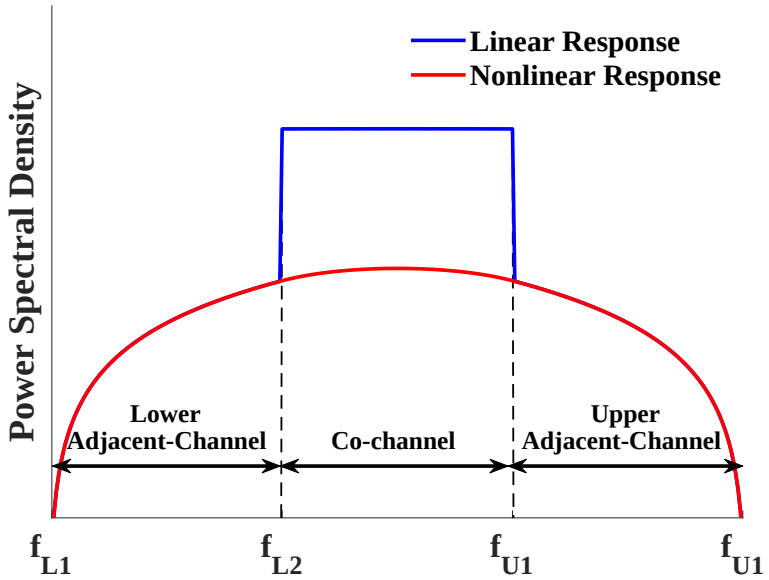

Figure 1.4: In-band distortion PSD.

Notch Based Techniques

Notch based techniques filter part of the test signal spectrum to make a nonlinear observation at the system output[1], as depicted in Fig. 1.5. The output PSD within the notch bandwidth provides an approximate measure of the co-channel uncorrelated nonlinear response, whereas the output PSD in the remaining co-channel frequencies provides an approximate

[1]The heuristic is to use a notch filter that removes less 10% of the total instantaneous bandwidth.

measure of the linear response. Classically, this measurement was performed with a notch at the carrier frequency [9, 10][2], but the notch can be placed anywhere within the excitation bandwidth to evaluate uncorrelated distortion locally [12].

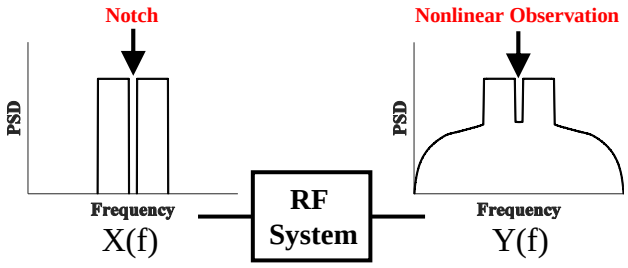

Figure 1.5: Notch based characterization technique block diagram.

Correlation Based Techniques

Correlation based techniques assume that the correlated system response is the linear response, and that the uncorrelated system response is the nonlinear response[3]. With this assumption, the correlation factor is the equivalent linear gain between the input, and linear output signals [13–16]. Therefore, after measuring the input, and output signals, it is possible to compute the equivalent gain, and obtain the linear, and nonlinear output responses.

Fig. 1.6 summarizes the correlation based characterization technique.

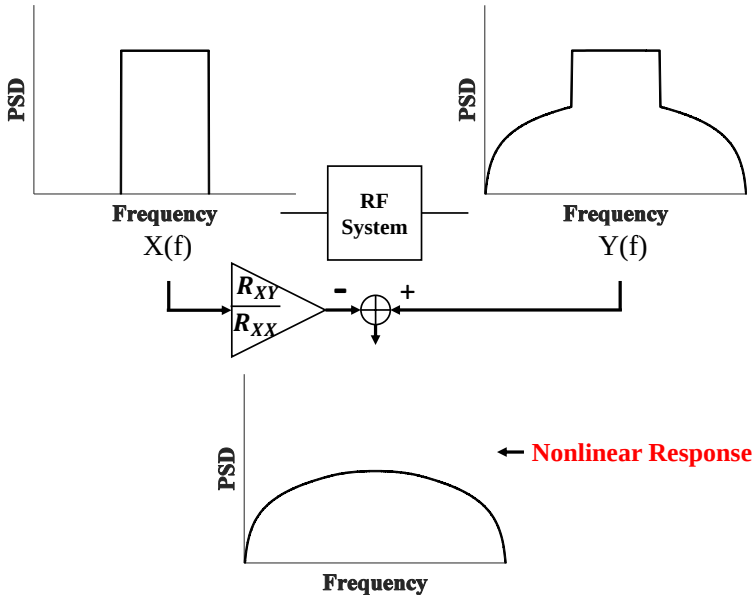

Figure 1.6: Correlation based characterization technique block diagram.

[2]In the absence of dynamics, the central notch location provides the worst case measurement of uncorrelated nonlinear distortion [11].

[3]Correlation based techniques interpret the correlated nonlinear response as part of the linear response.

Feed-Forward Based Techniques

Feed-forward based techniques feed the linear system response to the system output to isolate the nonlinear response, and then measure it [8, 17]. This method requires the prior knowledge of the linear system response, which can be obtained from small signal measurements. These techniques are the best suitable for scenarios in which input power level varies significantly. Fig. 1.7 summarizes the feed-forward based characterization technique.

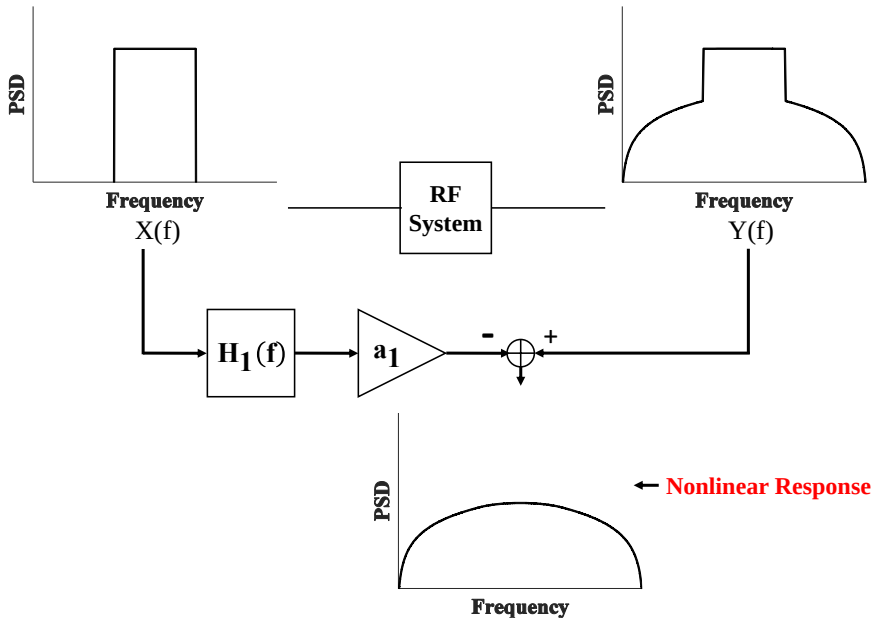

Figure 1.7: Feed-forward based characterization technique block diagram.

1.1.3 Linearity metrics

Linearity metrics define how the system linear, and nonlinear response measurements are processed to asses linearity. Classical Multi-tone metrics are linear/nonlinear ratios, that integrate power in interest bands: the adjacent-channel, and the co-channel [18, 19].

Adjacent-Channel Power Ratio (ACPR) is the ratio between the co-channel output power and the adjacent-channel distortion power. From Fig. 1.4, it is defined as:

$$\frac{\int_{f_{L2}}^{f_{U1}} S_y(f)df}{\int_{f_{L1}}^{f_{L2}} S_y(f)df + \int_{f_{U1}}^{f_{U2}} S_y(f)df} \tag{1.4}$$

ACPR can be measured from a simple spectral measurement of the output signal.

NPR is the ratio between the uncorrelated nonlinear output PSD and the correlated output PSD. From Fig. 1.8, it can be defined as:

$$NPR = \frac{\frac{1}{f_1 - f_{L2}} \int_{f_{L2}}^{f_1} S_y(f)df + \frac{1}{f_{U1} - f_2} \int_{f_2}^{f_{U1}} S_y(f)df}{\frac{1}{f_2 - f_1} \int_{f_1}^{f_2} S_y(f)df}. \tag{1.5}$$

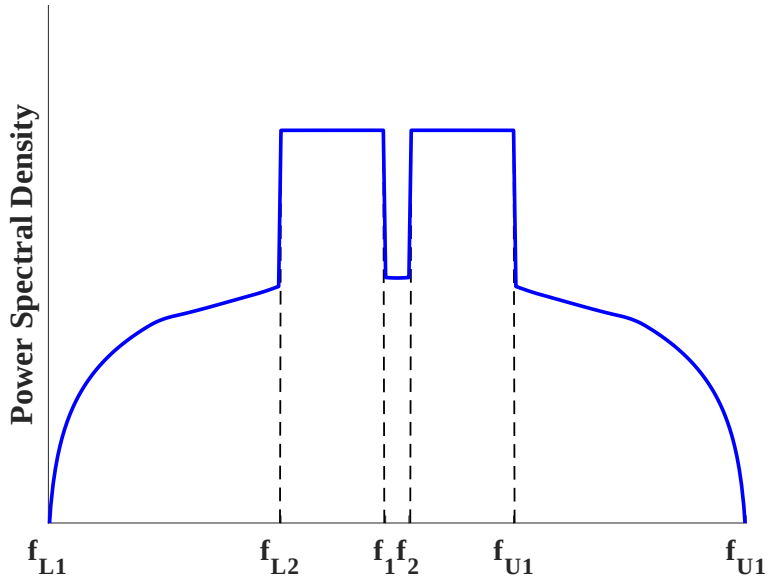

Figure 1.8: NPR evaluation bands.

NPR can be measured using correlation based techniques, or using notch based characterization techniques. Its first formulation assumes a notch based technique [9].

Co-Channel Power Ratio (CCPR) is the ratio between the co-channel nonlinear output power and the linear output power. From Fig. 1.4, it is defined as:

$$\frac{\int_{f_{L2}}^{f_{U1}} S_y(f)df}{\int_{f_{L2}}^{f_{U1}} S_{f_{nlin}}(f)df} \tag{1.6}$$

CCPR is measured using feed-forward characterization techniques, and accounts for both correlated and uncorrelated distortion [8, 11].

1.1.4 Linearity test signals

The nonlinear response, contrarily to the linear response, cannot be decomposed into the sum of the responses to each information component at the system output[4]. Thus, it must be measured with signals that replicate the real application modulation characteristics [20], or signals that force a wide variety of states, like random signals [9, 21].

For a long time, Continuous Wave (CW) and two-tones were the most widely used linearity test signals [18], but modern RF communication has amplitude, phase, and bandwidth characteristics that can no longer be represented by these test signals [21–23].

On the other hand, properly designed multi-tone signals produce well characterized waveforms that can simulate complex modulated RF signals and specific statistical distributions, like Additive White Gaussian Noise (AWGN). Furthermore, contrarily to real communication signals, multi-tones are easy to generate, measure, and replicate. They allow flexible statistical design with a reduced number of tones, and yield insight into distortion causing mechanisms [11, 21, 24–28]. Therefore, if possible, it is desirable to support future RF linearity characterization techniques on multi-tone test signals.

[4]Nonlinear systems do not enjoy superposition: $f_{nlin}[\sum_{n=1}^{\infty} \alpha_n x_n(t)] \neq \sum_{n=1}^{\infty} f_{nlin}[\alpha_n x_n(t)]$

A generic multi-tone signal is defined by (1.7).

$$x(t) = \sum_{q=1}^{Q} A_q cos(\omega_q t + \phi_q) \tag{1.7}$$

It consist of multiple sinusoidal waves with independent amplitude, A_q, frequency, ω_q, and phase, ϕ_q. For RF system linearity characterization purposes, the sinusoidal waves fit in a well-defined frequency grid, meaning that multi-tones are periodic and deterministic signals.

1.2 Motivation

Telecommunication is in constant evolution. As Fifth Generation (5G) technology is being deployed, researchers are already exploring the challenges and requirements for radio communication beyond 5G [29]. Each novel technology is expected to have higher capacity, more users, better energy efficiency, and lower cost than the previous one. But, more than improving specs, novel technologies aim to improve society in a tangible way. For example, future satellite technology aims to provide internet and mobile service coverage worldwide[5] [29]. To enable such technological leaps, RF hardware must be stretched beyond its current performance limits [30]. The same is true for RF linearity measurement science.

This work is aligned with the National Institute of Standard and Technology's goal to develop measurement science and standards for the next generations of wireless communication [31], namely the development of improved nonlinear device characterization and instrumentation techniques. It was kickstarted by the need to overcome the NPR characterization limitations found while characterizing the linearity of K-band Power Amplifier Monolitic Microwave Integrated Circuit designs for satellite application in a collaborative project with the European Space Agency [32].

In satellite applications, NPR is the linearity criterion [22, 33, 34], and the identity between NPR and Error Vector Magnitude (EVM) [14, 35–37] makes NPR aware of modulation error, which is relevant for mobile applications. But new linearity characterization challenges arise as these applications occupy broader bandwidths, and move to higher frequency bands, because nonlinear dynamics can no longer be neglected, and defining appropriate techniques, and metrics becomes increasingly complex. In fact, there are three major limitations that hinder the use of NPR in modern telecom: 1) NPR assumes static nonlinearities [12, 37], considering, at most, linear dynamics; 2) there is a lack of insight of how nonlinear dynamic effects manifest on the nonlinear response under broadband excitation; 3) the cumulative nature NPR hides the frequency dependence of the nonlinear response.

Furthermore, linearity metrics must provide insight about the nonlinear distortion limits for correct system operation. Without this, metrics become just blind marks to meet the requirement list. A debilitating weakness in this regard is the existent difficulty to perform measurements that yield comparable linearity metrics, especially when different test signals are used. This happens because there is no standard linearity characterization test signal, and it is not easy to establish identities between linearity metrics obtained using different test signals. These limitations create critical overarching problems. Designers do not have a universal metric to reference their linearity improved designs. Manufacturers cannot provide complete linearity characterization of their products, as it is impracticable to test them with

[5] 40 % of Earth still does not have access to internet, nor to mobile telecommunication services.

all communication signals. And application engineers cannot know a priori if a given device they purchase will comply to the linearity specifications of their application if that signal is not contemplated on the manufacturer's datasheet.

Actually, many more RF system linearity characterization limitations could be mentioned in the scope of novel telecommunication technologies, but for the sake of clarity, this document focuses only on nonlinear dynamic characterization, linearity metric identities, and test signal statistics, which are the object of study of this work.

1.3 State of the Art

1.3.1 Nonlinear Dynamic Characterization

The ability to detect and quantify nonlinear dynamics in broadband operation is essential for modern RF applications. Unfortunately, multi-tone RF system linearity characterization techniques and metrics capable of this are lacking. They can only be developed after understanding how dynamics manifest under multi-tone excitation, and how they can be measured.

Carvalho and Pedro explained how 3rd-order nonlinear dynamics manifest under equal magnitude two-tone excitation [38]. They demonstrated how baseband impedance variation produces strong adjacent channel distortion asymmetry when loads are dominantly reactive. Under equal magnitude two-tone excitation, a static system produces symmetrical adjacent channel distortion. Therefore, adjacent-channel distortion asymmetry is a measure of 3rd-order nonlinear dynamics. By comparing the measured adjacent channel distortion asymmetry with the expected static response it is possible to quantify nonlinear dynamics [39]. Therefore, by performing multiple two-tone measurements with different tone spacing, it is possible to detect and quantify dynamics within the RF system excitation bandwidth. For a long time, this was the most reliable RF nonlinear dynamic characterization procedure available. But, for several reasons, in modern RF applications this method has become obsolete. As stated, two-tone signals are not representative of modern communication scenarios. Furthermore, the circuit-level theory that supports this technique is hard to carry over to system-level linearity characterization, and it is too tightly bound to third-order nonlinearity and baseband dynamic mechanisms, which leads to incorrect results when the system under test manifests other nonlinear dynamic behaviors.

Martins *et. al.* [40] extrapolated RF system nonlinear dynamic characterization to multitone excitation signals. This work shows how to use multiple two-tone measurements to compute a multi-tone response, and evaluate adjacent-channel and co-channel distortion. From this endeavor, the authors drew two important qualitative considerations: adjacent-channel is mostly influenced by mid-band baseband distortion, whereas co-channel distortion is mostly influenced by baseband distortion near DC. They also noted that memory effects are observable in the shape of the distortion components. On the downside, this work, despite being a first step towards multi-tone linearity characterization, is highly influenced by [38], and suffers from the same limitations. Furthermore, its claim about memory effect observation is qualitative, and is not supported theoretically. More work is required to quantify nonlinear dynamic effects in comprehensive metrics. Beyond this, the use of multiple 2-tone measurements to reconstruct the multi-tone response is not generally valid, and is more laborious than truly performing a multi-tone characterization.

In [23], a multi-tone characterization technique was finally presented for the assessment of nonlinear dynamics. It uses an offset multi-tone, which is a multi-tone whose frequency

grid guarantees that each IMD product generated is unique[6], meaning that each nonlinear output frequency is composed of a single IMD product, and that output distortion and output signal are at distinct frequencies. Therefore, the nonlinear dynamics of different orders can be characterized directly, and simultaneously from the output response. This work evidences that offset multi-tone characterization is more sensitive than two-tone characterization, particularly near peaks and steep regions of the nonlinear dynamic response. However, offset multi-tones have scalability issues in terms of the number of tones, and in terms of the nonlinear orders that can be evaluated. Guaranteeing unique IMD products beyond third-order is increasingly difficult, and for higher orders it becomes impossible. Beyond this, the frequency sweep method used for in-band nonlinear dynamic observation is still tightly bound to the two-tone technique. Scalable RF multi-tone linearity characterization techniques require a categorically different approach to nonlinear dynamic detection.

This compilation of works evidences that the measurement of nonlinear dynamics requires tailored characterization techniques. It is not something that can be directly inferred from classical characterization approaches. In fact, existing multitone linearity metrics are unable to assess nonlinear dynamics, because they average the distortion power present inband by integrating the nonlinear response PSD. This hides nonlinear dynamic effects, which are frequency dependent by definition. Therefore, the use of NPR to assess the linearity of systems presenting long-term memory effects is misleading. Scalable multi-tone linearity characterization techniques, and quantifiable metrics to evaluate nonlinear dynamics effects in modern RF communication scenarios are missing, and are desperately required.

1.3.2 Linearity Metrics: identities and test signal statistics

Linearity measurements are complex, costly, time consuming, and require expertise. Therefore, it is desirable to be able to predict linearity metrics without having to measure them. This can be obtained from a good RF system model, or from the decomposition of the system output response. Figures of merit can be predicted either by computing the system output using the model, and evaluating the linearity metric, or by establishing an identity, i.e. a conversion factor, between linearity metrics measured at the system output.

The equivalent gain approach, presented in [13], accurately computes ACPR, NPR, and EVM under Code Devision Multiple Access (CDMA) signal excitation. This was achieved using a RF system model based on the AM-AM and AM-PM characteristics of the device under test. In [11], Pedro and Carvalho, assuming a 3rd-order nonlinear system, related two-tone and multi-tone figures of merit. They established identities between ACPR, NPR, CCPR, and Intermodulation Ratio (IMR). These identities were later expressed in terms of Third-Order Intercept Point (IP_3) [41]. In [35], a correlation based approach was used to decompose the RF system output response, and establish identities between Signal-to-Noise Ratio (SNR), and EVM. This linked system level metrics and nonlinear distortion. Since then, efforts were made to relate EVM with NPR [22, 36, 42]. In [37], a best linear approximation technique is used to obtain EVM, NPR, and ACPR from a single measurement, with the same setup. Indeed, many works have addressed and presented linearity metric identities. So, why is this still a relevant research topic? In part, because the published works based on modeling approaches are not valid in nonlinear dynamic scenarios. Also, because the correlation/best linear approximation strategies mentioned are valid as long as the test signal remains the

[6] An offset multi-tone is a standard multi-tone with most tones switched-off. The switch-off is designed to avoid IMD product overlap. In practice, this linearity characterization technique is notch based.

same, and with constant power level [12]. In fact, predicting linearity under different test signal statistics, and for different signal types is a major challenge.

Several studies report test-signal/linearity metric dependence. In [43], Aparin observed that in reserve link CDMA, linearity changes just by alternating between OQPSK and QPSK modulation schemes. In [44], the ACPR of the same device is measured with different multi-tones, and with a real communication signals. The authors observed that all ACPR metrics are different. No multi-tone was capable of reproducing the real communication signal ACPR. In [45], for the same device, the NPR measured with an IS-95 signal differs more than 5 dB from the NPR measured using a Gaussian signal.

Some have worked to formulate and interpret the influence of test signal statistics on linearity metrics. In [46], authors described modulated signals statistically. Then, with the aid of behavioral modeling, they computed the output auto-correlation function of a the nonlinear system, from which it is possible to compute and evaluate ACPR, effectively establishing the desired relationship between input statistics and linearity metrics. However, this approach is mathematically complex, and requires specific theoretical development for every desired input signal statistics, which makes it hard to use. Nonetheless, these considerations enabled Aparin to explain the linearity differences observed in [43] when alternating between OQPSK or QPSK modulation schemes in reverse link CDMA. These were imposed by differences in the high-order statistical moments of these signals. In [47], the initial steps on how to interpret linearity metrics in light of the test signal amplitude statistics were laid out. It explained the importance of the test signal PSD on the linearity metric, showing that the likelihood of nonlinear power levels is more important than maximum instantaneous power, evidencing the limitations of supporting the linearity analysis on Peak-to-Average Power Ratio (PAPR). In [48], it was added that to understand the linearity metric imposed by a given test signal, it is not enough to look to the signal spectrum and the amplitude statistics, it is necessary to consider the temporal waveform as a whole, i.e. to have in mind both the amplitude and phase of the test signal spectrum.

Despite these developments, the insight to interpret and predict linearity metrics measured with different test signals is still short, and in need of expansion.

1.4 Objectives

As stated, this work is aligned with the NIST's goal to develop measurement science and standards for the next generations of wireless communication. It aims to improve multi-tone linearity characterization techniques, and metrics. The major objectives are:

- To develop novel RF system multi-tone linearity characterization techniques and metrics capable of detecting nonlinear dynamics under broadband excitation;
- And to develop a universal framework to assess and compare RF system linearity when different test signals are used.

1.5 Assumptions

To avoid doubts and misinterpretations, here is list of assumptions implicit in this work.

List of assumptions:

- The RF system under test is time-invariant. It is not modified by characterization.
- The term *broadband system* is used interchangeably with *nonlinear dynamic system*. It does not refer to a specific bandwidth, carrier frequency, nor any ratio between the two.
- A broadband excitation is a test signal that excites the relevant nonlinear dynamics within the excitation bandwidth of a broadband system.
- RF system linearity is a function of the input test signal. Any thermal, bias, loading, or trapping effect that is not a function of the input test signal is not object of study.
- Nonlinear distortion is produced by the RF system. Mixing, video bandwidth, and baseband telecommunication subsystems are assumed to be ideal.

Chapter 2

Nonlinear dynamic detection under broadband excitation

As RF systems occupy broader bandwidths and move to higher frequency bands, the need to know how to detect nonlinear dynamics under broadband excitation increases, and defining appropriate linearity characterization techniques and metrics becomes more complex.

The existing approaches to nonlinear dynamic detection in RF systems rely on techniques developed under 2-tone excitation, but their theoretical validity under multi-tone excitation has not been demonstrated. Classical characterization techniques and metrics, such as NPR and ACPR, are often linked with nonlinear dynamic detection, but it is not proven if, nor how, they detect nonlinear dynamics. Furthermore, the validated techniques, like the unequally spaced multi-tone, have scalability issues.

This chapter revisits classical linearity characterization to understand and overcome its limitations, and presents a solution to detect nonlinear dynamics under broadband excitation.

2.1 Reference IMD profiles and nonlinear dynamic detection

Many works suggest that nonlinear dynamics manifest as a deviation of the observed IMD response from a reference response [36, 37, 40], but they do not explicitly define this reference. Without a reference it is not possible to quantify nonlinear dynamics, and qualitative observations are not rigorous. In this section, it is explained how to define static IMD reference profiles, and how to quantify nonlinear dynamics.

2.1.1 Static IMD Reference Profile

Fig. 2.1 portrays the static IMD profile concept.

Static nonlinear systems are generally described by (2.1).

$$y(t) = \sum_{n=0}^{\infty} a_n x(t)^n \tag{2.1}$$

For a given excitation, each monomial imposes a static spectral profile. The linear profile is an amplified replica of the input excitation spectrum:

$$Y_1(\omega) = a_1 \mathcal{F}\{x(t)\}, \tag{2.2}$$

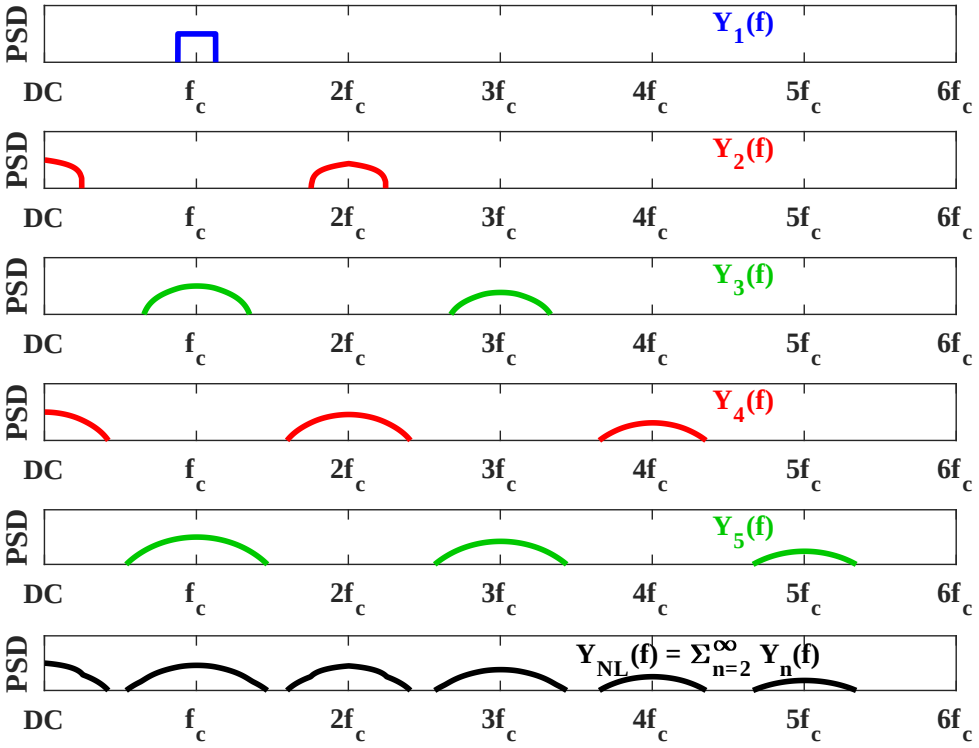

Figure 2.1: Static IMD profiles up to 5th-order, and corresponding full static IMD profile.

---

the nth-order profile is obtained by convoluting the lower order profile with the input signal:

$$Y_n(\omega) = \mathcal{F}\{a_n x(t) \cdot x(t)^{n-1}\} = a_n \mathcal{F}\{x(t)\} * \mathcal{F}\{x(t)^{n-1}\}, \tag{2.3}$$

the full static IMD profile is given by the overlap of all nonlinear order profiles:

$$Y_{\mathrm{NL}}(\omega) = \sum_{n=2}^{\infty} Y_n(\omega), \tag{2.4}$$

and the RF system linearity analysis focuses on the fundamental envelope IMD profile.

2.1.2 Static IMD profiles under multi-tone excitation

The nth-order response to an equal magnitude multi-tone

$$x(t) = \frac{1}{2} A \sum_{q=1}^{2Q} \cdot e^{j(\omega_{\mathrm{ex}q} t + \phi_{\mathrm{ex}q})}, \tag{2.5}$$

with excitation frequency vector

$$\boldsymbol{\omega_{ex}} = [-\omega_Q, \ \cdots, \ -\omega_1, \ \omega_1, \ \cdots, \ \omega_Q]^T, \tag{2.6}$$

and excitation phase vector

$$\boldsymbol{\phi_{ex}} = [-\phi_Q,\ \cdots,\ -\phi_1,\ \phi_1,\ \cdots,\ \phi_Q]^T, \tag{2.7}$$

is given by:

$$y_n(t) = \boldsymbol{g_n} \cdot e^{j[\boldsymbol{\omega_{IMD_n}} t + \boldsymbol{\phi_{IMD_n}}]}, \tag{2.8}$$

where $\boldsymbol{g_n}$ is the nth-order magnitude weighting vector,

$$\boldsymbol{g_n} = \frac{1}{2} a_n A^n \binom{n}{\boldsymbol{V_n}}, \tag{2.9}$$

and $\boldsymbol{\omega_{IMD_n}} t + \boldsymbol{\phi_{IMD_n}}$ is the nth-order IMD phase vector,

$$\boldsymbol{\omega_{IMD_n}} t + \boldsymbol{\phi_{IMD_n}} = [\boldsymbol{V_n} \cdot (\boldsymbol{\omega_{ex}} t + \boldsymbol{\phi_{ex}})]^T . \tag{2.10}$$

$\boldsymbol{V_n}$ is the nth-order mixing matrix,

$$\boldsymbol{V_n} = \left[\boldsymbol{v_1},\ \boldsymbol{v_2},\ \cdots,\ \boldsymbol{v_M}\right]^T, \tag{2.11}$$

that contains all M nth-order mixing vectors,

$$\boldsymbol{v_m} = [v_{m_1},\ v_{m_2},\ \cdots,\ v_{m_2 Q}]^T. \tag{2.12}$$

Each mixing vector is unique, and respects the following conditions: $v_{m_i} \in N_0$; $\sum v_{m_i} = n$. In summary, the nth-order IMD frequency, weight and phase are imposed by the input multi-tone excitation and the nth-order mixing matrix.

The nth-order static IMD profile at a given frequency, ω, is the phasor sum of all IMD products that overlap at ω:

$$K_n(\omega) = \sum_{i:\omega_{\mathrm{IMD}_{n_i}} = \omega} g_{n_i} \cdot e^{j\phi_{\mathrm{IMD}_{n_i}}} \tag{2.13}$$

Likewise, the full static IMD profile is the sum of all nth-order profiles that overlap at ω:

$$K(\omega) = \sum_{n=2}^{\infty} K_n(\omega) \tag{2.14}$$

for any equal magnitude multi-tone, for any nonlinear order.

With this formulation it is straightforward to distinguish between correlated and uncorrelated IMD profiles. The correlated profile considers IMD products that involve the excitation frequency in which they overlap:

$$K_n(\omega_q)_{\mathrm{corr}} = \sum_{i:\omega_{\mathrm{IMD}_{n_i}} = \omega_q \ \wedge\ \left(V_{n_i,Q-q+1} \neq 0 \ \vee\ V_{n_i,Q+q} \neq 0\right);\ q \in [1,Q]} g_{n_i} \cdot e^{j\phi_{\mathrm{IMD}_{n_i}}}, \tag{2.15}$$

whereas the uncorrelated profile does not:

$$K_n(\omega_q)_{\mathrm{uncorr}} = \sum_{i:\omega_{\mathrm{IMD}_{n_i}} = \omega_q \ \wedge\ V_{n_i,\{Q-q+1,Q+q\}} = 0;\ q \in [1,Q]} g_{n_i} \cdot e^{j\phi_{\mathrm{IMD}_{n_i}}}. \tag{2.16}$$

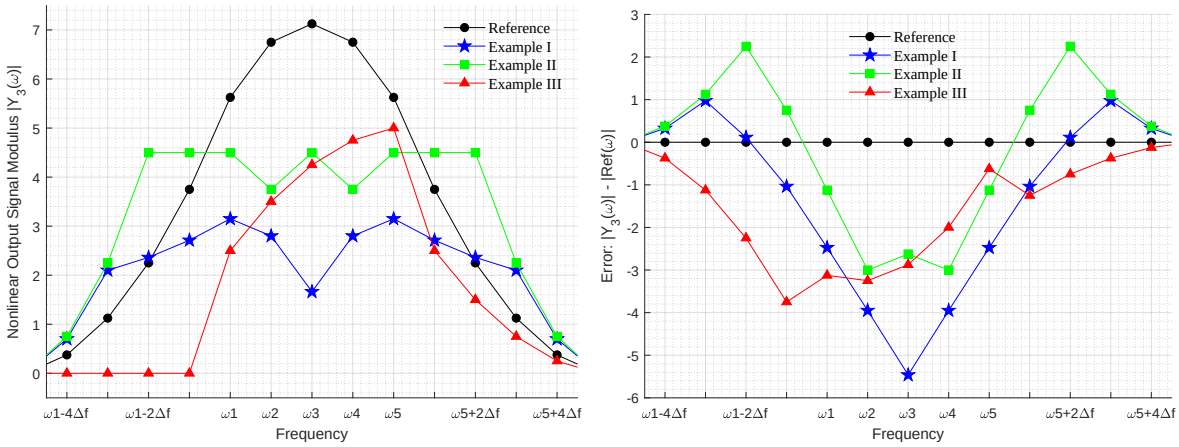

(a) Example IMD profiles.

(b) Example dynamic IMD error profiles.

Figure 2.2: Normalized numerical dynamic IMD profiles.

For equally spaced tones, the interest fundamental envelope bandwidth expands

$$\pm\frac{N-1}{2}\cdot(N_{\text{tones}}-1)\cdot\Delta f \tag{2.17}$$

beyond the instantaneous excitation bandwidth[1]. Where N is the largest odd-order in the system, N_{tones} is the number of excitation tones, and Δf is the carrier spacing.

2.1.3 Detecting Nonlinear Dynamics

Contrarily to memoryless systems, nonlinear dynamic systems filter the static IMD profile according to their frequency dependent response, changing $K(\omega)$. Therefore, nonlinear dynamics can be gauged in the error between the measured IMD profile and static reference IMD profile given by (2.14):

$$\text{Error}(\omega)=K_{\text{meas}}(\omega)-K_{\text{ref}}(\omega). \tag{2.18}$$

Constant error within the system bandwidth indicates attenuation/amplification, whereas frequency dependent error indicates the presence of nonlinear dynamics[2]. Fig. 2.2 plots the IMD profiles and dynamic error curves obtained through numerical computation of three example scenarios that use a 5-tone excitation[3]. The frequency dependent error confirms the presence of nonlinear dynamics.

2.2 Classical nonlinear dynamic mechanism: Review, IMD profile analysis, and limitations

The classic nonlinear dynamic mechanism is depicted in Fig. 2.3. It has two interfering branches: a static 3rd-order branch, and a dynamic 3rd-order branch. The dynamics are imposed at baseband by $H_2(\omega)$, before the IMD conversion to the fundamental carrier.

[1] Formula (2.17) assumes that even and odd order profiles do not overlap.

[2] Dynamics are detected at frequencies in which $\frac{\partial\text{Error}(\omega)}{\partial\omega}\neq 0$

[3] For numerical example details, refer to [nprJ1, Sec. IV.], attached at the end of this chapter.

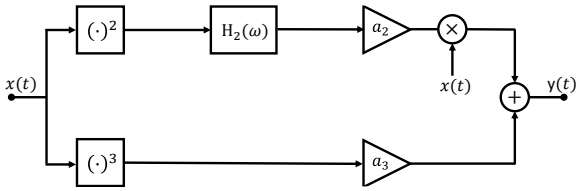

Figure 2.3: Classic IMD mechanism block diagram.

For an equal magnitude 2-tone excitation signal, the envelope 3rd-order static reference IMD profile, given by (2.13), has equal lower and upper adjacent-channel IMD power[4], regardless of the excitation phase vector. Therefore, in these conditions, adjacent channel IMD asymmetry and adjacent channel IMD variation with carrier spacing are indicators of 3rd-order dynamics. These features, and the classical nonlinear dynamic mechanism, were used in [38, 39] to explain and detect baseband dynamics observed at RF. Under multi-tone excitation, several IMD products overlap at each fundamental envelope IMD frequency, and the excitation phase vector affects the reference 3rd-order IMD profile given by (2.13). Thus, adjacent channel features are not sufficient to detect baseband nonlinear dynamics. Note that such analysis fails to detect the nonlinear dynamics present in the Example I and Example II symmetrical IMD profiles plotted in Fig. 2.2a.

As explained in section 2.1.3, under multi-tone excitation, baseband dynamics are detected by the observation of frequency dependent error betweeen the classic mechanism IMD profile and the 3rd-order static reference profile. The classical mechanism IMD profile is given by the sum of the static and dynamic branch 3rd-order IMD profiles. The static branch IMD profile is equal to the reference. The dynamic branch IMD profile is dependent on the baseband dynamics that enter into play before the IMD conversion from 2nd-order to 3rd-order. Expression (2.19) formulates this conversion:

$$\begin{aligned} y_n(t) &= a_n\ x(t)^{n-1} \cdot x(t) \\ y_3(t) &= \frac{a_3}{a_2} \cdot y_2(t) \cdot \frac{1}{2} \cdot A \cdot \sum_{q=1}^{2Q} e^{j(\omega_{\mathrm{ex}_q} t + \phi_{\mathrm{ex}_q})} \\ K_3(\omega_{\mathrm{IMD}_3}) &= \frac{a_3}{a_2}\frac{1}{2} A \sum_{\substack{i,k:\ \omega_{\mathrm{IMD}_{2_i}} + \omega_{\mathrm{ex}_q} = \omega_{\mathrm{IMD}_3}}} K_2(\omega_{\mathrm{IMD}_{2_i}}) \cdot e^{j\phi_{\mathrm{ex}_q}} \end{aligned} \tag{2.19}$$

Basically, each 2nd-order IMD frequency, $\omega_{\mathrm{IMD}_{2_i}}$, converts to the 3rd-order IMD frequency $\omega_{\mathrm{IMD}_{2_i}} + \omega_{ex_q}$. Before the conversion, $H_2(\omega)$ filters each 2nd-order IMD product, $K_2(\omega_{\mathrm{IMD}_{2_i}})$, introducing dynamics that are observable at RF, as the static and dynamic branch IMD profiles interfere with each other.

The classic nonlinear dynamic mechanism was a fundamental tool to understand the influence of baseband dynamics in RF systems, and it is still useful to conceptualize nonlinear dynamics in broadband scenarios, but its applicability is limited. An obvious limitation is that it is bound to 3rd-order, but the limitations span beyond this. Different systems of equal nonlinear order can produce the same profile for the same excitation signal. For instance, if the filter $H_3(\omega)$, in the 3rd-order dynamic system in Fig. 2.4, is given by:

[4] $|K_3(2\omega_1 - \omega_2)|^2 = |K_3(2\omega_2 - \omega_1)|^2$

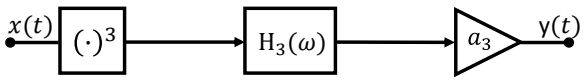

Figure 2.4: 3rd-order dynamic mechanism block diagram.

$$H_3(\omega) = \frac{K_{3_{\text{classic}}}(\omega)}{K_3(\omega)}, \tag{2.20}$$

where $K_{3_{\text{classic}}}$ is the IMD profile of the classic nonlinear dynamic mechanism, the resulting fundamental envelope IMD profile is equal to the one produced by the classic mechanism[5].

The major problem of mechanism based IMD analysis is its use out of context, regardless of the test signal excitation, or the system nonlinearity. For example, some characterization procedures are tailored to specific nonlinear dynamic mechanisms [37, 40]. When using them, one must know this, and be certain that the system under test complies with the assumptions, because invalid assumptions lead to incorrect experimental results.

Static reference IMD profiles enable general characterization techniques to detect nonlinear dynamics that avoid making assumptions about the mechanism that produces them.

2.3 Classical linearity metric limitations

NPR was developed to measure signal to distortion ratio in real communication scenarios. In memoryless scenarios, classical NPR[6] is guaranteed to measure the worst signal to distortion ratio, but in nonlinear dynamic scenarios classical NPR is misleading.

Table 2.1 lists the central notch distortion power, NP, evaluated at ω_3 for each example in Fig. 2.2a. In Example I, the IMD profile minimum occurs at the central frequency. Here, classical NPR not only underestimates the signal to distortion ratio, it also fails to detect nonlinear dynamics. By comparing Example I NP, NP = 2, with the reference NP, NP = 50.8, it is possible to circumvent nonlinear dynamic blindness. But this NP reference is not enough to fix classic NPR. Any dynamics within the notch are hidden, as nonlinear power accumulates, and any dynamics outside the notch are lost, making it impossible to distinguish IMD scenarios that are similar within the notch, but different outside the notch. Note that Example II and Example III have similar NP values, but very distinct IMD profiles[7].

Table 2.1: IMD power at the central frequency

Metric	Example I	Example II	Example III	Reference
NP ($\lvert Y_3(\omega)\rvert^2$)	2.0	20.1	18.1	50.8

Table 2.2 lists the lower and upper adjacent channel distortion power, $\text{ACP}_\text{L}/\text{ACP}_\text{U}$, for each example in Fig. 2.2a. Once again, without a reference ACP, it is not possible to detect dynamics. With the aid of the reference ACP, it is possible to detect dynamics in

[5] Find numerical examples of this in [nprJ1, Sec. V.], attached at the end of this chapter.
[6] A NPR measurement with a central notch.
[7] The same conclusions can be drawn from an analysis based on CCPR.

Example II and Example III[8], and to distinguish these nonlinear dynamic scenarios[9], but it is not possible to detect the nonlinear dynamics present in Example I. This happens because the Example I IMD profile area above and bellow the reference IMD profile in the adjacent channel is similar, therefore, the accumulation of adjacent channel distortion power hides nonlinear dynamics, making Example I ACP, ACP = 19.5, and reference ACP, ACP = 20.5, very similar. Furthermore, note that in ACP the adjacent channel IMD profile trend differences between Example I and Example II are lost. ACP informs that Example II is above the reference, true, and that Example I is on top of the reference, not true.

Table 2.2: IMD power at the adjacent channels

Metric	Example I	Example II	Example III	Reference
$\mathrm{ACP_L}$ ($\lvert Y_3(\omega)\rvert^2$)	19.5	46.1	0.0	20.5
$\mathrm{ACP_U}$ ($\lvert Y_3(\omega)\rvert^2$)	19.5	46.1	9.1	20.5

In short, the inhability of classical system level linearity metrics to detect nonlinear dynamics is twofold: they do not specify a static reference metric, and, by definition[10], they hide nonlinear dynamics in the nonlinear distortion integrals. In other words, classical linearity metrics lack frequency resolution to detect nonlinear dynamics. Reliable nonlinear dynamic characterization, capable of measuring both IMD profile level and trend, requires the definition of a static IMD reference and the measurement of both adjacent-channel and co-channel IMD with sufficient resolution frequency.

2.4 Swept NPR

From the presented developments, it is possible to extract a list of essential features a reliable nonlinear dynamic RF system characterization technique must have. It must:

- specify a static IMD reference profile in agreement with the input excitation;
- capture the frequency dependent error between measured and reference IMD profiles;
- perform full inband IMD characterization: adjacent channel + co-channel;
- perform magnitude and phase measurements;
- and avoid blind nonlinear dynamic mechanism assumptions.

Swept NPR was developed to comply with these essential features. It consists of performing multiple NPR measurements, sweeping the notch location along the excitation bandwidth, to obtain a full in-band uncorrelated IMD profile.

This technique is performed using an equal amplitude multi-tone test signal, therefore, the full inband response is given by:

[8] Example ACP differ more than a factor of two from the reference ACP.
[9] Example II has a symmetrical ACP, and Example III has asymmetrical ACP.
[10] Recall the definitions in section 1.1.3.

$$\sum_{n=0}^{\infty} K_{n_d}(\omega) \quad , \quad \omega \in \text{inband} \tag{2.21}$$

where $K_{n_d}(\omega)$ is the dynamic weighting phasor of order n observed at the system output[11].

Using (2.15) and (2.16), the response can be decomposed in correlated and uncorrelated components:

$$\sum_{n=0}^{\infty} K_{n_d}(\omega) = \sum_{n=0}^{\infty} K_{n_d}(\omega)_{\text{corr}} + \sum_{n=0}^{\infty} K_{n_d}(\omega)_{\text{uncorr}} \tag{2.22}$$

In swept NPR, the correlated response is interpreted as the linear response[12], and the uncorrelated response as the interest nonlinear IMD profile. The key for a successful characterization is to understand how to decouple these responses. The uncorrelated IMD profile can then be used to detect dynamics when compared with a static IMD reference profile.

2.4.1 Measuring the full in-band uncorrelated IMD profile

By definition, the correlated response is restricted to the excitation bandwidth frequencies, i.e. to the co-channel, whereas the uncorrelated IMD profile spans along co-channel and adjacent channel frequencies. Therefore, under a full spectrum multi-tone excitation[13], the adjacent-channel uncorrelated nonlinear response is observable, but in the co-channel correlated and uncorrelated responses overlap. These must be decoupled.

Note that in (2.15) and (2.16) if a single excitation tone, ω_{off}, is turned off, all IMD phasors correlated with the ω_{off} excitation phasor are switched off, but all uncorrelated phasors that fall in ω_{off} are preserved. Thus, the co-channel uncorrelated IMD response can be measured by switching off a single excitation tone, taking a measurement, recording the uncorrelated IMD at the switched off excitation frequency, sweeping the switched off tone along the co-channel, and repeating this process until all excitation frequencies are characterized. This is the swept NPR concept, that is illustrated in Fig. 2.5 for a 5-tone signal.

Finally, the uncorrelated IMD profile is decoupled by combining the adjacent channel and co-channel uncorrelated IMD observations obtained from multiple measurements. The adjacent channel uncorrelated IMD is obtained from a single full-spectrum measurement, whereas each co-channel IMD component is obtained from a swept NPR measurement. After decoupling the uncorrelated IMD profile, the correlated response is obtained by subtracting the uncorrelated IMD profile from the full spectrum-response initially measured, using (2.22).

The Swept-NPR measurement procedure is summarized in Fig. 2.6 flowchart.

2.4.2 Defining a static IMD profile reference

To define a static IMD profile reference, it is necessary to determine the nonlinear order of the RF system, and the weight of each static nonlinear order on the response. One approach to do this is to use input/output observations under full spectrum multi-tone excitation to

[11] $K_{n_d}(\omega)$ can be understood as the result of the static weighting phasor, given by (2.13), being filtered by the system memory effects.

[12] As usual from a communication perspective [12, 35].

[13] I.e. a multi-tone with all tones on.

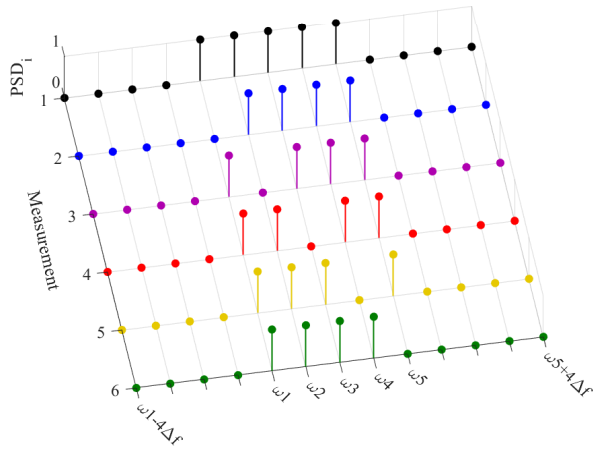

Figure 2.5: 5-tone example of the swept tone characterization steps.

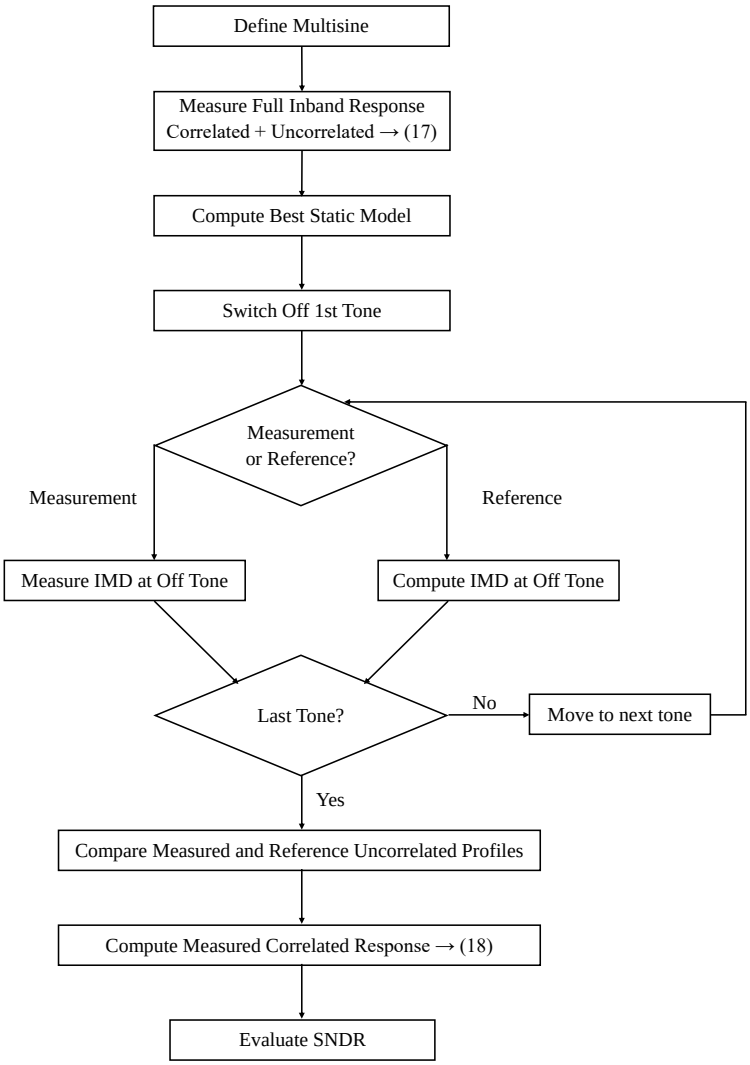

Figure 2.6: Swept NPR characterization flowchart.

extract the best static model of the system in a least squares sense [19, 39], and then use this model to compute the static IMD profile reference[14].

The static IMD reference computation is similar to the uncorrelated IMD profile measurement, but instead of performing measurements, numerical replicas of the experimental signals are applied to the best static model. First a full spectrum excitation is applied to compute the adjacent channel static IMD reference, and then swept-tone NPR signals are applied to compute the co-channel uncorrelated IMD reference.

The static IMD reference extraction procedure is summarized in Fig. 2.6 flowchart.

2.4.3 Signal to noise distortion ratio

When detecting dynamics in nonlinear system responses, it continues to be important to assess the linearity level, conveyed by a SNDR in classic linearity metrics. In the proposed method this can be evaluated as follows:

$$SNDR = \frac{\text{Correlated Power}}{\text{Uncorrelated Power}} \tag{2.23}$$

The correlated power is the commutative power of the correlated inband response, whereas the uncorrelated power is the commutative power of the uncorrelated IMD profile. This formulation accounts for all the power in-band, i.e. co-channel and adjacent channel power.

SNDR, combined with a dynamic error profile, effectively overcomes the aforementioned limitations of classical linearity metrics.

2.4.4 Characterization example

Lets compare the swept NPR characterization of a memoryless device, ERA-2+, with the characterization of a nonlinear dynamic device, ZVA-213-S+. The measurements are performed using two different test signals: an additive white Gaussian Noise 101-tone, and a phase aligned 5-tone. The devices operate at different carriers, but both signals occupy 100 MHz of instantaneous bandwidth, and excite the devices with -10 dBm[15].

Fig. 2.7 plots the error curves between measured and reference IMD profiles. For the ERA-2+ device, the error is lower than 1 dB for both signals, and the curves are almost horizontal in the whole band. Therefore, the swept NPR measurement confirms that this device is memoryless. For the ZVA-213-S+ device, the error can be higher than 3 dB, and there are several measurements points in which the derivative of the error is not zero, confirming that the ZVA-213-S+ is a nonlinear dynamic device.

Table. 2.3 lists the SNDR for each measurement scenario, providing a linearity level that complements the dynamic detection information given by the error curves.

Table 2.3: Experimental SNDR

Metric	ERA (5-tones)	ZVA (5-tones)	Era (101-tones)	ZVA (101-tones)
SNDR (dB)	28.0	24.3	28.8	25.8

[14]This approach minimizes the error between reference and measured IMD profiles, therefore, the corresponding dynamic error is the minimum error, not the absolute error.

[15]For details about the characterization, refer to [nprJ1, Sec. VII.], attached at the end of this chapter.

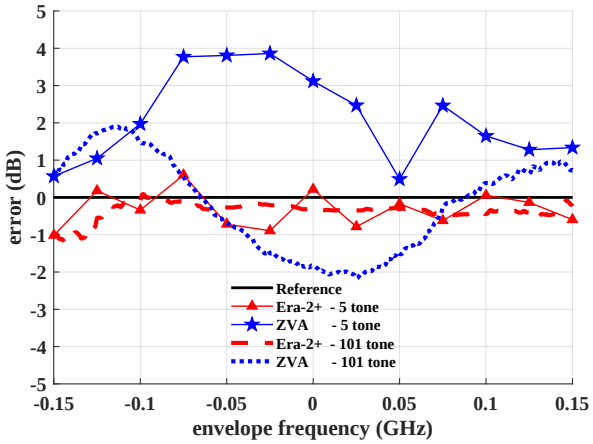

Figure 2.7: Measured dynamic error profiles.

In summary, a swept-tone NPR characterization is capable of distinguishing nonlinear dynamic scenarios from static scenarios using the error profiles, and is capable of evaluating IMD power levels with SNDR, regardless of the multi-tone signal used.

2.5 Swept-Notch NPR vs Multi-Notch NPR

Prior to the development of swept-NPR, the scientific community and industry [37, 42, 50] resorted to multi-notch NPR, hoping to overcome the limitations of classical linearity metrics to detect nonlinear dynamics. Fig. 2.8 depicts the difference between swept-notch, and multi-notch NPR. Multi-notch places multiple notches along the system excitation bandwidth. The idea was that the observation of asymmetrical IMD along the excitation bandwidth implied the presence of nonlinear dynamics, just like in 2-tone IMR. As already explained, IMD symmetry features alone do not detect nonlinear dynamics under multi tone excitation reliably. But the critical limitation of multi-notch NPR is that notching affects IMD outside the notch, therefore, with multiple notches, each notch affects every other notch.

To exemplify this critical limitation, lets consider a normalized static 3rd-order nonlinearity. Table. 2.4 lists, for different linearity characterization techniques, the IMD weight observed at each co-channel frequency when the nonlinearity is excited with a phase aligned 5-tone signal with different tones switched off[16]. The CCPR row[17] lists the full IMD weight, contemplating both correlated and uncorrelated IMD. The swept-tone NPR rows, list, highlighted in bold, the uncorrelated IMD weight at the switched-off tone. This is the uncorrelated IMD weight under full-spectrum excitation[18]. These rows also evidence that switching off a single tone reduces IMD in the whole excitation bandwidth. The multi-notch NPR rows evidence that the uncorrelated IMD weight observed at ω_2 is highly dependent on which other tone is switched-off, demonstrating how multi-notch NPR measurements can corrupt full-spectrum uncorrelated IMD evaluation, even for memoryless scenarios.

In nonlinear dynamics scenarios, the advantage of swept-notch NPR over multi-notch NPR

[16]For IMD computation details, refer to [nprC2, Sec. II.], attached at the end of this chapter.
[17]The row in which all tones are switched-on.
[18]Recall from section 2.4.1, that switching off a single tone cancels all correlated IMD, and preserves all uncorrelated IMD at the switched off frequency.

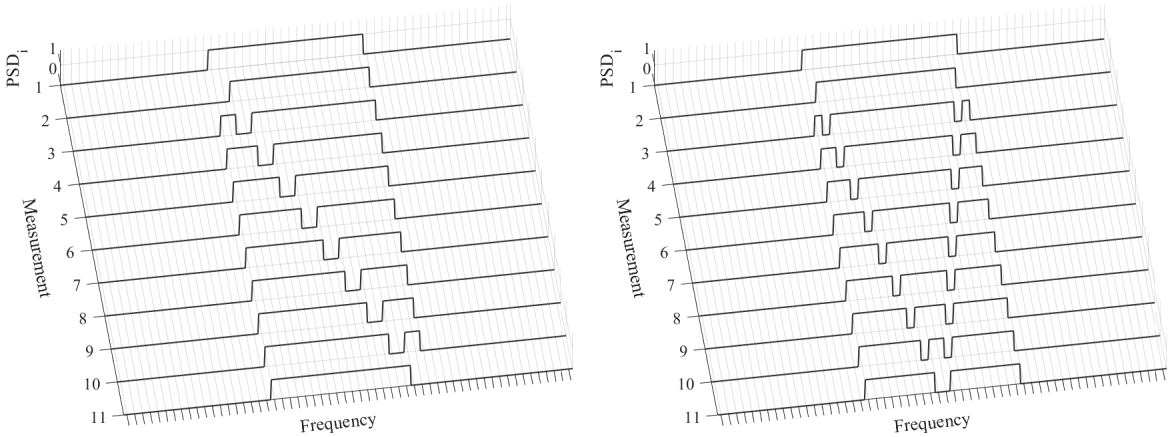

(a) Swept notch NPR. (b) Swept multi-notch NPR.

Figure 2.8: Difference between swept-notch and swept multi-notch NPR.

Table 2.4: Normalized IMD power at ω_n as excitation tones are switched off.

Characterization Technique	off tones	ω_1	ω_2	ω_3	ω_4	ω_5
CCPR	all on	5.625	6.750	7.125	6.750	5.625
Swept NPR	ω_1	**2.250**	3.750	4.500	4.500	3.750
Swept NPR	ω_2	3.000	**2.625**	3.750	3.375	3.375
Swept NPR	ω_3	3.375	3.375	**2.250**	3.375	3.375
Swept NPR	ω_4	3.375	3.375	3.375	**2.625**	3.000
Swept NPR	ω_5	3.750	4.500	4.500	3.750	**2.250**
Multi-Notch NPR	$\omega_2 + \omega_1$	0.350	1.125	2.250	2.625	2.250
Multi-Notch NPR	$\omega_2 + \omega_3$	1.875	0.750	0.375	1.875	1.875
Multi-Notch NPR	$\omega_2 + \omega_4$	2.250	0.000	2.625	0.000	2.250

is reinforced. Table. 2.5 lists the number of IMD products converted from 2nd-harmonic to the co-channel frequencies in a classical nonlinear dynamic system under a 5-tone excitation[19]. Note that IMD observed at nearby excitation frequencies is mostly converted from the same 2nd-harmonic IMD frequencies. Most IMD products converted to ω_2, ω_3, and ω_4 are converted from IMD frequencies between $-1\Delta f$ and $1\Delta f$ of the 2_{nd} harmonic, whereas most IMD products converted to ω_1, and ω_5 are converted from different IMD frequencies, only the IMD products converted from the 2_{nd} harmonic, 0Δf, are shared. Thus, notches in different frequency bands can introduce errors in the uncorrelated IMD measurements imposed by the dynamics observed in each frequency band. This is problematic. Alternatively, a single notch can always be narrowed so that dynamics do not vary significantly within its bandwidth.

Fig. 2.9 plots in the same graph swept NPR measurements of an Era2-+ device obtained from swept-tone NPR, swept-notch NPR, and multi-notch NPR characterization techniques[20]. As explained, the swept-tone NPR corresponds to a correct measurement of uncorrelated IMD, it is the reference NPR measurement. The swept-notch measurement is performed by sweeping a notch that occupies 10 % of the excitation bandwidth along the co-channel, as depicted in Fig. 2.8. The multi-notch measurement is performed using two notches. Each notch occupies

[19]For computation details, refer to [nprC1, Sec. II.], attached at the end of this chapter.
[20]For characterization details, refer to [nprC2, Sec. III.], attached at the end of this chapter.

Table 2.5: Number of IMD products converted to ω_q from frequencies spaced nΔf from the 2nd-harmonic.

nΔf	-4	-3	-2	-1	0	1	2	3	4
ω_1	1	2	3	4	5	0	0	0	0
ω_2	0	2	3	4	5	4	0	0	0
ω_3	0	0	3	4	5	4	3	0	0
ω_4	0	0	0	4	5	4	3	2	0
ω_5	0	0	0	0	5	4	3	2	1

5 % of the excitation bandwidth, so that the total notch bandwidth is equivalent to the swept-notch measurement. The notches are swept as depicted in Fig. 2.8. The swept-notch NPR is almost a vertically translated replica of the swept-tone NPR, with a constant error of 0.6 dB. The multi-notch NPR measurement distorts uncorrelated IMD, because it is not a vertically translated replica of the reference profile. Note that from 5.64-5.68 GHz the reference is constant and the multi-notch NPR increases monotonically.

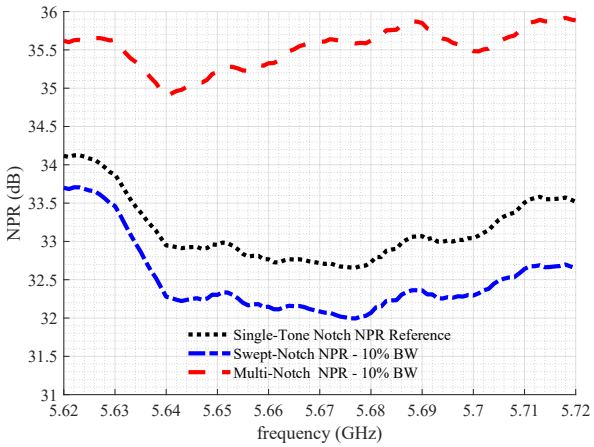

Figure 2.9: Experimental results: swept NPR vs multi-notch NPR.

In conclusion, in respect to uncorrelated IMD characterization, there is no swept-notch NPR vs multi-notch NPR trade-off. Multi-notch NPR characterization techniques corrupt uncorrelated IMD measurements, swept-notch measurements, with adequate notch bandwidth, should be used instead. And since both procedures require an equal number of measurements to fully cover the co-channel if an equivalent notch bandwidth is used, there is simply no point in using multi-notch NPR

Support Articles

"Swept Notch NPR for Linearity Assessment of Systems Presenting Long-Term Memory Effects"

Figueiredo, Piacibello, Camarchia, and Carvalho

2020 95th ARFTG Microwave Measurement Conference (ARFTG)

Swept Notch NPR for Linearity Assessment of Systems Presenting Long-Term Memory Effects

Ricardo Figueiredo*†, Anna Piacibello‡, Vittorio Camarchia‡,Nuno Borges Carvalho*†
*Universidade de Aveiro, Portugal, †Instituto de Telecomunicações, Portugal, ‡Politecnico di Torino, Italy.

***Abstract*—Mobile and Satellite applications are progressively moving towards broader bandwidths, so nonlinear long-term memory effects manifested by RF Transmitters must not be neglected. This trend evidences the need for more informative and robust broadband linearity metrics.**

This work proposes swept notch noise power ratio to capture co-channel long-term memory effects, moving the scientific discussion toward the definition of useful metrics for broadband nonlinear memory assessment.

***Index Terms*—intermodulation distortion, long-term memory effects, nonlinear, noise power ratio.**

I. Introduction

Broadband transmitters suffer from long-term memory effects that cannot be neglected. Moreover, existing linearity metrics lack robustness to guide standardization, design and to define safe operation regimes in terms of long-term memory.

Noise power ratio (NPR) is the traditional benchmark for Satellite PA linearity assessment [1], [2]. NPR characterization consists in exciting a device with a band-limited addictive white Gaussian noise (AWGN) signal with a central notch, as shown in Fig. 1, and evaluate the ratio between the output power spectral density (oPSD) within the AWGN excitation and the oPSD within the notch [3]. NPR is thus given by

$$NPR = \frac{oPSD_{AWGN}}{oPSD_{Notch}}. \quad (1)$$

In other words, NPR averages the intermodulation distortion (IMD) within the notch for a given signal oPSD. Note that this NPR definition is a narrow-band approximation, since it assumes that evaluating the IMD within the central notch provides the best approximation for the average IMD along the signal bandwidth.

Several works have studied how IMD manifests in-band [4]–[6], and it is well documented that for the memoryless case the uncorrelated IMD maximum occurs at the central excitation frequency. Thus, the use of a central notch when evaluating NPR is reasonable in a memoryless system since this tends to overestimate the average IMD. However, results shown in the aforementioned studies also indicate that in the presence of long-term memory effects the uncorrelated IMD maximum might no longer occur at the central excitation frequency. Thus, the use of NPR to assess the linearity of systems presenting long-term memory effects might be misleading, and must therefore be critically studied.

978-1-7281-0951-0/20/$31.00 ©2020 IEEE

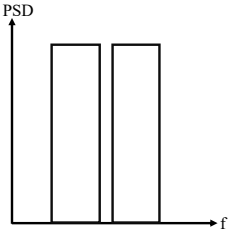

Fig. 1: Noise Power Ratio Excitation Signal.

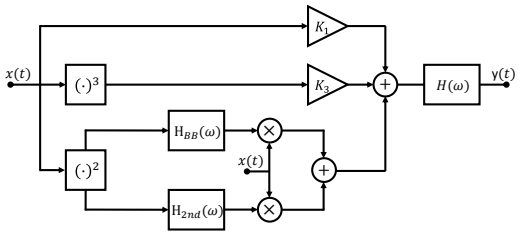

Fig. 2: Broadband RF System Model Under Study.

This work presents that study, tackling NPR linearity assessment limitations in the presence of long-term memory effects. First, we explain how different long-term memory effects can produce different co-channel IMD profiles along the signal bandwidth and how NPR might misrepresent system linearity in such scenarios. Then, we propose the swept notch NPR characterization procedure, which is capable of capturing long-term memory effects along the signal bandwidth. The novel characterization procedure is corroborated with experimental results.

II. Impacts of Long-Term Memory Effects on NPR

To exemplify how long-term memory effects can impose different co-channel IMD profiles along the signal bandwidth, a demonstrative three-slice model, based on [7] and shown in Fig. 2, is used. It is composed by a dominant linear slice, a 3_{rd} order memoryless nonlinearity and a 3_{rd} order nonlinearity with memory imposed by upconverted baseband components and downconverted 2nd harmonic components. Since we want to analyze memory effects, let's consider an operation regime where the nonlinearity with memory is dominant over the memoryless nonlinearity, i.e. IMD is mostly imposed by the 3_{rd} slice. Let's also consider that the system is excited by a multi-sine with equally spaced tones.

In such scenario, after the squarer, $(\cdot)^2$, IMD components appear at frequencies

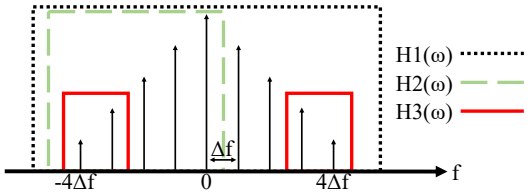

Fig. 3: IMD products near DC and 2_{nd} harmonic for a 5 tone excitation and examples of possible H_{BB} and H_{2nd} filter profiles: $H_1(\omega)$; $H_2(\omega)$; $H_3(\omega)$.

TABLE I: Number of IMD products up/down converted to ω_n from frequencies spaced $n\Delta f$ from DC and 2_{nd} Harmonic.

$n\Delta f$	-4	-3	-2	-1	0	1	2	3	4
ω_1	1	2	3	4	5	0	0	0	0
ω_2	0	2	3	4	5	4	0	0	0
ω_3	0	0	3	4	5	4	3	0	0
ω_4	0	0	0	4	5	4	3	2	0
ω_5	0	0	0	0	5	4	3	2	1

$$\omega_{2nd} = \omega_{q1} + \omega_{q2}, \tag{2}$$

where ω_{q1} and ω_{q2} can take the value of any tone frequency of the multi-sine excitation, either positive or negative. Thus, products where $sgn(\omega_{q1}) \neq sgn(\omega_{q2})$ constitute baseband IMD, while products where $sgn(\omega_{q1}) = sgn(\omega_{q2})$ constitute second harmonic IMD. Fig. 3 displays these IMD products around DC and the 2_{nd} harmonic for a 5 tone excitation.

After the $H_{BB}(\omega)$ and the $H_{2nd}(\omega)$ filters, signals are mixed with $x(t)$. This operation generates IMD at the following frequencies

$$\omega_{3rd} = \omega_{2nd} + \omega_{q3}, \tag{3}$$

where w_{q3} can take the value of any tone frequency of the multi-sine excitation, either positive or negative. Thus, some baseband IMD is up-converted to the co-channel, while some 2_{nd} harmonic IMD is down-converted. However, the number of IMD products converted to each excitation tone depends on the separation from either DC or the 2_{nd} harmonic of the IMD products shown in Fig. 3. This dependence is listed in Table I for a 5 tone excitation. As shown, more products overlap near the central frequency, ω_3, as expected in a memoryless system.

After laying this out, it is easy to understand how the memory introduced by filters $H_{BB}(\omega)$ and $H_{2nd}(\omega)$ can affect differently the co-channel IMD. If both filters have the profile of $H_1(\omega)$ in Fig. 3, co-channel IMD is not affected and presents a memoryless-like profile. However, if both filters have the profile of $H_3(\omega)$ in Fig. 3, only products spaced $\pm 3\Delta f$ and $\pm 4\Delta f$ from DC or the 2_{nd} harmonic are converted to the co-channel, meaning that no IMD products fall on ω_3, generating a central IMD minimum. On the other hand, if $H_{BB}(\omega)$ has the profile of $H_3(\omega)$ in Fig. 3 and $H_{2nd}(\omega)$ has the profile of $H_2(\omega)$ in Fig. 3, the number of IMD products monotonically decreases from ω_1 to ω_5. To illustrate these ideas a 101-tone excitation, replicating AWGN, with 1 MHz bandwidth at a carrier of 3 MHz is used to excite the system in Fig. 2. $H_{BB}(\omega)$ and $H_{2nd}(\omega)$ are designed using the principles previously described. Fig. 4 shows both the signal oPSD and the uncorrelated co-channel IMD obtained through simulation.

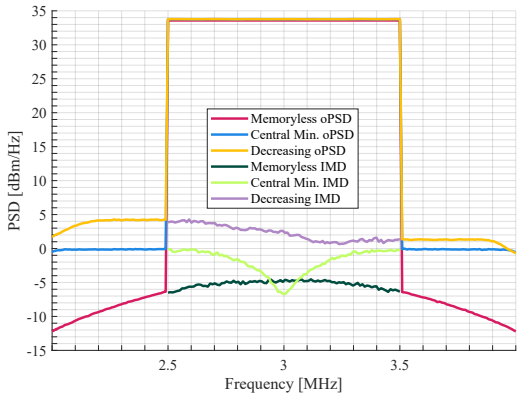

Fig. 4: Simulation results of the output PSDs and co-channel distortion PSD for each scenario described.

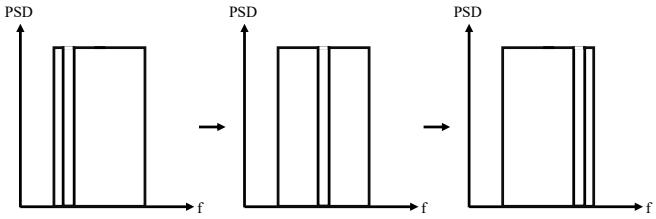

Fig. 5: Swept Notch NPR Excitation Concept.

What is important to retain from this demonstrative analysis is that a classical NPR characterization procedure is unable to detect co-channel IMD variations due to long-term memory effects, like the decreasing IMD shown in Fig. 4; and that in some cases, like the central minimum co-channel IMD scenario portrayed in Fig. 4, a classical NPR characterization can critically underestimate IMD. Thus, better broadband linearity metrics are required.

III. Swept Notch NPR

A. Concept

The Swept Notch NPR concept consists in performing several NPR characterizations in which the notch is swept along the co-channel, as shown in Fig. 5, instead of performing a single measurement with a central notch.

The premise is that by doing this it is not only possible to determine the best co-channel frequency to evaluate the average co-channel IMD, as it is also possible to detect co-channel IMD variations due to long-term memory effects.

Fig. 6 presents the swept notch NPR simulation results for each scenario displayed in Fig. 4. Each "step" on the graph corresponds to a NPR measurement performed within the notch located in that co-channel frequency region. The notch used occupies 5% of the co-channel. As shown, swept notch NPR is capable of characterizing long-term memory effects

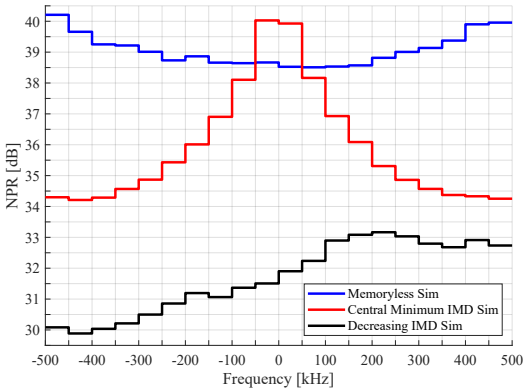

Fig. 6: Simulated swept notch NPR of each described scenario.

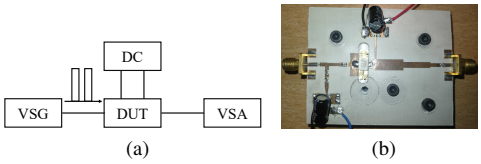

Fig. 7: NPR Characterization: (a) Setup; (b) Device under test (DUT).

along the co-channel, as it captures the inverted trend of IMD. Once again, this graph shows the ineptitude of classical NPR characterization to evaluate IMD in caricature scenarios like the central minimum IMD, where it would underestimate the maximum IMD by 6 dB.

B. Experimental Validation

To validate the swept notch NPR proposal, this characterization procedure was tested experimentally. The setup, presented in Fig. 7a, consists in a R&S SMW200A VSG to generate the excitation signal and a R&S FSW VSA to measure the device under test (DUT) output signal. A 1001-tone excitation, replicating AWGN, with -10 dBm average power is used. The notch occupies 5% of the co-channel. Two DUTs are tested, the GaN PA shown in Fig. 7b biased near class B, and an ERA-2+ PA from mini-circuits. The GaN PA is excited with a 100 MHz signal at both 2.6 GHz and 3.5 GHz, while the ERA-2+ is excited with a 50 MHz signal at 5.67GHz. Fig. 8 presents the swept notch NPR measurement of the ERA-2+, while Fig. 9 presents the measurements of the GaN PA.

The ERA-2+ NPR varies around 18.4 dB and the swept notch NPR profile along the co-channel strongly indicates a memoryless behaviour, since NPR tends to improve toward the edges of the co-channel and to degrade toward the center, as observed in the memoryless case simulations presented in Fig. 6, and as theoretically explained in II.

The GaN PA NPR varies around 37.5 dB. The NPR profile along the co-channel at 3.5 GHz also tends to indicate a memoryless behaviour, but some asymmetry about the central frequency is observed between lower and upper frequencies in the co-channel, which might be due to long-term memory ef-

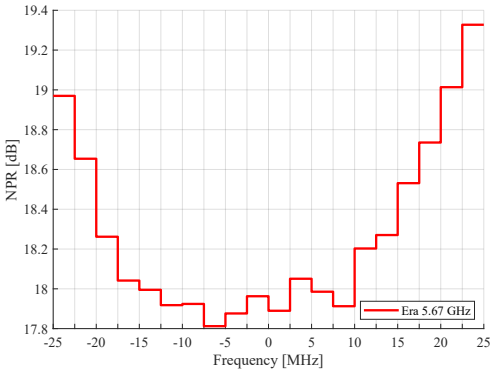

Fig. 8: Measured swept notch NPR of the ERA-2+ DUT at 5.67 GHz.

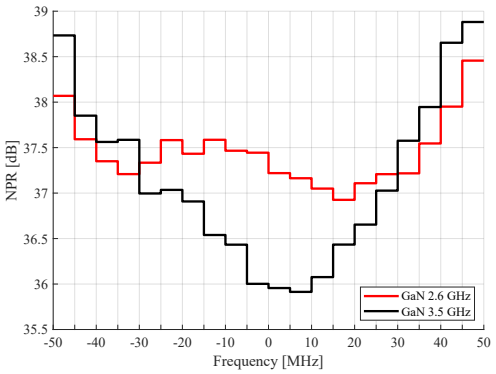

Fig. 9: Measured swept notch NPR of the GaN DUT at 2.6 GHz and 3.5 GHz.

fects. On the other hand, the NPR profile along the co-channel at 2.6 GHz clearly deviates from the memoryless profile, as NPR oscillates around 37 dB and 37.5 dB between -45 MHz and 40 MHz, indicating more strongly the manifestation of long-term memory effects. Such profile is distinct from those simulated and shown in Fig. 6, meaning that the memory mechanisms of this GaN PA DUT probably differ from those described in the multi-slice model for conceptualization.

Note that although we cannot guarantee the co-channel IMD variations observed are only due to long-term memory effects, these results validate the ability of swept notch NPR to capture both co-channel IMD profiles that resemble the memoryless profile, and that differ from the memoryless profile, and thus the ability of swept notch NPR to characterize co-channel IMD profile variations due to long-term memory effects.

IV. Conclusion

This work evidences the limitations of NPR to assess linearity in the presence of long-term memory effects.

To overcome such limitations, a swept notch NPR characterization procedure to detect the impacts of long-term memory effects on co-channel IMD was proposed and validated.

Further work is required to transform swept notch NPR in a quantifiable memory metric capable of extracting useful long-

term memory effect models. But swept notch NPR is already an initial step toward more robust and informative broadband linearity metrics.

ACKNOWLEDGMENT

The work of Ricardo Figueiredo was supported by the Fundação para a Ciência e Tecnologia (F.C.T.) under Ph.D. Grant SFRH/BD/146935/2019.

This work is supported by the European Regional Development Fund (FEDER), through the Regional Operational Programme of Lisbon (POR LISBOA 2020) and the Competitiveness and Internationalization Operational Programme (COMPETE 2020) of the Portugal 2020 framework [Project INFANTE with Nr. 024534 (POCI-01-0247-FEDER-024534)]

REFERENCES

[1] G. Lasser, M. R. Duffy, and Z. Popović, "Dynamic dual-gate bias modulation for linearization of a high-efficiency multistage pa," *IEEE Transactions on Microwave Theory and Techniques*, 2019.

[2] S. Din, A. M. Morishita, N. Yamamoto, C. Brown, M. Wojtowicz, and M. Siddiqui, "High-power k-band gan pa mmics and module for npr and pae," in *2017 IEEE MTT-S International Microwave Symposium (IMS)*. IEEE, 2017, pp. 1838–1841.

[3] J. C. Pedro and N. B. Carvalho, *Intermodulation distortion in microwave and wireless circuits*. Artech House, 2003.

[4] J. P. Martins and N. B. Carvalho, "Co-channel and adjacent channel distortion in microwave amplifiers presenting memory," in *2007 European Microwave Conference*. IEEE, 2007, pp. 40–43.

[5] J. P. Martins, N. B. Carvalho, and J. C. Pedro, "Intermodulation distortion of third-order nonlinear systems with memory under multisine excitations," *IEEE transactions on microwave theory and techniques*, vol. 55, no. 6, pp. 1264–1271, 2007.

[6] S. Farsi, P. Draxler, H. Gheidi, B. K. Nauwelaers, P. Asbeck, and D. Schreurs, "Characterization of intermodulation and memory effects using offset multisine excitation," *IEEE Transactions on Microwave Theory and Techniques*, vol. 62, no. 3, pp. 645–657, 2014.

[7] A. Walker, M. Steer, K. Gard, and K. Gharaibeh, "Multi-slice behavioral model of rf systems and devices," in *2004 IEEE Radio and Wireless Conference*. IEEE, 2004, pp. 71–74.

"Issues of Multi-Notch NPR Characterization Procedures"

Figueiredo and Carvalho

2021 97th ARFTG Microwave Measurement Conference (ARFTG)

Issues of Multi-Notch NPR Characterization Procedures

Ricardo Figueiredo*†, Nuno Borges Carvalho*†
*DETI, Universidade de Aveiro, Portugal, †Instituto de Telecomunicações, Aveiro, Portugal.

***Abstract*—This work exposes limitations of multi-notch NPR, which have been neglected, that make experimental results hard to compare with classic NPR measurements. In fact, it demonstrates, theoretically and experimentally, how swept-notch NPR is a better linearity metric than multi-notch NPR, particularly in the presence of nonlinear dynamic effects. This calls for the replacement of multi-notch NPR by swept-notch NPR.**

***Index Terms*—characterization, intermodulation distortion, linearity, memory effects, noise power ratio, nonlinear distortion.**

I. Introduction

Noise power ratio (NPR) is a central linearity metric in modern RF communications. It is the linearity criterion for satellite applications [1], and the establishment of an identity between NPR and error vector magnitude (EVM) makes it a consistent metric in several levels of analysis [2], [3], increasing the NPR relevance for mobile and wireless applications.

As these technologies occupy larger instantaneous bandwidths, and nonlinear dynamic effects become non-negligible, the classical NPR procedure has to be adjusted. In such scenarios, multi-notch NPR is an approach that has been followed both by the scientific community and industry [3]–[5]. However, multi-notch NPR measurements are difficult to compare with results obtained using the classical procedure [4]. Beyond this, in the presence of long-term memory effects, iterative procedures, highly based on experimental heuristics, are required to obtain consistent results [3].

This work revisits the fundamental issues of NPR - [6]–[8] - to explain how multi-notch NPR differs from classical NPR characterization, whereas swept-notch NPR is compatible with classical NPR. This work also evidences why swept-notch NPR is the preferred characterization method in the presence of nonlinear dynamic effects [9]. The presented theoretical analysis is supported by experimental validation.

II. Issues of Multi-Notch NPR

A. Problem Statement

The discussion on the fundamental issues of NPR started with the claim that NPR is an optimistic linearity metric, because it does not capture correlated intermodulation distortion (IMD) [6], [7]. This claim was answered [8], noting that in most applications input power levels remain constant. Under such conditions, correlated IMD is desired signal, and only uncorrelated IMD should be considered signal distortion. Thus, uncorrelated IMD can be gauged at a given excitation frequency, ω_{q}, by switching-off that excitation frequency. This corresponds to the classic NPR procedure. In [8], it was also noted that the notch can be placed in any frequency band to measure uncorrelated IMD, and thus evaluate NPR. However, it did not address the fact that switching-off ω_{q} does not only eliminate correlated IMD at ω_{q}, it also eliminates uncorrelated IMD power that is present in other frequency bands under the full-spectrum excitation. This is an important reason why multi-notch NPR is often not comparable with classic NPR. In [4], it was experimentally observed that in multi-notch measurements uncorrelated IMD power is dependent on notch location, and dependent on the type of excitation signal. No theoretical explanation was provided for this, but it was stated that a multi-notch method with randomly spread notch locations is more consistent.

978-0-7381-1249-7/21/$31.00

B. Problem Analysis

To evidence the implications of multi-notch NPR, lets consider a 3rd-order memoryless system, as assumed in prior art [6]–[8]. For such systems, the full IMD response under multi-tone excitation can be computed from (1).

$$y_{NL_3}(t) = \frac{1}{2^3} a_3 \left[\sum_{\substack{q=-Q \\ q\neq 0}}^{Q} A \cdot e^{j(\omega_q t + \phi_q)} \right]^3 \tag{1}$$

For the sake of exemplification, lets consider that this system is under a 5-tone excitation. This excitation is not a practical NPR characterization signal. Nonetheless, the analysis of this simple example highlights behaviors observed in practice in a comprehensive manner. This evidences the problem under study, and provides ideas for possible solutions. Also, assume that $\mathrm{A} = \mathrm{a}_3 = 1$.

Table. I provides the IMD weight observed at each co-channel frequency, ω_1 to ω_5, when the excitation tones listed in the first column are switched-off. For example, the last row lists the IMD weight observed at each excitation frequency, ω_1 to ω_5, when both ω_1 and ω_3 tones are switched-off.

TABLE I: IMD at ω_{n} as excitation tones are switched off.

off tones	ω_1	ω_2	ω_3	ω_4	ω_5
all on	5.625	6.750	7.125	6.750	5.625
ω_1	**2.250**	3.750	4.500	4.500	3.750
ω_2	3.000	**2.625**	3.750	3.375	3.375
ω_3	3.375	3.375	**2.250**	3.375	3.375
ω_4	3.375	3.375	3.375	**2.625**	3.000
ω_5	3.750	4.500	4.500	3.750	**2.250**
$\omega_2 + \omega_1$	0.350	1.125	2.250	2.625	2.250
$\omega_2 + \omega_3$	1.875	0.750	0.375	1.875	1.875
$\omega_2 + \omega_4$	2.250	0.000	2.625	0.000	2.250
$\omega_1 + \omega_3$	0.750	1.875	1.125	1.875	1.875

The row in which all tones are switched-on lists the full IMD weight, i.e. it contemplates both correlated and uncorrelated IMD, as evaluated by CCPR [7].

The rows in which only one tone is switched-off, corresponding to a classical NPR characterization, list the correct evaluation of uncorrelated IMD weight at the switched-off tone, highlighted in bold. This is the uncorrelated IMD weight under full-spectrum excitation. These rows also evidence that performing a classical NPR characterization affects IMD in other frequency bands. In fact, such artifacts, even though not directly addressed at the time, are observable in the experimental NPR results disclosed in [7]. Furthermore, note that neaby tones are the most influenced, in terms of IMD power reduction, when switching-off a single tone, as expected [10].

The rows in which two tones are switched-off represent the multi-notch NPR characterization. By analyzing the rows in which ω_2 is off, it is perceptible that uncorrelated IMD weight at ω_2 is highly dependent on which other tone is also switched-off. Similar theoretical analysis has already been noted in [6] for a 3-tone excitation, but this notion was somehow forgotten in the scope of multi-notch NPR. When ω_1 and ω_2 are off, the uncorrelated IMD weight at ω_2 is reduced by $57\ \%$. When ω_3 and ω_2 are off, the uncorrelated IMD weight at ω_2 is reduced by $71\ \%$. When ω_4 and ω_2 are off, the uncorrelated IMD weight at ω_2 is reduced by $100\ \%$. Note that in multi-notch characterization, the scenario with the highest impact on the uncorrelated IMD measure is not necessarily the scenario in which nearby frequencies are switched-off. If uncorrelated IMD at ω_1 and ω_3 is obtained from the last row computation, it can be concluded that uncorrelated IMD is lower at ω_1, thus it is higher at ω_3. However, single off-tone measures, which provide the correct IMD weight under full-spectrum excitation, indicate that uncorrelated IMD is equal at these frequencies. These are just some examples that demonstrate how multi-notch NPR measurements corrupt full-spectrum uncorrelated IMD evaluation, even for memoryless scenarios. Such theoretical examples explain the difficulties in obtaining equivalent NPR metrics from multi-notch NPR and classic NPR procedures reported in [4].

In truth, for a memoryless scenario there is no need for multi-notch, nor swept-notch measurements. It is well-known that memoryless NPR is maximum at the band extremes, minimum at the central frequency, and that it follows a parabolic shape throughout the co-channel [6], [9]. Nonetheless, it is important to mention that in this scenario a swept-notch NPR characterization, performed with a sufficiently narrow notch, is guaranteed to capture the correct uncorrelated IMD trend under full-spectrum excitation, whereas the same cannot be guaranteed for every possible multi-notch NPR characterization, performed with an equivalent total notch bandwidth.

In a nonlinear dynamic scenario it is easy to show that switching-off nearby tones is preferable. Table. II recalls the number of IMD products converted from DC and 2_{nd} harmonic to the co-channel in a typical nonlinear dynamic system under a 5-tone excitation, as was first presented in [9].

As shown, IMD observed at nearby excitation frequencies is mostly converted from the same IMD frequencies. Most IMD products converted from the 2_{nd} harmonic to ω_2, ω_3, and ω_4 are converted from the same IMD frequencies, whereas most IMD products converted from the 2_{nd} harmonic to ω_1, and ω_5 are converted from different IMD frequencies (only $0\Delta\mathrm{f}$ products are shared). Thus, multiple notches in different bands can always introduce errors in the uncorrelated IMD evaluation if they are affected by different dynamics, whereas it is always possible to narrow a single notch so that dynamics do not vary significantly within it. This is very problematic for multi-notch approaches, particularly because existing methods work best for larger notch bandwidths [3], which impose a larger interference. Therefore, it is preferred to sweep a single notch when evaluating NPR in the presence of nonlinear dynamics.

TABLE II: Number of IMD products up/down converted to ω_{q} from frequencies spaced $\mathrm{n}\Delta\mathrm{f}$ from DC and 2_{nd} harmonic.

$\mathrm{n}\Delta\mathrm{f}$	-4	-3	-2	-1	0	1	2	3	4
ω_1	1	2	3	4	5	0	0	0	0
ω_2	0	2	3	4	5	4	0	0	0
ω_3	0	0	3	4	5	4	3	0	0
ω_4	0	0	0	4	5	4	3	2	0
ω_5	0	0	0	0	5	4	3	2	1

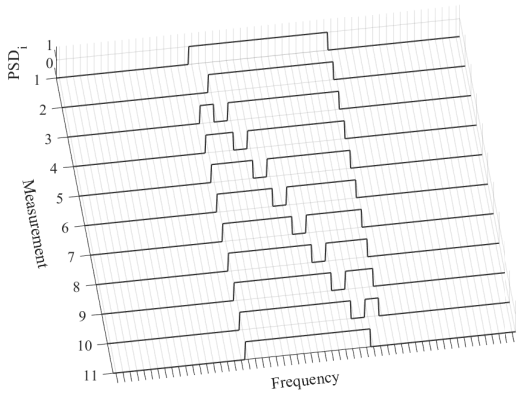

Fig. 1: Swept-Notch NPR characterization procedure.

III. Experimental Validation

A. Validation Experiments

Three experiments are carried out to verify that swept-notch NPR is a preferred characterization technique over multi-notch NPR, as theoretically explained in II. First, NPR measurements in which a single-tone is switched-off are performed, covering all co-channel frequencies, to obtain the correct uncorrelated IMD response under full-spectrum excitation. Then, a swept-notch NPR characterization, with $10\ \%$ notch bandwidth, is done as depicted in Fig. 1. Finally, a multi-notch NPR characterization, with $10\ \%$ total notch bandwidth, is carried out as depicted in Fig. 2. At last, the swept-notch NPR, and multi-notch NPR are compared with the reference NPR to validate which approach provides better results.

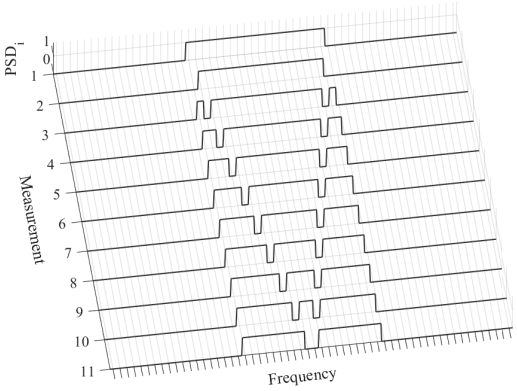

Fig. 2: Multi-Notch NPR characterization procedure.

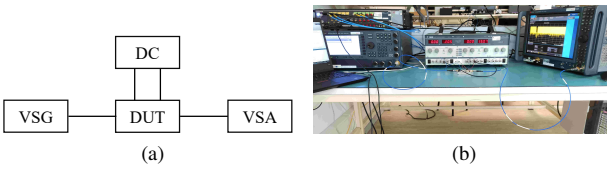

Fig. 3: Experimental Setup: (a) Schematic; (b) Picture.

B. Full-Spectrum Excitation

The input full-spectrum signal used is a 101-tone excitation, designed to resemble band-limited additive white Gaussian noise. This is a typical NPR characterization signal [11]. During the experiments, signal power and signal bandwidth were fixed at -10 dBm and 100 MHz, respectively.

C. Devices Under Test

Two devices were characterized: an Era-2+ [12], which is a mostly memoryless device, and a ZVA-213-S+ [13], which is a wideband amplifier likely to manifest nonlinear dynamic effects. The Era-2+ board operates from 5.55 GHz to 5.75 GHz, having a $P_{1\text{dB}}$ of 11 dBm. It is biased with 8.4 V, consuming 50 mA. When excited at 5.67 GHz, it outputs an average envelope power of 1 dBm. The ZVA-213-S+ operates from 800 MHz to 21 GHz, having a $P_{1\text{dB}}$ of 24 dBm. It is biased with 12 V, consuming 340 mA. When excited at 18 GHz, it outputs an average envelope power of 15.6 dBm.

D. Experimental Setup

The experimental bench is depicted in Fig. 3. The VSG is composed by a Keysight M8190A AWG and a Keysight E8361C PSG. The AWG generates the input waveform, and the PSG up-converts it to the desired carrier frequency, while controlling the envelope signal power. The Keysight N9041B UXA VSA captures the output waveform. The DC supply is a TTI PL330DP. This bench is calibrated to capture the desired waveform synchronously at the output port.

E. Experimental Result Analysis

The Era-2+ and ZVA-213-S+ output power spectral density (PSD) under full-spectrum excitation, and co-channel uncorrelated IMD response for each experiment are depicted in Fig. 4 and Fig. 5, respectively. What is most noticeable is that multi-notch NPR significantly underestimates uncorrelated IMD for both devices, whereas the swept-notch NPR uncorrelated IMD measurement is mostly overlapped with the single-tone reference. The NPR curve analysis throughout the band provides more details, and further insight into the problem at hand.

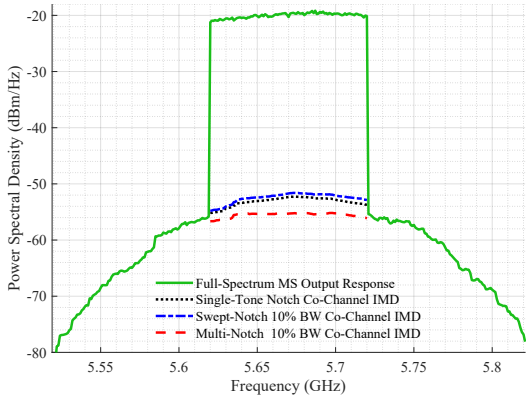

Fig. 4: Era-2+ - Full-Spectrum PSD response, and co-channel uncorrelated IMD obtained from each experiment.

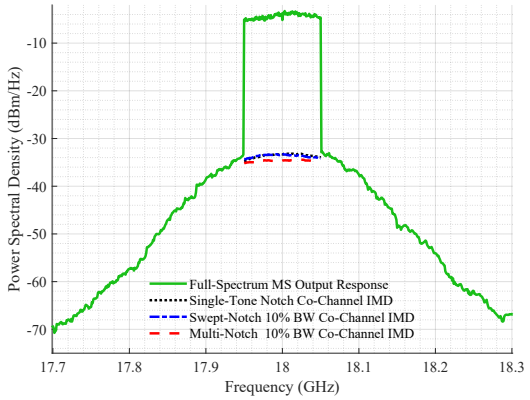

Fig. 5: ZVA-213-S+ - Full-Spectrum PSD response, and co-channel uncorrelated IMD obtained from each experiment.

Fig. 6 depicts the Era2-+ NPR profiles. The reference NPR ranges between 32.7-34.1 dB throughout the band. It is roughly memoryless, since NPR is higher at the band edges, minimum at the central frequency, and the profile resembles a parabolic shape. The multi-notch NPR ranges between 35-36 dB. Throughout the band, the minimum error in relation to the reference is 1.5 dB, the maximum error is 3 dB, and the average error is 2 dB. The NPR profile is distorted, because it is not a vertically translated replica of the reference profile. Note that from 5.64-5.68 GHz the reference is constant and the multi-notch NPR increases monotonically. This portrays how multi-notch NPR can corrupt the uncorrelated IMD distribution in relation to the full-spectrum excitation. The swept-notch NPR ranges between 32-33.7 dB. It is mostly a vertically translated replica of the reference profile, with a constant error of 0.6 dB. This means swept-notch NPR

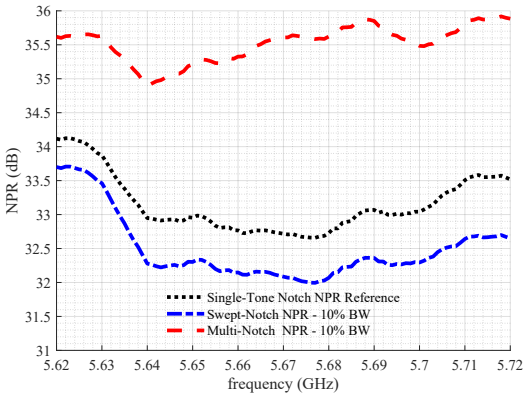

Fig. 6: Era-2+ - results from NPR experiments.

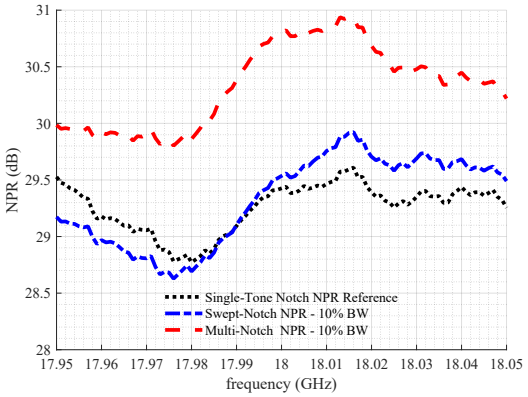

Fig. 7: ZVA-213-S+ - results from NPR experiments.

preserves the uncorrelated IMD distribution in relation to the full-spectrum excitation.

Fig. 7 depicts the ZVA-213-S+ NPR profiles. The reference NPR ranges between 28.8-29.6 dB throughout the band. The profile indicates dynamic behavior: it decreases from 17.95-17.98 GHz, increases from 17.98-18 GHz, and is constant from 18-18.05 GHz. This is not the memoryless parabolic profile. The multi-notch NPR ranges between 30-31 dB. Throughout the band, the minimum error in relation to the reference is 0.4 dB, the maximum error is 1.4 dB, and the average error is 1 dB. In this case, only a slight shape distortion is observed between 17.95-17.98 GHz, where NPR is constant, instead of decreasing. Apart from this, the NPR profile is mostly a vertically translated replica of the reference. The swept-notch NPR ranges between 28.7-29.9 dB, having a maximum error of 0.4 dB in relation to the reference. This profile is almost overlapped with the reference. For this device, the multi-notch NPR scheme used preserves the correct NPR profile, for the most part. Nonetheless, the swept-notch NPR metric is better, overlapping with the reference.

Overall, it was observed that for the scenarios tested, swept-notch NPR always provided better NPR metrics than multi-notch NPR, i.e. the NPR metric is closer to the reference NPR correspondent to the uncorrelated IMD power present in the full-spectrum excitation. This agrees with and validates the theoretical predictions presented in II. As both procedures require an equal number of measurements to fully cover the co-channel, there is no point in using multi-notch NPR.

IV. Conclusion

This work provided theoretical and experimental proofs to demonstrate that swept-notch NPR obtains better linearity metrics than multi-notch NPR. This is an important contribution to consider for future research, and industry standards that aim to use NPR as a linearity metric. Swept-notch NPR is a characterization technique that provides the required robustness to assess linearity in the presence of nonlinear dynamic effects. Nonetheless, remember that classic NPR procedures are typically sufficient for memoryless systems.

Acknowledgment

The work of Ricardo Figueiredo was supported by the Fundação para a Ciência e Tecnologia (F.C.T.) under Ph.D. Grant SFRH/BD/146935/2019.

References

[1] C. Boulanger, A. Mallet, J. Puech, L. Lapierre, and J. Sombrin, "A new criterion for power amplifier comparison and optimisation," in *IEE Seminar on Microwave and RF Power Amplifiers (Ref. No. 2000/118)*. IET, 2000, pp. 1–1.

[2] J. B. Sombrin, "On the formal identity of evm and npr measurement methods: Conditions for identity of error vector magnitude and noise power ratio," in *2011 41st European Microwave Conference*. IEEE, 2011, pp. 337–340.

[3] K. Freiberger, H. Enzinger, and C. Vogel, "A noise power ratio measurement method for accurate estimation of the error vector magnitude," *IEEE Transactions on Microwave Theory and Techniques*, vol. 65, no. 5, pp. 1632–1645, 2017.

[4] E. Van Nechel, Y. Rolain, and J. Lataire, "Extracting improved figures of merit for characterizing nonlinear devices using multisine excitation signals," in *2018 91st ARFTG Microwave Measurement Conference (ARFTG)*. IEEE, 2018, pp. 1–4.

[5] R. . Schwarz. (2016) Noise power ratio signal generation and measurement. [Online]. Available: https://www.rohde-schwarz.com/us/applications/npr-application-note_56280-15651.html

[6] J. C. Pedro and N. B. De Carvalho, "On the use of multitone techniques for assessing rf components' intermodulation distortion," *IEEE Transactions on Microwave Theory and Techniques*, vol. 47, no. 12, pp. 2393–2402, 1999.

[7] J. C. Pedro and N. B. de Carvalho, "Characterizing nonlinear rf circuits for their in-band signal distortion," *IEEE Transactions on Instrumentation and Measurement*, vol. 51, no. 3, pp. 420–426, 2002.

[8] A. Geens, Y. Rolain, W. Van Moer, K. Vanhoenacker, and J. Schoukens, "Discussion on fundamental issues of npr measurements," *IEEE Transactions on Instrumentation and Measurement*, vol. 52, no. 1, pp. 197–202, 2003.

[9] R. Figueiredo, A. Piacibello, V. Camarchia, and N. B. Carvalho, "Swept notch npr for linearity assessment of systems presenting long-term memory effects," in *2020 95th ARFTG Microwave Measurement Conference (ARFTG)*, 2020, pp. 1–4.

[10] N. B. De Carvalho and J. C. Pedro, "A comprehensive explanation of distortion sideband asymmetries," *IEEE Transactions on Microwave Theory and Techniques*, vol. 50, no. 9, pp. 2090–2101, 2002.

[11] T. Reveyrand, D. Barataud, J. Lajoinie, M. Campovecchio, J.-M. Nebus, E. Ngoya, J. Sombrin, and D. Roques, "A novel experimental noise power ratio characterization method for multicarrier microwave power amplifiers," in *55th ARFTG Conference Digest*, vol. 37. IEEE, 2000, pp. 1–5.

[12] Mini-Circuits. (2021) Drop-in monolithic amplifier. [Online]. Available: https://www.minicircuits.com/pdfs/ERA-2+.pdf

[13] ——. (2021) Super ultra wideband amplifier. [Online]. Available: https://www.minicircuits.com/pdfs/ZVA-213-S+.pdf

"Nonlinear Dynamic RF System Characterization: Envelope Intermodulation Distortion Profiles—A Noise Power Ratio-Based Approach"

Figueiredo, Carvalho, Piacibello, and Camarchia

IEEE Transactions on Microwave Theory and Techniques

Nonlinear Dynamic RF System Characterization: Envelope Intermodulation Distortion Profiles, a Noise Power Ratio Based Approach

Ricardo Figueiredo , *Graduate Student Member, IEEE*, Nuno Carvalho, *Fellow, IEEE*, Anna Piacibello, *Member, IEEE*, and Vittorio Camarchia, *Senior Member, IEEE*

***Abstract*—As radio-frequency (RF) applications occupy larger bandwidths, nonlinear dynamics become non-negligible. This work presents a theoretical framework capable of quantifying the impacts of nonlinear dynamic effects on RF systems through the observation of intermodulation distortion (IMD) profiles produced under multi-tone excitation. This framework defines static reference profiles, and quantifies inband nonlinear dynamic effects as the error between measured and reference profiles. This analysis demonstrates that classic linearity metrics, such as noise power ratio (NPR), adjacent channel power ratio, and co-channel power ratio do not have sufficient frequency resolution to reliably evaluate the impacts of nonlinear dynamics manifested in the IMD profiles produced by broadband RF systems. These observations result in a list of general characterization guidelines to overcome the limitations of classical linearity metrics in the assessment of nonlinear dynamics, and in the proposal and experimental validation of a novel method, swept-tone NPR, for the characterization of IMD profiles affected by nonlinear dynamic effects. Beyond this, the classic nonlinear dynamic mechanism, responsible for IMD asymmetry, is analyzed under multi-tone excitation at the system-level for the first time, and the limitations of mechanism based IMD analysis in the presence of nonlinear dynamic effects are evidenced with theoretical examples.**

***Index Terms*—Characterization, intermodulation distortion, memory effects, multitone excitation, noise power ratio.**

I. Introduction

MODERN radio-frequency (RF) communication systems, namely mobile and satellite applications, are occupying ever broader bandwidths and moving to higher frequency bands. This trend raises novel intermodulation distortion (IMD) characterization challenges, because nonlinear dynamic effects can no longer be neglected, thus the definition of appropriate IMD characterization techniques, and appropriate linearity metrics, becomes an increasingly complex problem. In the context of satellite applications, noise power ratio (NPR) has already been defined as the linearity criterion [1], [2], [3]. Beyond this, the establishment of an identity between NPR and error vector magnitude (EVM) [4], [5], [6], [7] makes NPR a consistent linearity metric in several levels of analysis, which is an indicator of its potential relevance for mobile applications as they move towards broader bandwidths. However, despite of the NPR inherent potential and initial hopes of its application in domains such as design optimization, behavioral modeling, memory effect characterization, and predistortion [2], [8], [9], it continues to be mostly used as a final design validation metric [10], [11], whereas simpler linearity metrics continue to be preferred for the aforementioned tasks.

Recently, it was demonstrated that unequally spaced multi-tone load-pull characterization techniques can be effectively used to guide power amplifier design trade-offs [12], [13]. This technique is compatible with classical NPR characterization in narrowband memoryless scenarios [14].

This was an important step towards the adoption of appropriate characterization techniques and appropriate linearity metrics in modern RF system design, as well as the development of novel instrumentation techniques that enable coherent vector signal analysis and facilitate the fast evaluation of NPR in modern equipment [15]. However, in the authors' opinion there are three major factors preventing the generalized use of NPR: 1) studies addressing NPR characterization often assume static nonlinearities [7], [16], considering only linear dynamic effects; 2) there is a lack of insight of how nonlinear dynamic effects can manifest in the IMD response under broadband excitation; 3) nonlinear dynamic effects imply a frequency dependent IMD response, but the cumulative nature of classic linearity metrics [17], such as NPR, adjacent channel power ratio (ACPR), and co-channel power ratio (CCPR) hide the frequency dependence of the IMD response. There is therefore a need to better understand how nonlinear dynamic effects manifest under broadband excitation, and to understand how to define linearity metrics to capture them.

The work presented in [18] was an important step towards the understanding of nonlinear dynamics in RF systems, as it

Manuscript received February 8, 2021; revised April 225, 2021; accepted May 16, 2021. Date of publication Month Day, Year; date of current version Month Day, Year. This work is funded by FCT/MCTES through national funds and when applicable co-funded EU funds under the project UIDB/50008/2020-UIDP/50008/2020. The work of Ricardo Figueiredo was supported by FCT and EU through FSE and Programa Operacional Regional Centro under Ph.D. Grant SFRH/BD/146935/2019. *(Corresponding author: Ricardo Figueiredo.)*

Ricardo Figueiredo, and Nuno Carvalho are with the Departamento de Eletrónica, Telecomunicações e Informática, Instituto de Telecomunicações, Universidade de Aveiro, Campus Universitário de Santiago, 3810-193 Aveiro, Portugal (e-mail: ricardofigueiredo@ua.pt; nbcarvalho@ua.pt).

Anna Piacibello is with the is with the Department of Electronics and Telecommunications, Politecnico di Torino, 10129 Turin, Italy, and also with the Microwave Engineering Center for Space Applications (MECSA), 00133 Rome, Italy (e-mail: anna.piacibello@polito.it).

Vittorio Camarchia is with the Department of Electronics and Telecommunications, Politecnico di Torino, 10129 Turin, Italy (e-mail: vittorio.camarchia@polito.it).

Color versions of one or more of the figures in this article are available online at https://ieeexplore.ieee.org.

Digital Object Identifier

explains how memory effects can manifest through adjacent channel asymmetry observations. However, this explanation is presented in a circuit-level perspective that is hard to carry over to the system-level. Beyond this, the focus of the analysis is mostly on 2-tone characterization, while not expanding on the multi-tone scenario in a comprehensive manner. The work is also too tightly bound to specific third-order nonlinear dynamic mechanisms.

In [19], the multi-tone scenario is addressed, establishing a relationship between 2-tone and multi-tone measurements. This allowed the developments presented in [18] to be applied to compute multi-tone responses of nonlinear dynamic RF systems. The work presents a qualitative analysis of nonlinear dynamic effects, stating that these effects can be noted in the shape of distortion components, but a quantitative analysis is missing. The evaluation of IMD is done using ACPR and CCPR, which hide the frequency dependence of the IMD response. Beyond this, the nonlinear dynamic effect explanation remains at the circuit-level, despite the study being developed at the system-level, and the work remains too tightly bound to specific third-order nonlinear dynamic mechanisms. Furthermore, the use of 2-tone characterization is ultimately more laborious than multi-tone characterization, and has critical limitations regarding signal statistics, frequency domain resolution, and sensitivity.

These limitations of 2-tone characterization strategies have already been addressed in [20]. In that study an offset multi-sine strategy is proposed to characterize nonlinear dynamic RF systems. Offset multi-sines have the advantage of allowing for separate characterization of co-channel IMD distortion, and separate characterization of each nonlinear order, but the disadvantage of scalability as bandwidth, number of tones, and nonlinear order increase. In [20], a qualitative detection of nonlinear dynamic effects is observed through IMD spectral response variation as decoupling capacitors are adjusted, but an insightful analysis is missing.

In a previous work [21], we have already exposed the limitations of classic NPR characterization techniques to capture nonlinear dynamic effects within the system co-channel, and proposed a novel characterization procedure to overcome those limitations. However, despite insightful, this work lacks a formal representation of the IMD mechanisms, and a quantitative analysis of the proposed linearity metric.

In this work we:

1) Present a theoretical framework capable of analyzing IMD profiles produced under multi-tone excitation and detecting the impacts of nonlinear dynamic effects in a quantitative manner;
2) Analyze the classic nonlinear dynamic mechanism responsible for IMD asymmetry, presented in [18], under multi-tone excitation at the system-level for the first time;
3) Further expose the limitations of classic characterization techniques, and linearity metrics, to evaluate the IMD profiles affected by nonlinear dynamics;
4) Explain the limitations of mechanism based IMD analysis in the presence of nonlinear dynamic effects;
5) Detail general characterization guidelines for a reliable evaluation of dynamic IMD profiles, produced by nonlinear dynamic RF systems;
6) Propose a novel characterization method, swept-tone NPR, for the characterization of IMD profiles affected by nonlinear dynamic effects, and validate it experimentally.

This work is organized as follows. Section II presents the theoretical framework. Section III uses this framework to analyze the classic nonlinear dynamic mechanism at the system-level. Section IV analyzes three numerical dynamic IMD profile examples produced by the classic mechanism. The analysis focuses on the importance of defining reference responses, and on the limitations of classical linearity metrics. Section V addresses the limitations of mechanism based IMD analysis in the presence of nonlinear dynamic effects. Section VI discusses the implications of this work on characterization techniques and linearity metrics, detailing general characterization guidelines, and proposing a specific characterization method, swept-tone NPR. Section VII present the experimental validation of the swept-tone NPR characterization, which also serves as the experimental proof for the theoretical framework presented. Finally, Section VIII draws the major conclusions.

II. Nonlinear Dynamic RF Systems Revisited

This section presents the theoretical framework used throughout this work to analyze nonlinear dynamic effects in RF systems. Here, foundational concepts are revisited from the IMD profile point of view. This framework consists of a frequency domain analysis performed at the system-level, i.e. an analysis focused only on input/output signal observations. This contrasts with the conventional analysis performed at the circuit-level, focused on baseband impedance variation [18]. As stated, the object of the presented analysis is the spectral IMD profile produced under multi-tone excitation.

The aim is to use IMD profiles to measure nonlinear dynamic effects. This implies computing the static IMD profile, explaining how dynamic effects change the static IMD profile, and explaining how to measure those changes. The ultimate goal of this analysis is to provide insight on how to improve multi-tone linearity metrics, such as NPR, ACPR and CCPR, to be able to gauge nonlinear dynamic effects.

A. Static IMD Profile - Concept

Static nonlinear systems can be generally described by the polynomial in (1).

$$y_{\mathrm{NL}}(t) = \sum_{n=0}^{\infty} a_n x(t)^n \tag{1}$$

By shifting the analysis to the frequency domain it is easier to notice that, for a given excitation, each polynomial term imposes a specific spectral response profile. The linear spectral profile is an amplified replica of the input excitation spectrum, whereas each nonlinear profile can be obtained through the convolution theorem, as expressed in (2).

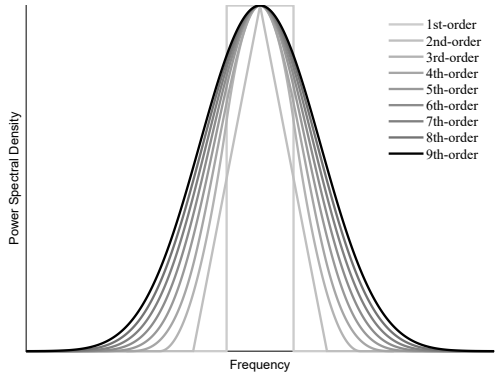

Fig. 1. Normalized envelope IMD profiles produced by a Gaussian excitation up to the 9th-order. These envelope profiles are overlapped for the sake of visualization, but they do not all overlap in the same envelope carriers. The envelope carrier frequencies for each nonlinear order are given by (3).

$$Y_{\mathrm{NL_n}}(\omega) = \mathcal{F}\{a_n x(t)\cdot x(t)^{n-1}\} = a_n \mathcal{F}\{x(t)\} * \mathcal{F}\{x(t)^{n-1}\} \tag{2}$$

As an example, let us consider a band-limited additive white Gaussian noise (AWGN) excitation signal, used in classic NPR characterization. As shown in Fig. 1, the linear envelope profile is an amplified version of the input excitation rectangular spectrum. The second-order envelope profile is triangular, resultant from the convolution of the input rectangular spectrum with itself. The remaining higher-order envelope profiles can be roughly approximated by Gaussian pulses, or by inverted parabolas when observed in logarithmic scale [22]. Note that Fig. 1 depicts the correct shape of the envelope IMD profiles, but does not represent the exact amplitude relations, as all profiles are normalized to the same peak value.

For a given order n, the full frequency response is obtained by replicating the nth-order envelope profile in each of the envelope carrier frequencies, f_{c_n}, given by (3).

$$f_{\mathrm{c}_n} = \begin{cases} \pm f_{\mathrm{c}} \cdot (2\cdot k) & \text{if n even}, \quad k \in [0, \frac{n}{2}] \\ \pm f_{\mathrm{c}} \cdot (2\cdot k + 1) & \text{if n odd}, \quad k \in [0, \frac{n-1}{2}] \end{cases} \tag{3}$$

In (3), f_c is the fundamental carrier frequency, and $k \in N_0$.

The full static IMD response is given by the overlap of all nonlinear order responses. However, the linearity analysis is mostly concerned with inband IMD - the envelope IMD centered at f_c (co-channel frequencies + adjacent channel frequencies, as defined in [17]) - because RF systems filter out of band IMD before transmission - i.e. the envelope IMD centered around DC and high-order harmonic frequencies is typically filtered by RF transmitters. Therefore, throughout this work when referring to the IMD profile, it is meant as the inband IMD profile.

B. Static IMD Profile - Multi-Tone Excitations

In modern NPR characterization, analog noise sources were replaced by reliable digital signal generators [9], [23]. These procedures are based on equal amplitude multi-tone signals designed to resemble AWGN. Expression (4) describes a Q-tone signal.

$$x(t) = \frac{1}{2}\sum_{q=1}^{2Q} A \cdot e^{j(\omega_{\mathrm{ex}_q} t + \phi_{\mathrm{ex}_q})} \tag{4}$$

In (4), ω_{ex_q} is the q-th element of the excitation frequency vector, given by (5), and ϕ_{ex_q} is the q-th element of the excitation phase vector, given by (6).

$$\boldsymbol{\omega_{ex}} = [-\omega_Q,\ \cdots,\ -\omega_1,\ \omega_1,\ \cdots,\ \omega_Q] blue^T \tag{5}$$

$$\boldsymbol{\phi_{ex}} = [-\phi_Q,\ \cdots,\ -\phi_1,\ \phi_1,\ \cdots,\ \phi_Q]^T \tag{6}$$

For a general static nonlinear system, the nth-order response, assuming a multi-tone excitation, is given by (7). This response is obtained by inserting (4) into (1) [17], [23].

$$y_{\mathrm{NL}_n}(t) = \frac{1}{2^n} a_n \left[\sum_{q=1}^{2Q} A \cdot e^{j(\omega_{\mathrm{ex}_q} t + \phi_{\mathrm{ex}_q})}\right]^n \tag{7}$$

Using the multinomial theorem, (7) can be expressed as (8).

$$y_{\mathrm{NL}_n}(t) = \frac{1}{2^n} a_n A^n \sum_{|\boldsymbol{v}|=n} \binom{n}{\boldsymbol{v}} \prod_{q=1}^{2Q} \left[e^{j(\omega_{\mathrm{ex}_q} t + \phi_{\mathrm{ex}_q})}\right]^{v_q} \tag{8}$$

Each nth-order mixing vector, $\boldsymbol{v}$, is unique, and $\sum v_i = n$.

$$\boldsymbol{v} = [v_1,\ v_2,\ \cdots,\ v_{2Q}]^T; \quad v_i \in N_0 \tag{9}$$

Mixing vectors determine the IMD frequencies of each order, and weight the IMD product magnitude and phase.

The notation can be further simplified into (10).

$$y_{\mathrm{NL}_n}(t) = \boldsymbol{g} \cdot e^{j[\boldsymbol{\omega_{IMD}} t + \boldsymbol{\phi_{IMD}}]} \tag{10}$$

This notation is achieved by defining the nth-order mixing matrix, $\boldsymbol{V}$. This matrix contains all m nth-order mixing vectors, as expressed in (11).

$$\boldsymbol{V} = \begin{bmatrix} \boldsymbol{v_1}^T \\ \boldsymbol{v_2}^T \\ \vdots \\ \boldsymbol{v_m}^T \end{bmatrix} \tag{11}$$

In (10), $\boldsymbol{g}$ is the magnitude weighting vector, given by (12), and $\boldsymbol{\omega_{IMD}} t + \boldsymbol{\phi_{IMD}}$ is the IMD phase vector, given by (13).

$$\boldsymbol{g} = \frac{1}{2} a_n A^n \binom{n}{\boldsymbol{V}} = \frac{1}{2} a_n A^n \begin{bmatrix} \binom{n}{\boldsymbol{v_1}} \\ \binom{n}{\boldsymbol{v_2}} \\ \vdots \\ \binom{n}{\boldsymbol{v_m}} \end{bmatrix} \tag{12}$$

$$\boldsymbol{\omega_{IMD}} t + \boldsymbol{\phi_{IMD}} = [\boldsymbol{V} \cdot (\boldsymbol{\omega_{ex}} t + \boldsymbol{\phi_{ex}})]^T \tag{13}$$

The resulting nth-order weighting phasor, at any frequency ω, is given by the phasor sum described in (14).

$$K_n(\omega) = \sum_{i:\omega_{\mathrm{IMD}_i}=\omega} g_i \cdot e^{j\phi_{\mathrm{IMD}_i}} \tag{14}$$

$K_n(\omega)$ represents the nth-order static IMD response produced under multi-tone excitation. Therefore, the IMD frequencies generated by each nonlinear order, as well as their weight and phase, are imposed by the input multi-tone excitation and the respective mixing matrix. This means that the static IMD profile is defined by the input excitation and by the nonlinear orders of the system. Thus, if the multi-tone excitation resembles AWGN (statistically), the envelope profiles generated by each order will be discretized versions of the envelope profiles shown in Fig. 1.

It is also useful to distinguish between correlated and uncorrelated IMD weighting phasors. These can be computed using (15) and (16), respectively.

$$K_n(\omega_q)_{\text{corr}} = \sum_{i:\omega_{\text{IMD}_i}=\omega_q \ \wedge \ (V_{i,Q-q+1}\neq 0 \ \vee \ V_{i,Q+q}\neq 0);\ q\in[1,Q]} g_i \cdot e^{j\phi_{\text{IMD}_i}} \tag{15}$$

$$K_n(\omega_q)_{\text{uncorr}} = \sum_{i:\omega_{\text{IMD}_i}=\omega_q \ \wedge \ V_{i,\{Q-q+1,Q+q\}}=0;\ q\in[1,Q]} g_i \cdot e^{j\phi_{\text{IMD}_i}} \tag{16}$$

C. Detecting Nonlinear Dynamics

Memory observations imply a system whose response is dependent on excitation frequency. This dependence can be mathematically expressed by a deviation of the magnitude and phase weights - the g_i's and the ϕ_{IMD_i}'s in (14) - from the static IMD reference, depending on the frequency terms involved in each IMD product. Magnitude and phase variations with frequency are represented, at the system level, by frequency filters. When analyzing linearity, it is also important to distinguish linear dynamic effects [7] - the dynamic effects that affect the first-order response - from nonlinear dynamic effects - the dynamic effects that affect the static IMD profiles. Thus, the practicality of describing nonlinear dynamic systems using multi-slice models [24].

When using two-tone test signals, nonlinear dynamics can be identified though observations of IMD asymmetry, or though observations of intermodulation distortion ratio variation with carrier spacing [18], [25]. However, in a multi-tone scenario the observation of these features is not a sufficient condition for the detection of nonlinear dynamics, as already noted in [18]. As far as the authors' knowledge goes, a systematic way to detect nonlinear dynamic effects from IMD profile observations under multi-tone excitation has not yet been presented in the literature. Meanwhile, the aforementioned qualitative criteria based on the 2-tone scenario continue to be used to detect nonlinear dynamics under multi-tone excitation [19], [20].

Note that the theoretical tools presented provide sufficient insight to address this issue. In Section II-B it was shown that the static IMD profile is imposed by the input multi-tone excitation, and by the system nonlinear order. As mentioned, nonlinear dynamics filter the static IMD profile, changing $K_n(\omega)$. Thus, for a given multi-tone excitation, nonlinear dynamics should be gauged as the error between the measured dynamic IMD profile and the static reference IMD profile. This approach can be viewed as an extension of the memory metric, proposed in [25] for the 2-tone excitation, to the multi-tone excitation scenario for systems of any nonlinear order. One advantage of this solution over the one presented in [18] is that it does not impose limitations on the multi-tone excitation characteristics.

In fact, it is the specification of the static reference response in agreement with the input excitation that allows the notion of expected IMD response, which, as a consequence, allows the detection of nonlinear dynamics. This becomes evident by transposing the classic analysis, presented in [18], to the system-level. It uses an equal magnitude 2-tone excitation, and assumes a third-order system. By computing the static third-order weighting phasor in these conditions, using (14), one IMD product falls in the lower adjacent channel, one IMD product falls in the upper adjacent channel, and these IMD products have the same weight. This implies that a memoryless system must have a flat adjacent-channel IMD response. Therefore, adjacent channel IMD asymmetry and adjacent channel IMD variation with carrier spacing become indicators of nonlinear dynamic effects. It is the understanding of the reference that gives meaning to the IMD profile analysis!

For systems of any order under multi-tone excitation, it is difficult to intuitively guess the static reference IMD profile because many IMD phasors overlap at inband IMD frequencies, as also expressed in (14). Despite this, expected IMD responses are often assumed without computing the reference [5], [7], [19], [20], [21]. This imposes important limitations on the IMD profile analysis. One is that it is not possible to do objective comparisons, and qualitative observations might not be rigorous. Another one is that small changes in the input signal characteristics can affect the reference, therefore, not computing the reference can lead to erroneous considerations. This is most problematic when the experimental setup is compensated, or the experimental results are processed, based on incorrect assumptions about the IMD response. Thus, the importance of specifying the static IMD reference response under multi-tone excitation when evaluating nonlinear dynamics, as proposed here.

III. Classic Nonlinear Dynamic RF Mechanism

When addressing nonlinear dynamic RF systems, the classic mechanism, first explained in [18], is often assumed. To complement the circuit-level analysis presented in [18], this section presents an in-depth system-level analysis, focused on the IMD profile response under multi-tone excitation.

The classic nonlinear dynamic mechanism is depicted in the schematic of Fig. 2. It consists of a static nonlinear branch and a nonlinear dynamic branch. These two branches add, interfering with each other, to produce the resultant output envelope IMD profile.

The static nonlinear branch consists of a third-order nonlinearity. Thus, the static branch IMD profile contribution is directly computed from (14), substituting for third-order.

The nonlinear dynamic branch consists of a second-order nonlinearity that is filtered before being remixed with the input signal. It can be viewed as a special case of a dynamic third-order nonlinearity in which IMD is filtered at baseband and second-harmonic before manifesting at the fundamental

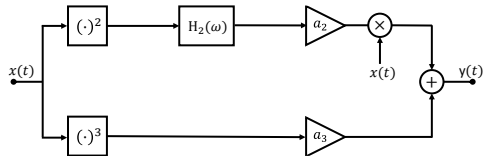

Fig. 2. Classic nonlinear dynamic mechanism model. This model addresses nonlinear dynamics (the linear path is omitted).

and third-harmonic frequencies. If not for $H_2(\omega)$, this branch would also constitute a static third-order nonlinearity. To understand the contribution of the nonlinear dynamic branch to the resultant envelope IMD profile, we must know exactly how second-order IMD products convert to third-order IMD frequencies in this branch. To do that, let us first neglect the impacts of $H_2(\omega)$ and address only the nonlinear conversion.

From (7), it is possible to decompose any nonlinearity of order n as the product of a nonlinearity of order n-1 with the input excitation, as shown in (17).

$$y_{\mathrm{NL}_n}(t) = a_n \; x(t)^{n-1} \cdot x(t) \tag{17}$$

Thus, the static conversion of a second-order nonlinearity to a third-order nonlinearity is mathematically described by (18).

$$y_{\mathrm{NL}_3}(t) = \frac{a_3}{a_2} \cdot y_{\mathrm{NL}_2}(t) \cdot \frac{1}{2} \cdot A \cdot \sum_{q=1}^{2Q} e^{j(\omega_{\mathrm{ex}_q} t + \phi_{\mathrm{ex}_q})} \tag{18}$$

Note that each second-order IMD frequency, ω_{IMD_2}, converts to the third-order IMD frequency $\omega_{\mathrm{IMD}_2} + \omega_{ex_q}$. Therefore, the conversion gain, given by (19), can be derived from (14).

$$K_3(\omega_{\mathrm{IMD}_3}) = \frac{a_3}{a_2}\frac{1}{2}A \sum_{\forall \omega_{\mathrm{IMD}_2} + \omega_{\mathrm{ex}_q} = \omega_{\mathrm{IMD}_3};\; q \in [1,2Q]} K_2(\omega_{\mathrm{IMD}_2}) \cdot e^{j\phi_{\mathrm{ex}_q}} \tag{19}$$

Equation (19) establishes the phasor relationship between static second-order IMD profiles and static third-order IMD profiles. $H_2(\omega)$ affects the magnitude and phase of each second-order IMD product, captured in $K_2(\omega_{\mathrm{IMD}_2})$. This ultimately deviates the nonlinear dynamic branch IMD profile from the static third-order IMD profile.

Therefore, the sum of the static and dynamic branches, that produces the resultant IMD profile, is a phasor sum at every third-order IMD frequency. This means that, when analyzing the classic nonlinear dynamic mechanism at the system-level under multi-tone excitation, the nonlinear dynamics introduced by $H_2(\omega)$ should be gauged as the error between the resultant IMD profile and the static third-order IMD reference profile.

IV. Dynamic IMD Profiles - Example Analysis

This section analyses distinct examples of dynamic IMD profiles produced by the classic nonlinear dynamic RF mechanism. These examples serve the following purposes:

1) to validate numerically the presented theory;
2) to emphasize the need for a static reference to make sense of IMD profiles;
3) to evidence the limitations of classic multi-tone linearity metrics in the presence of nonlinear dynamic effects.

Before the example analysis, the example systems, the input stimulus, the IMD reference profile, and the computation method are presented to parameterize the numerical examples.

A. Example Systems

As stated, all examples follow the block diagram of the classic nonlinear dynamic system, depicted in Fig. 2.

For the sake of simplicity, all the static gains, a_2 and a_3, are normalized to 1, and only the filter structure, $\mathrm{H}_2(\omega)$, is varied. Three examples are considered for analysis. The $\mathrm{H}_2(\omega)$ filters of examples I, II and III are described in Table. I, Table. II, and Table. III, respectively.

B. Input Stimulus

In this example analysis, the input stimulus is an equal magnitude 5-tone excitation, equally spaced and phase aligned. The amplitude, A from (4), is normalized to 1.

Note that this is not a standard NPR excitation. The NPR excitation has higher number of tones - i.e. higher frequency domain resolution - and the tone phases are designed to mimic band-limited AWGN statistical characteristics. This input stimulus simplification is done for the sake of intelligibility of the numerical examples, without loss of generality.

The validity of this approach is provided from (8) to (14). Note that varying the number of tones changes the the mixing matrix, thus varying the number of IMD frequencies generated, as expressed in (13). Also, tone phase manipulations change the weight phasor sum at each IMD frequency, as expressed in (14). Thus, changing multi-tone excitation parameters changes the domains of analysis - IMD frequency and IMD power - but this does not impact the analysis tools presented, as long as the IMD reference profile is defined in agreement with the input multi-tone excitation.

C. IMD Reference Profile

As mentioned in Section III, the reference for the classic mechanism is a static third-order IMD profile. But before computing the reference, the IMD frequency domain of analysis has to be specified in agreement with the input multi-tone excitation.

For equally spaced tones, the adjacent channel expands

$$\pm \frac{n-1}{2} \cdot (N_{\mathrm{tones}} - 1) \cdot \Delta f \tag{20}$$

beyond the co-channel. Where n can be any odd-order, N_{tones} is the number of excitation tones, and Δf is the carrier spacing. Equation (20) can be derived from (13).

Therefore, for the 5-tone input stimulus, the third-order IMD reference profile ranges from $\omega_1 - 4\Delta f$ to $\omega_5 + 4\Delta f$. Given this information, the IMD reference profile is computed at the interest IMD frequencies from (14), substituting for third-order with a_3 normalized to 1. The IMD reference profile is listed in Table. IV and depicted in Fig. 3.

Here it is assumed that the lowest IMD frequency is higher than DC. It is also assumed that third-order IMD envelope

TABLE I
$H_2(\omega)$ FILTER OF EXAMPLE 1.

$H_2(\omega)$	$-4\Delta f$	$-3\Delta f$	$-2\Delta f$	$-\Delta f$	REF	Δf	$2\Delta f$	$3\Delta f$	$4\Delta f$
$\lvert H_2(\omega)\rvert$	1	1	0.75	0.75	0.75	0.75	0.75	1	1
$\angle H_2(\omega)$	0	0	π	π	π	π	π	0	0

TABLE II
$H_2(\omega)$ FILTER OF EXAMPLE 2.

$H_2(\omega)$	$-4\Delta f$	$-3\Delta f$	$-2\Delta f$	$-\Delta f$	REF	Δf	$2\Delta f$	$3\Delta f$	$4\Delta f$
$\lvert H_2(\omega)\rvert$	1	1	1	1	1	1	1	1	1
$\angle H_2(\omega)$	0	0	0	π	π	π	0	0	0

TABLE III
$H_2(\omega)$ FILTER OF EXAMPLE 3.

$H_2(\omega)$	$-4\Delta f$	$-3\Delta f$	$-2\Delta f$	$-\Delta f$	REF	Δf	$2\Delta f$	$3\Delta f$	$4\Delta f$
$\lvert H_2(\omega)\rvert$	1	1	1	1	1	1	1	1	1
$\angle H_2(DC)$	π	π	π	π	0	π	π	π	π
$\angle H_2(2\omega_3)$	π	π	π	π	π	0	0	0	0

TABLE IV
REFERENCE FUNDAMENTAL ENVELOPE STATIC THIRD-ORDER PROFILE - 5-TONE EXCITATION

$\omega_1-4\Delta f$	$\omega_1-3\Delta f$	$\omega_1-2\Delta f$	$\omega_1-1\Delta f$	ω_1	ω_2	ω_3	ω_4	ω_5	$\omega_5+1\Delta f$	$\omega_5+2\Delta f$	$\omega_5+3\Delta f$	$\omega_5+4\Delta f$
0.375	1.125	2.25	3.75	5.625	6.75	7.125	6.75	5.625	3.75	2.25	1.125	0.375

profiles centered at the fundamental and at the third-harmonic frequencies do not overlap. Such assumptions avoid image channel overlap, which simplify the example analysis. Note, however, that the theoretical tools presented are also valid in such scenarios. In case of image channel overlap, the third-order IMD reference profile differs from the one presented here, in accordance to the specific scenario.

D. Classic Mechanism - Numerical Computation Method

As explained in Section III, the classic mechanism IMD profile is given by the phasor sum of the IMD profiles produced by the static and dynamic branches. Therefore, the IMD profile numerical computation starts by the independent computation the IMD profiles imposed by each branch.

The static branch is a third-order nonlinearity. Thus, the static branch IMD profile is given by the reference IMD profile, as explained in Section IV-C.

The dynamic branch performs a frequency conversion from second-order IMD frequencies to third-order IMD frequencies. So, before computing the IMD profile, the conversion domain has to be specified in agreement with the 5-tone input stimulus. As noted in IV-C, the third-order IMD profile ranges from $\omega_1-4\Delta f$ to $\omega_5+4\Delta f$. Around DC, second-order IMD ranges from $-4\Delta f$ to $+4\Delta f$. Around the second harmonic, second-order IMD ranges from $2\omega_3-4\Delta f$ to $2\omega_3+4\Delta f$. Note that second-order IMD frequencies are computed from (13).

After specifying the conversion domain, the conversion gain of each IMD product is computed from (19). Table. V lists the static conversion gain from DC, whereas Table. VI lists the static conversion gain from the second harmonic. As expected, these conversions differ by a factor of 2.

The dynamic effects, introduced by $H_2(\omega)$, are computed by scaling the static conversion gain tables - Table. V and Table. VI - at each second-order IMD frequency. The scaling factor is the phasor response of $H_2(\omega)$ at each IMD frequency.

At this point, the dynamic branch IMD profile is computed in two steps. First, add Table. V and Table. VI after applying $H_2(\omega)$ filtering. Second, compute the line element sum of the resulting table. For a memoryless conversion, the dynamic branch IMD profile coincides with the reference, as expected.

Finally, the classic mechanism IMD profile is given by the sum of the static branch IMD profile and dynamic branch IMD profile. For a memoryless conversion, this also coincides with the reference, amplified by 3 dB, as expected.

E. Example Analysis

The IMD profiles produced by each numerical example, computed as described in Section IV-D, are depicted in Fig. 3.

These IMD profiles present rather unusual trends. Example I presents a co-channel IMD minimum at the central frequency, instead of a IMD maximum. Example II presents co-channel IMD oscillation, having equal power at the start, middle and end of the band, while having lower power at intermediate frequencies ω_2 and ω_4. Example III presents strong adjacent channel asymmetry, and co-channel IMD power increases monotonically along the co-channel.

However, one must remember that IMD profile trends alone do not objectively inform about nonlinear dynamics. The meter

TABLE V
STATIC CONVERSION TABLE FROM DC TO FUNDAMENTAL FOR THE 5 TONE INPUT STIMULUS

	$DC-4\Delta f$	$DC-3\Delta f$	$DC-2\Delta f$	$DC-\Delta f$	DC	$DC+\Delta f$	$DC+2\Delta f$	$DC+3\Delta f$	$DC+4\Delta f$
$\omega_1-4\Delta f$	0.25	0	0	0	0	0	0	0	0
$\omega_1-3\Delta f$	0.25	0.5	0	0	0	0	0	0	0
$\omega_1-2\Delta f$	0.25	0.5	0.75	0	0	0	0	0	0
$\omega_1-\Delta f$	0.25	0.5	0.75	1	0	0	0	0	0
ω_1	0.25	0.5	0.75	1	1.25	0	0	0	0
ω_2	0	0.5	0.75	1	1.25	1	0	0	0
ω_3	0	0	0.75	1	1.25	1	0.75	0	0
ω_4	0	0	0	1	1.25	1	0.75	0.5	0
ω_5	0	0	0	0	1.25	1	0.75	0.5	0.25
$\omega_5+\Delta f$	0	0	0	0	0	1	0.75	0.5	0.25
$\omega_5+2\Delta f$	0	0	0	0	0	0	0.75	0.5	0.25
$\omega_5+3\Delta f$	0	0	0	0	0	0	0	0.5	0.25
$\omega_5+4\Delta f$	0	0	0	0	0	0	0	0	0.25

TABLE VI
STATIC CONVERSION TABLE FROM SECOND HARMONIC TO FUNDAMENTAL FOR THE 5 TONE INPUT STIMULUS

	$2\omega_3-4\Delta f$	$2\omega_3-3\Delta f$	$2\omega_3-2\Delta f$	$2\omega_3-\Delta f$	$2\omega_3$	$2\omega_3+\Delta f$	$2\omega_3+2\Delta f$	$2\omega_3+3\Delta f$	$2\omega_3+4\Delta f$
$\omega_1-4\Delta f$	0.125	0	0	0	0	0	0	0	0
$\omega_1-3\Delta f$	0.125	0.25	0	0	0	0	0	0	0
$\omega_1-2\Delta f$	0.125	0.25	0.375	0	0	0	0	0	0
$\omega_1-\Delta f$	0.125	0.25	0.375	0.5	0	0	0	0	0
ω_1	0.125	0.25	0.375	0.5	0.625	0	0	0	0
ω_2	0	0.25	0.375	0.5	0.625	0.5	0	0	0
ω_3	0	0	0.375	0.5	0.625	0.5	0.375	0	0
ω_4	0	0	0	0.5	0.625	0.5	0.375	0.25	0
ω_5	0	0	0	0	0.625	0.5	0.375	0.25	0.125
$\omega_5+\Delta f$	0	0	0	0	0	0.5	0.375	0.25	0.125
$\omega_5+2\Delta f$	0	0	0	0	0	0	0.375	0.25	0.125
$\omega_5+3\Delta f$	0	0	0	0	0	0	0	0.25	0.125
$\omega_5+4\Delta f$	0	0	0	0	0	0	0	0	0.125

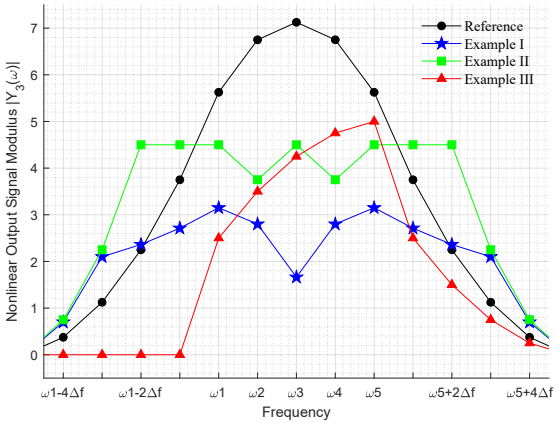

Fig. 3. IMD profiles obtained through numerical simulation: static reference and nonlinear dynamic examples.

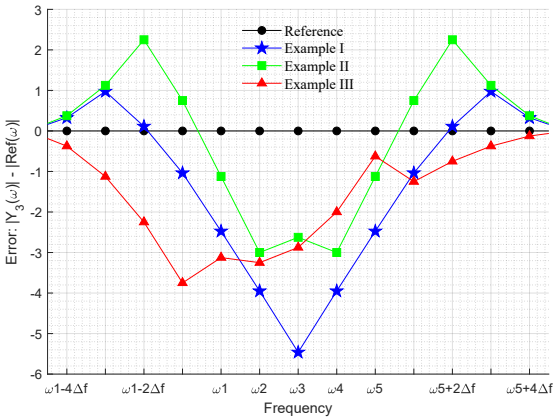

Fig. 4. IMD profile error. Positive error indicates IMD above the static reference. Negative error indicates IMD bellow the static reference.

for nonlinear dynamic quantification is the frequency dependence of the error between the IMD profile and reference, not the IMD profile trend. As shown in Fig. 4, this error is frequency dependent for each example, confirming the presence of nonlinear dynamics. Note how these are good examples of how distinct the impacts of nonlinear dynamics on the IMD profile can be. For instance, Example I and Example II expose the limitations of expecting nonlinear dynamics to manifest

TABLE VII
IMD POWER EVALUATION USING CLASSIC LINEARITY METRICS

Metric	$\mathrm{ACP_L}$	$\mathrm{ACP_U}$	NP	CCP
Reference	20.5	20.5	50.8	205.2
Example I	19.5	19.5	2.0	36.5
Example II	46.1	46.1	20.1	88.9
Example III	0.0	9.1	18.1	84.1

through asymmetric IMD profiles/asymmetric errors.

These examples also expose the limitations of classic multi-tone linearity metrics, such as ACPR, NPR and CCPR, in the assessment of nonlinear memory effects. Note that these metrics cannot quantify nonlinear dynamics, because they do not specify a static reference in accordance with the input stimulus. Beyond this, even if a reference is postulated, the integrals, explicit in the definition of these metrics [26], hide the frequency dependence of the IMD response. Thus, these metrics cannot gauge the frequency dependence of the error between measurement and reference IMD profiles, they can only gauge the difference between measured and reference IMD power within the evaluation bandwidth. This power error can incorrectly account a frequency independent error as nonlinear dynamics. It can also mask nonlinear dynamics whenever these do not translate into total IMD power errors within the evaluation bandwidth. This means that these metrics, in their classical formulation, lack frequency resolution to accurately evaluate nonlinear dynamics.

To evidence how relevant information regarding nonlinear dynamics is lost in classic linearity metrics, IMD power, as evaluated by ACPR, CCPR and NPR, is listed in Table. VII. $\mathrm{ACP_L}$ denotes the IMD power sum from $\omega_1 - 4\Delta f$ to $\omega_1 - \Delta f$, as evaluated by $\mathrm{ACPR_L}$. $\mathrm{ACP_U}$ denotes the IMD power sum from $\omega_1 + \Delta f$ to $\omega_1 + 4\Delta f$, as evaluated by $\mathrm{ACPR_U}$. NP denotes the IMD power at ω_3, as evaluated by a classic NPR measurement with a central notch. CCP denotes the IMD power sum from ω_1 to ω_5, as evaluated by CCPR. Note that IMD power is adimensional because the numerical example signals are adimensional.

Consider the ACP. In Example III the ACP measure detects not only the presence of nonlinear dynamic effects in the L-band and in the U-band, but it is also capable of detecting the large error difference between the L-band and the U-band. However, in Example I the ACP error is too marginal to confidently detect the existing nonlinear dynamic effects. Beyond this, the perception of the IMD frequencies in which IMD power is above or bellow the reference, as observed in Fig. 4, is lost. This happens because the coarse ACP analysis loses the frequency resolution required to detect these features imposed by nonlinear dynamic effects. It is no longer possible to relate IMD power to specific IMD frequency bands. Also, observe how ACP is not indicative of the CCP, and vice-versa.

NP detects the absolute IMD error at the central frequency, ω_3, but it is not indicative of the error variations that occur at other co-channel frequencies. Observe that Example II and Example III have similar NP, but these examples manifest very distinct co-channel IMD profiles (refer to Fig. 3 and Fig. 4). This evidences the importance of using swept-notch NPR measurements [21].

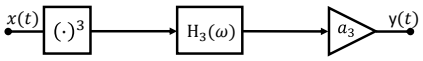

Fig. 5. Third-order dynamic nonlinear system model. This model addresses nonlinear dynamics, thus the linear path is not presented.

The use of CCP does not necessarily provide a better insight than NP. As already explained, Example II IMD power oscillates along the co-channel, whereas Example III IMD power monotonically increases along the co-channel. The CCP coarse analysis does not have sufficient frequency resolution to appropriately capture these variations imposed by nonlinear dynamic effects. This is the reason why CCP indicates similar IMD power levels for both scenarios.

The presented analysis indicates that a reliable characterization of IMD profiles affected by nonlinear dynamic effects requires the measurement of both adjacent-channel and co-channel IMD, with sufficient resolution frequency. Then, the analysis of the measured IMD profile has to be performed in relation to the static IMD reference profile.

V. LIMITATIONS OF MECHANIM BASED IMD ANALYSIS

As stated in Section III, in RF systems the IMD analysis is often performed assuming the classic nonlinear dynamic mechanism. However, IMD analysis based on specific mechanisms have strong limitations in terms of range of applicability. If the system under test differs from the analysis mechanism, the analysis is no longer valid. An obvious limitation of the classic mechanism is that it is strongly bound to third-order nonlinearity.

Range of applicability limitations directly translate into experimental setups and procedures in which specific nonlinear mechanisms are assumed prior to measurement. Studies [7] and [19] are good examples of nonlinear characterization based on specific mechanisms. When following this approach, one must be careful, because whenever incorrect assumptions are made in experiments, these translate into errors in the experimental results.

The limitations of mechanism based IMD analysis span beyond the nonlinear order of the system, because different systems, of equal nonlinear order, can produce the same response for a given excitation. Remember, from Section III, that a static second-order nonlinearity up-converted to third-order is indistinguishable from a static third-order nonlinearity. In fact, it is a static third-order nonlinearity. Beyond this, it is possible to have a different third-order system that produces the IMD profiles generated by the classic mechanism in Section IV-E, for the same excitation signal.

Consider the third-order nonlinear dynamic mechanism depicted in Fig. 5. It consists of a static third-order nonlinearity followed by a filter, $H_3(\omega)$. The static nonlinear contribution is given by (14), substituting for third-order. The filter, $H_3(\omega)$, affects the magnitude and phase of each IMD product captured in $K_3(\omega)$. For the example scenario described in Section IV, the static third-order contribution is given by the

IMD reference profile, after normalizing a_3 to 1. The dynamic effects, introduced by $H_3(\omega)$, scale the IMD reference profile. The scaling factor is the phasor response of $H_3(\omega)$ at each third-order IMD frequency. Thus, this mechanism can produce exactly the IMD profiles shown in Fig. 3, for the same excitation, if $H_3(\omega)$ is given by the normalization of the example IMD profiles by the static IMD reference profile. Table. VIII, Table. IX, and Table. X list the $H_3(\omega)$ filters, obtained through normalization, that produce the IMD profiles of Example I, Example II, and Example III, respectively.

Therefore, general experimental setups and procedures must avoid making assumptions about the nonlinear dynamic mechanism of the system under test. Such considerations must be made based on the analysis of unbiased experimental results. Specific experimental setups and procedures should only be used when there is prior knowledge about the system, and there is a need for a tailored characterization.

VI. Nonlinear Dynamic RF System Characterization

So far, the presented work brought important insights into the analysis of the IMD response produced by nonlinear dynamic RF systems, exposing relevant limitations of existing linearity metrics on the quantification of nonlinear dynamics.

This section reframes those insights from a characterization perspective, summarizing the major contributions of this work in a way that they can be instrumentally used to improve characterization techniques, and linearity metrics, on the assessment of nonlinear dynamics.

Beyond this, these contributions are used to propose a novel characterization procedure that overcomes the most critical limitations of standard procedures.

A. General Guidelines for Procedures and Metrics

The major contributions already presented can be summarized in a list of general guidelines for more reliable experimental procedures and linearity metrics, as follows:

1) Specify a static IMD reference profile in agreement with the input excitation: It was shown that IMD profiles are highly dependent on the input excitation. The definition of a reference avoids the misinterpretation of the experimental results. Beyond this, nonlinear dynamics are detected through the frequency dependence of the error between measured IMD profile and IMD reference;

2) Avoid blind mechanism based characterization: It was explained that mechanism based characterization has a very restrictive range of validity, and that incorrect assumptions can lead to experimental errors. Instead of blindly assumming a nonlinear dynamic mechanism, start from unbiased experimental results before moving to a mechanism based analysis;

3) Perform full inband IMD characterization: It was shown that in the presence of nonlinear dynamics, adjacent-channel IMD trends are not necessarily indicative of co-channel IMD trends, and vice-versa. Capturing both adjacent-channel and co-channel IMD allows for a more comprehensive understanding of the nonlinear dynamic mechanism being characterized;

4) Perform magnitude and phase measurements: The theoretical formulation evidences that important information about system dynamics is concealed in the phase of the overlapping IMD products at each IMD frequency. Therefore, magnitude and phase measurements are preferred over power measurements;

5) Use frequency dependent linearity metrics: It was demonstrated that informative linearity metrics must capture the frequency dependence of the measured IMD profile in relation to the reference with sufficient frequency resolution.

B. Swept-Tone NPR

Given the aforementioned guidelines, this section proposes a reliable characterization method, based on classic NPR procedures, to measure IMD profile responses produced by nonlinear dynamic RF systems.

First, the input stimulus has to be specified. For the swept-tone NPR the input excitation can be any equal amplitude multi-tone signal, with equally spaced tones. For those signals, the full inband response is given by (21), where $K_{n_d}(\omega)$ is the dynamic weighting phasor of order n, observed at the system output. It results from the static weighting phasor, given by (14), being filtered by the system memory effects.

$$\sum_{n=0}^{\infty} K_{n_d}(\omega) \quad , \quad \omega \in \text{inband} \tag{21}$$

From (15) and (16), this inband IMD response can be decomposed in correlated IMD and uncorrelated IMD components, as expressed in (22).

$$\sum_{n=0}^{\infty} K_{n_d}(\omega) = \sum_{n=0}^{\infty} K_{n_d}(\omega)_{\text{corr}} + \sum_{n=0}^{\infty} K_{n_d}(\omega)_{\text{uncorr}} \tag{22}$$

In RF systems the desired response is the correlated response, because correlated IMD components can be used to regenerate communication signals at the receiver [4], [16]. Thus, from an RF system perspective, the uncorrelated IMD response is the interest nonlinear response to be measured.

From a characterization perspective, the full inband response, given by (21), is measured with a full spectrum multi-tone excitation. This measurement fully captures the adjacent-channel portion of the uncorrelated nonlinear envelope response, but overlaps correlated and uncorrelated responses at the co-channel frequencies.

From (15) and (16), it is perceptible that if a single excitation tone, ω_{off}, is turned off, all IMD phasors correlated with the ω_{off} excitation phasor are also switched off, but all uncorrelated phasors that fall in ω_{off} are preserved. Thus, the co-channel uncorrelated IMD response can be measured by switching off a single excitation tone, taking a measurement, recording the uncorrelated IMD at the switched off excitation frequency, sweeping the switched off tone along the co-channel, and repeating this process until all excitation frequencies are characterized in terms of uncorrelated IMD. To illustrate this procedure, the swept-tone NPR excitation signals, for a 5-tone input stimulus, are shown in Fig. 6.

TABLE VIII
$H_3(\omega)$ FILTER THAT PRODUCES EXAMPLE 1 RESPONSE FOR THE THIRD-ORDER DYNAMIC NONLINEAR CASE

$H_3(\omega)$	$-6\Delta f$	$-5\Delta f$	$-4\Delta f$	$-3\Delta f$	$-2\Delta f$	$-\Delta f$	REF	Δf	$2\Delta f$	$3\Delta f$	$4\Delta f$	$5\Delta f$	$6\Delta f$
$\lvert H_3(\omega)\rvert$	2	2	1.1	0.74	0.56	0.4	0.2	0.4	0.56	0.74	1.1	2	2
$\angle H_3(\omega)$	0	0	0	0	0	0	0	0	0	0	0	0	0

TABLE IX
$H_3(\omega)$ FILTER THAT PRODUCES EXAMPLE 2 RESPONSE FOR THE THIRD-ORDER DYNAMIC NONLINEAR CASE

$H_3(\omega)$	$-6\Delta f$	$-5\Delta f$	$-4\Delta f$	$-3\Delta f$	$-2\Delta f$	$-\Delta f$	REF	Δf	$2\Delta f$	$3\Delta f$	$4\Delta f$	$5\Delta f$	$6\Delta f$
$\lvert H_3(\omega)\rvert$	2	2	2	1.2	0.8	$\frac{5}{9}$	$\frac{12}{19}$	$\frac{5}{9}$	0.8	1.2	2	2	2
$\angle H_3(\omega)$	0	0	0	0	0	0	0	0	0	0	0	0	0

TABLE X
$H_3(\omega)$ FILTER THAT PRODUCES EXAMPLE 3 RESPONSE FOR THE THIRD-ORDER DYNAMIC NONLINEAR CASE

$H_3(\omega)$	$-6\Delta f$	$-5\Delta f$	$-4\Delta f$	$-3\Delta f$	$-2\Delta f$	$-\Delta f$	REF	Δf	$2\Delta f$	$3\Delta f$	$4\Delta f$	$5\Delta f$	$6\Delta f$
$\lvert H_3(\omega)\rvert$	0	0	0	0	$\frac{4}{9}$	$\frac{14}{27}$	$\frac{34}{57}$	$\frac{19}{27}$	$\frac{8}{9}$	$\frac{2}{3}$	$\frac{2}{3}$	$\frac{2}{3}$	$\frac{2}{3}$
$\angle H_3(\omega)$	0	0	0	0	0	0	0	0	0	0	0	0	0

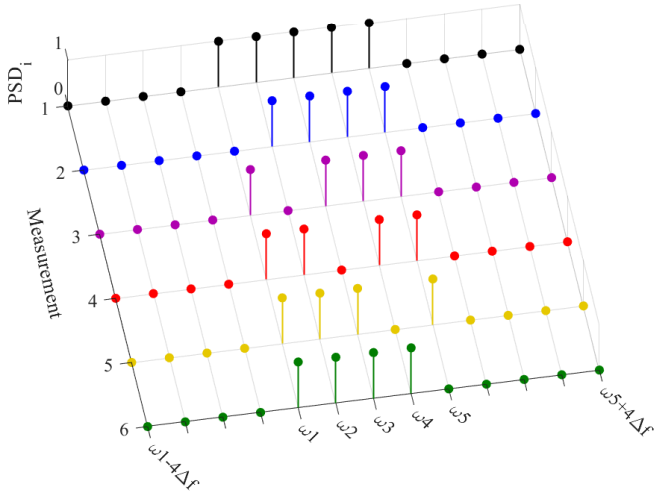

Fig. 6. Swept-tone notch NPR excitation signals PSD, assuming a 5-tone excitation.

The aforementioned measurements characterize the full inband response and the uncorrelated inband response. These measurements allow for the computation of the correlated inband response through (22), by subtracting the uncorrelated inband response from the full inband response.

It is now important to define the static reference IMD envelope profile. One approach to define the static reference is to use system input/output observations. With the full spectrum multi-tone excitation input/output observations, the best static model can be computed in a least squares sense [25], [26]. Then, the swept-tone NPR excitations can be applied to this model to compute the co-channel uncorrelated IMD response. With this, the best static reference IMD profile can be defined. Note that in this process no assumptions are made about the system, and no processing is done on the experimental results. But assumptions are made about the static reference, which instead of capturing the real a_n values from (1), it optimizes the a_n values to minimize error in the least squares sense. This means that deviations of the measured uncorrelated IMD profile from the static reference uncorrelated IMD profile are measures of the minimum dynamic deviations, not absolute deviation measures.

Lets finally address the linearity metrics. When evaluating linearity it continues to be important to measure the signal to noise distortion ratio (SNDR), as postulated in classic linearity metrics. In the proposed method this can be easily evaluated by (23).

$$SNDR = \frac{\text{Correlated Power}}{\text{Uncorrelated Power}} \tag{23}$$

Following the formulation in (22), the correlated power is given the commutative power of the correlated inband response spectrum - linear power + correlated IMD power - whereas the uncorrelated power is given the commutative power of the uncorrelated inband response spectrum - adjacent-channel uncorrelated IMD power + co-channel uncorrelated IMD power. These powers are directly obtained by computing the cumulative power of the correlated inband response and the uncorrelated inband response, respectively, which are measured as explained above.

However, system nonlinear dynamics cannot be neglected. To capture nonlinear dynamics, the SNDR measure has to be accompanied by the uncorrelated IMD profile and the reference IMD profile. The error between these profiles quantifies the variations due to nonlinear dynamic effects. These profiles can also be presented in relation to the correlated power, thus expressing the SNDR variation along the adjacent channel and co-channel. Note how this overcomes the aforementioned limitations of ACPR, NPR and CCPR.

The full characterization method proposed is summarized in the flowchart of Fig. 7.

To speed up characterization in a practical application scenario, the experimental procedure can be simplified by swiping a small bandwidth notch instead of a single tone

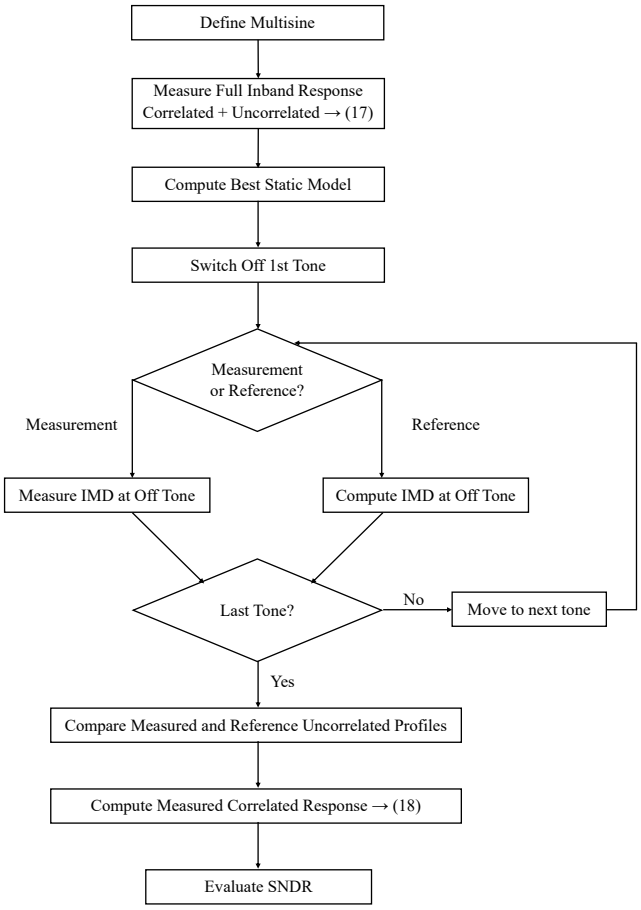

Fig. 7. Characterization method flowchart.

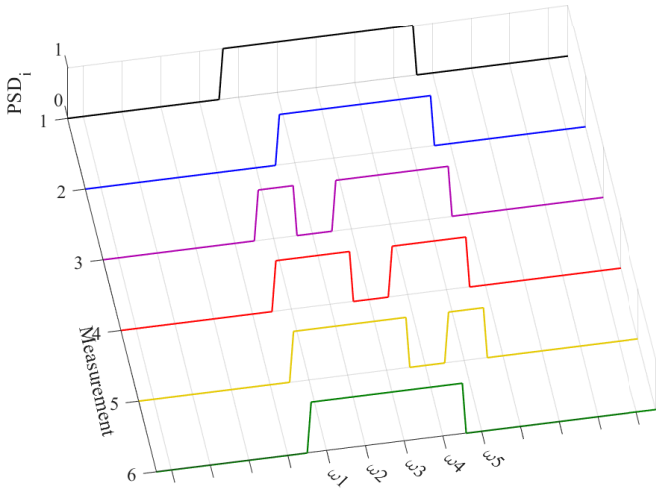

Fig. 8. Swept notch NPR excitation signals PSD, proposed in [21].

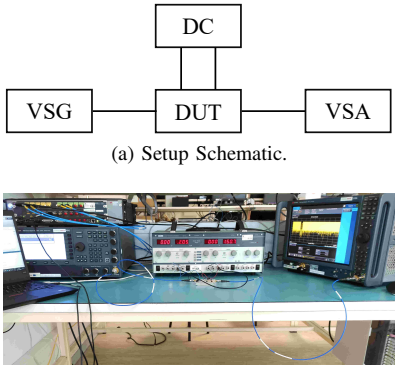

(a) Setup Schematic.

(b) Setup Picture.

Fig. 9. Experimental Setup.

notch, as proposed in [21]. The swept-notch NPR exitation signals for such a scenario are shown in Fig. 8. The IMD profile observations using this method are valid as long as the system is slowly varying along the co-channel, when compared to the notch bandwidth, i.e. as long as the notch provides sufficient frequency resolution to capture the existing nonlinear dynamic effects. Note, however, that this modification does not allow for the computation of the correlated response as previously formulated in (22).

VII. Experimental Validation

The main objective of this section is to validate the theoretical contributions of this work experimentally. Namely, evidencing the limitations of classical metrics - ACPR, NPR and CCPR - in the assessment of nonlinear dynamics, and evidencing the usefulness of the general characterization guidelines proposed to overcome those limitations. This is achieved by comparing the IMD profile obtained from the proposed swept-tone NPR procedure with IMD power measures obtained from classical procedures.

Before advancing into the experimental result analysis, the swept-tone NPR experimental validation is described in terms of experimental setup, input stimulus, and devices-under-test (DUTs).

A. Experimental Setup

The experimental setup is designed and configured to perform the swept-tone NPR procedure described in Fig. 7.

The experimental bench is depicted in Fig. 9. The VSG is composed of a Keysight M8190A AWG and a Keysight E8361C PSG. The AWG is used to generate the desired input baseband I/Q waveform, whereas the PSG serves to up-convert this baseband waveform to the desired carrier frequency, while controlling the envelope signal power. The Keysight N9041B UXA VSA function is to capture the input/output I/Q waveforms. The TTI PL330DP DC supply is used to bias the DUTs.

The DC supply is controlled manually, whereas the VSG and VSA equipments are remotely controlled to follow the procedure depicted in Fig. 7 closely. The bench is calibrated to capture the desired I/Q waveforms synchronously at the input and output ports.

B. Input Stimulus

As explained in Section VI-B, the swept-tone NPR specifies the input excitation as any equal amplitude multi-tone signal, with equally spaced tones. Before experimentation, this signal has to be parameterized in power level, bandwidth and number of tones. Note that the specification of bandwidth and the number of tones imposes the carrier spacing, which is the resolution frequency of the swept-tone NPR procedure.

During the experiments, signal power and signal bandwidth were fixed at -10 dBm and 100 MHz, respectively, whereas the number of tones was varied. Two input stimulus were used, one with 5-tones and another with 101-tones. In other words, one with 25 MHz resolution frequency and another with 1 MHz resolution frequency.

The 5-tone signal has phase aligned tones. This signal is similar to the one used for theoretical exemplification, which allows a familiar transition from the theoretical analysis to the experimental analysis. The idea is to show that signals with these characteristics can also be used to measure IMD and nonlinear dynamics in practical scenarios.

The 101-tone excitation has randomized phases, designed following the guidelines presented in [27] to resemble AWGN. This signal corresponds to a typical NPR characterization signal. The idea is to show that the presented concepts also apply to characterization signals used for the evaluation of classic linearity metrics.

C. Devices Under Test

During the experimental procedure, two devices were characterized: an Era-2+ [28], and a ZVA-213-S+ [29].

The Era-2+ is a stable off-the-shelf device known to be memoryless. It is used to validate the static reference IMD profile extraction procedure followed in swept-tone NPR characterization. The Era-2+ board operates from 5.55 GHz to 5.75 GHz, having a $P_{1_{\mathrm{dB}}}$ of 11 dBm. It is biased with 8.4 V, consuming 50 mA. It is excited at a 5.67 GHz carrier. For the input-stimulus with -10 dBm input power, it outputs an envelope power of 1 dBm, which is in agreement with the typical gain of 10.7 dB.

The ZVA-213-S+ is a wideband amplifier of interest for Ku-band radar and satellite applications. Its large operation bandwidth is an indicator for the manifestation of nonlinear dynamic effects. This device is used to validate the ability of swept-tone NPR to gauge nonlinear dynamics. The ZVA-213-S+ board operates from 800 MHz to 21 GHz, having a $P_{1_{\mathrm{dB}}}$ of 24 dBm. It is biased with 12 V, consuming 340 mA. It is excited at an 18 GHz carrier. For the input-stimulus with -10 dBm input power, it outputs an envelope power of 15.6 dBm, which is in agreement with the typical gain of 26 dB.

D. Experimental Result Analysis

The experimental results are presented in Table. XI and from Fig. 10 to Fig. 15. Table. XI contains all SNDR measures and classical linearity metrics measures. The results from Fig. 10 to Fig. 12 refer to swept-tone NPR measures done with the

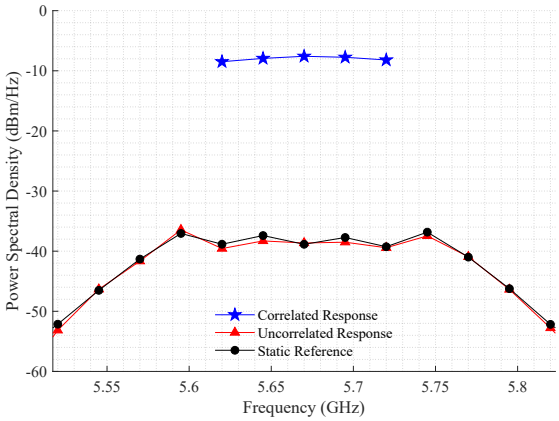

Fig. 10. Era-2+ - 5-tone excitation - correlated response and uncorrelated IMD profiles (Measurement and Reference).

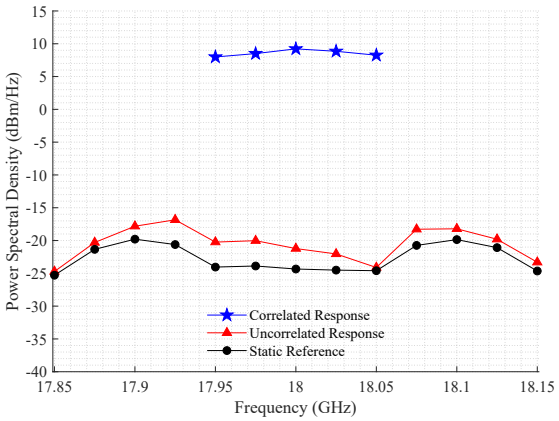

Fig. 11. ZVA-213-S+ - 5-tone excitation - correlated response and uncorrelated IMD profiles (Measurement and Reference).

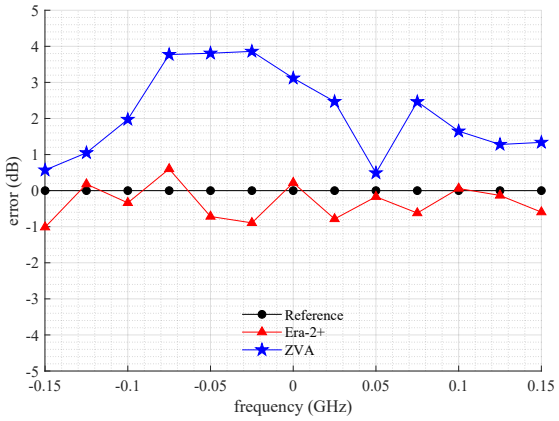

Fig. 12. 5-tone excitation - error between uncorrelated response and reference profile (Era-2+ and ZVA-213-S+). The error curves, even though referent to different carrier frequencies, are plotted in the same graph to facilitate the comparison between the two dynamic behaviors.

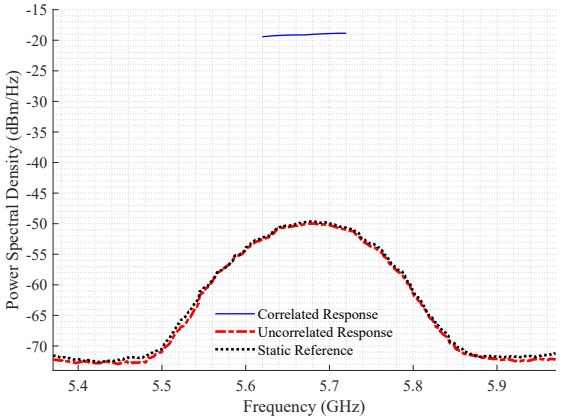

Fig. 13. Era-2+ - 101-tone excitation - correlated response and uncorrelated IMD profiles (Measurement and Reference).

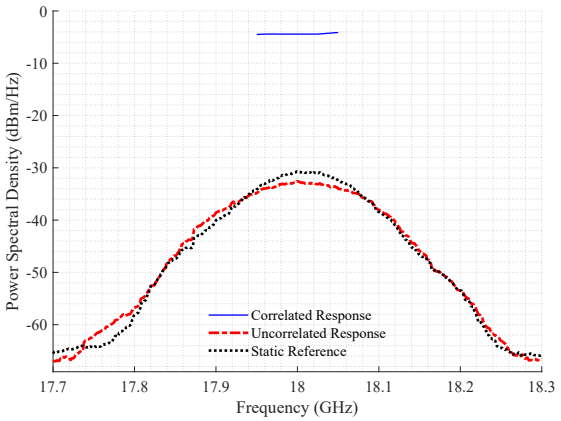

Fig. 14. ZVA-213-S+ - 101-tone excitation - correlated response and uncorrelated IMD profiles (Measurement and Reference).

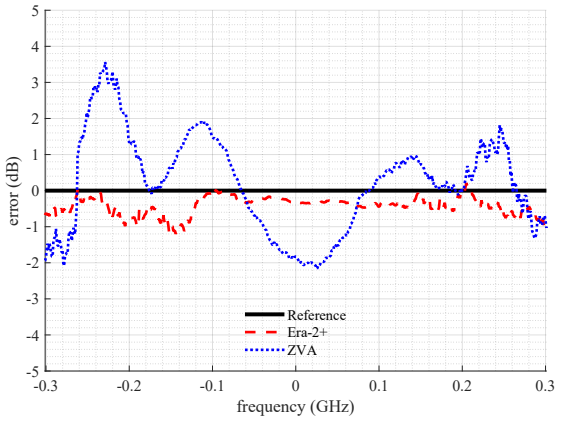

Fig. 15. 101-tone excitation - error between uncorrelated response and reference profile (Era-2+ and ZVA-213-S+). The error curves, even though referent to different carrier frequencies, are plotted in the same graph to facilitate the comparison between the two dynamic behaviors.

TABLE XI
EXPERIMENTAL RESULTS: IMD POWER METRICS AND SNDR

Metric	$\mathrm{ACPR_L}$	$\mathrm{ACPR_U}$	NPR	CCPR	**SNDR**
Unit	dB	dB	dB	dB	**dB**
Era_m (5-tones)	33.9	34.4	30.7	30.8	**28.0**
Era_r (5-tones)	34.2	33.9	30.8	30.3	**27.6**
Zva_m (5-tones)	28.6	29.0	29.8	29.9	**24.3**
Zva_r (5-tones)	30.6	30.5	32.6	32.6	**26.2**
Era_m (101-tones)	52.4	47.3	26.9	30.2	**28.8**
Era_r (101-tones)	50.9	46.5	27.1	29.9	**28.5**
Zva_m (101-tones)	47.1	41.8	22.9	27.8	**25.8**
Zva_r (101-tones)	48.3	41.3	21.7	26.1	**24.8**

5-tone excitation, whereas the results from Fig. 13 to Fig. 15 refer to swept-tone NPR measures done with the 101-tone excitation. For each measurement performed, each metric was also evaluated taking into account the reference profile, instead of the measured uncorrelated IMD profile. These results are also listed in Table. XI to aid the result analysis.

Lets start with the Era-2+ characterization performed with 5-tones. As shown in Fig. 10, the uncorrelated IMD profile and the reference profile overlap. Fig. 12 confirms this assessment, showing that for this device the error between uncorrelated IMD profile and reference is mostly constant throughout the band, and that the magnitude of the error never exceeds 1 dB. Beyond this, the error between uncorrelated IMD profile and the reference profile for all the metrics listed in Table. XI never exceeds 0.5 dB. All these results evidence a memoryless behavior, as expected. The swept-tone NPR measure provides more frequency resolution than the metrics listed in Table. XI, which for this memoryless scenario does not provide any additional information.

The advantages of the swept-tone NPR measures are clear in the 5-tone experimental results of the ZVA-213-S+ device. As shown in Fig. 11, the uncorrelated IMD profile is above the reference throughout the band. The most noticeable feature of these profiles is the decreasing error between the uncorrelated IMD profile and the reference along the co-channel frequencies. For this device, the error curve, shown in Fig. 12, reveals more details. It can be noted that lower-band adjacent-channel error increases towards the co-channel, whereas higher-band adjacent-channel error is mostly constant, around 1.5 dB. The frequency dependence of the error between uncorrelated IMD profile and reference confirms the presence of nonlinear dynamics in the IMD response of the ZVA-213-S+ device. Regarding $\mathrm{ACPR_L}$ and $\mathrm{ACPR_U}$ metrics, a 1.5 dB error is measured between the uncorrelated IMD profile and the reference profile evaluations, as listed in Table. XI. These metrics can detect that the uncorrelated IMD profile is above the reference, but loose the information regarding the adjacent-channel error trend. Similar considerations can be made about the NPR and CCPR metrics. Errors of 2.8 dB can detect that the uncorrelated IMD profile is above the reference, but the perception that the error decreases along the co-channel is lost. In the presence of nonlinear dynamics, it is clear that swept-tone NPR measurements can provide detailed information that

classic metrics neglect.

Now, consider the Era-2+ characterization performed with 101-tones. Once again, the uncorrelated IMD profile and the reference overlap, as show in Fig. 13. For this excitation the error between the uncorrelated IMD profile and the reference remains constant throughout the band, and lower than $1\ \mathrm{dB}$ in modulus, as depicted in Fig. 15. Apart from the adjacent-channel measures, all metrics agree with the reference metric with an error lower than $0.3\ \mathrm{dB}$, as listed in Table. XI. The adjacent channel error is slightly larger - $1.5\ \mathrm{dB}$ - because these measures are taken at lower powers, where small absolute errors translate into larger relative errors. Despite this limitation in the evaluation of ACPR, the experimental results, particularly the error curves in Fig. 15, confirm the memoryless behaviour of the Era-2+, now under a 101-tone excitation.

Finally, lets analyze the ZVA-213-S+ characterization performed with 101-tones. Once again, the uncorrelated IMD profile and the reference do not overlap, as shown in Fig. 14. But the uncorrelated IMD trend is now more complex than observed for the 5-tone excitation. There are several frequency bands in which the uncorrelated IMD profile is either above, bellow, or overlapped with the reference, as can be clearly observed in Fig. 15. Once again, the frequency dependence of the error between uncorrelated IMD profile and reference confirms the presence of nonlinear dynamics in the IMD response of the ZVA-213-S+ device. It is interesting to contrast the error profile, depicted in Fig. 15, with classical linearity measures, listed in Table. XI. The $\mathrm{ACPR_L}$ measure is $1.2\ \mathrm{dB}$ bellow the reference $\mathrm{ACPR_L}$. Looking into the error curve it is perceptible that this skew occurs because in the lower-band adjacent-channel the cumulative uncorrelated IMD power above the reference is higher than the cumulative uncorrelated IMD power bellow the reference. In the higher-band adjacent channel the impacts of the cumulative analysis are more severe, because the amount of comulative uncorrelated IMD power above and bellow the reference is similar. Therefore, the error between the uncorrelated IMD profile and the reference in the $\mathrm{ACPR_U}$ measure is only $0.5\ \mathrm{dB}$, which can mask the detection of nonlinear dynamics. Note, again, how the cumulative nature of classic linearity metrics mask important features of IMD profiles containing nonlinear dynamic effects. Regarding the NPR and CCPR, errors of $1.2\ \mathrm{dB}$ and $1.7\ \mathrm{dB}$ are measured in relation to the reference, respectively. These errors detect that the uncorrelated IMD profile is bellow the reference in the co-channel, but the perception of the error trend is lost.

It is now important to compare the experimental results obtained for the 5-tone excitation with the results obtained for the 101-tone excitation. For the Era-2+, the uncorrelated IMD responses and the error trends reinforce each other, confirming the memoryless behavior of the device. The same can be said for the ZVA-213-S+ device, in the sense that nonlinear dynamic effects are detected with both signals. However, more work is required to establish an identity between these two regimes of operation in order to be able to perform a direct comparison between the results obtained from each excitation, because IMD profiles and error trends are dependent on input excitation, as previously explained. The ACPR and NPR measures vary significantly from one excitation to the other, which makes them difficult to compare. The CCPR measure is similar for the memoryless scenario, but in the presence of memory effects errors can be as large as $6.5\ \mathrm{dB}$. However, the SNDR measures, evaluated as defined in (23), agree within a $1.5\ \mathrm{dB}$ error margin.

Regarding linearity metrics, in a memoryless scenario all metrics evaluated provide IMD measures with similar levels of confidence. In the presence of nonlinear dynamics, the error profile obtained from swept-tone NPR is the most informative metric. The remaining metrics can be misleading, as demonstrated by the experiments. In sum, swept-tone NPR is capable of reliably distinguishing nonlinear dynamic scenarios from memoryless scenarios, while accurately evaluating IMD power levels.

Regarding the device under test performance evaluation, the Era-2+ device is a static nonlinear device that exhibits a $28.8\ \mathrm{dB}$ SNDR at $1\ \mathrm{dBm}$ of output power when excitated at $5.67\ \mathrm{GHz}$, whereas the ZVA-213-S+ device is a nonlinear dynamic device that exhibits a $25.8\ \mathrm{dB}$ SNDR at $15.6\ \mathrm{dBm}$ of output power when excitated at $18\ \mathrm{GHz}$. In these conditions the Era-2+ SNDR is $3\ \mathrm{dB}$ higher than the ZVA-213-S+, meaning that a higher portion of the output power is desired signal power. In that sense, it can be said that Era-2+ device is more linear at delivering $1\ \mathrm{dBm}$ of output power at a $5.67\ \mathrm{GHz}$ carrier, than the ZVA-213-S+ device at delivering $15.6\ \mathrm{dBm}$ of output power at an $18\ \mathrm{GHz}$ carrier. This analysis is not an absolute comparison of the performance of the devices, because the regimes of operation are too distinct, it is just to provide an idea of how to use the proposed metrics to evaluate both dynamics and linearity.

As a final note, observe that it was the definition of the static reference that allowed an objective interpretation of the experimental results for every linearity metric considered.

VIII. Conclusion

This work presented a theoretical framework capable of analyzing IMD profiles produced under multi-tone excitation and detecting the impacts of nonlinear dynamic effects. This analysis exposed critical limitations of classic linearity metrics in the assessment of IMD responses produced by nonlinear dynamic RF systems, and allowed for the definition of general characterization guidelines to overcome those limitations.

Based on these contributions, a novel characterization method, based on classic NPR procedures, for the characterization of IMD profiles affected by nonlinear dynamic effects was proposed and validated experimentally.

The proposed method, swept-tone NPR, contemplates several advantages over previous works addressing NPR characterization, as the novel method:

1) does not require an AWGN excitation. It is consistent for different multi-tone excitation statistics, and can be adapted to excitations used in practical scenarios;
2) it captures full inband IMD (adjacent-channel + co-channel IMD)

3) it separates the correlated inband response, from the uncorrelated inband response. This allows for an accurate evaluation of inband SNDR;
4) it is capable of distinguishing memoryless scenarios from nonlinear dynamic scenarios;
5) it defines a frequency dependent metric, which allows for the detection fine IMD profile features introduced by nonlinear dynamic effects, both in adjacent channel and co-channel frequencies;
6) it is not bound to specific nonlinear mechanisms.

The general characterization guidelines presented are good practices that allow for the definition of novel characterization methods, or for the adaptation of exiting methods, to reliably capture IMD profiles affected by nonlinear dynamic effects in accordance to specific RF application constraints. This is particularly important, as RF applications continue to expand towards broader instantaneous bandwidths and nonlinear dynamic effects become more relevant.

Further work is required to establish direct relationships between experimental results obtained with different excitation signals, but the initial results presented here indicate the ability to correctly characterize IMD power level while detecting nonlinear dynamic effects.

The developments presented in this work can be used in design, modeling and compensation of nonlinear dynamic RF systems. However, future developments are required in this regard, so that reliable linearity metrics, contemplating nonlinear dynamic effects in broadband scenarios, are integrated in these fields, finally replacing simpler, but invalid, metrics in these domains of application.

REFERENCES

[1] C. Boulanger, A. Mallet, J. Puech, L. Lapierre, and J. Sombrin, "A new criterion for power amplifier comparison and optimisation," in *IEE Seminar on Microwave and RF Power Amplifiers (Ref. No. 2000/118)*, 2000, pp. 1/1–1/6.

[2] A. Mallet, F. Gizard, T. Reveyrand, L. Lapierre, and J. Sombrin, "A new satellite repeater amplifier characterization system for large bandwidth NPR and modulated signals measurements," in *2002 IEEE MTT-S International Microwave Symposium Digest (Cat. No.02CH37278)*, vol. 3, 2002, pp. 2245–2248 vol.3.

[3] P. Medrel, T. Reveyrand, A. Martin, P. Bouysse, J.-M. Nébus, and J. Sombrin, "Time domain envelope characterization of power amplifiers for linear and high efficiency design solutions," in *WAMICON 2013*, 2013, pp. 1–6.

[4] K. M. Gharaibeh, K. G. Gard, and M. B. Steer, "Accurate estimation of digital communication system metrics-SNR, EVM and /spl rho/in a nonlinear amplifier environment," in *64th ARFTG Microwave Measurements Conference, Fall 2004.*, 2004, pp. 41–44.

[5] J. B. Sombrin, "On the formal identity of EVM and NPR measurement methods: conditions for identity of error vector magnitude and noise power ratio," in *2011 41st European Microwave Conference*, 2011, pp. 337–340.

[6] Y. Rolain, M. Zyari, E. Van Nechel, and G. Vandersteen, "A measurement-based error-vector-magnitude model to assess non linearity at the system level," in *2017 IEEE MTT-S International Microwave Symposium (IMS)*, 2017, pp. 1429–1432.

[7] E. Van Nechel, Y. Rolain, and J. Lataire, "Extracting improved figures of merit for characterizing nonlinear devices using multisine excitation signals," in *2018 91st ARFTG Microwave Measurement Conference (ARFTG)*, 2018, pp. 1–4.

[8] J. Lajoinie, E. Ngoya, D. Barataud, J. Nebus, J. Sombrin, and B. Rivierre, "Efficient simulation of NPR for the optimum design of satellite transponders SSPAs," in *1998 IEEE MTT-S International Microwave Symposium Digest (Cat. No.98CH36192)*, vol. 2, 1998, pp. 741–744 vol.2.

[9] T. Reveyrand, D. Barataud, J. Lajoinie, M. Campovecchio, J.-M. Nebus, E. Ngoya, J. Sombrin, and D. Roques, "A novel experimental noise power ratio characterization method for multicarrier microwave power amplifiers," in *55th ARFTG Conference Digest*, vol. 37, 2000, pp. 1–5.

[10] S. Din, A. M. Morishita, N. Yamamoto, C. Brown, M. Wojtowicz, and M. Siddiqui, "High-power K-band GaN PA MMICs and module for NPR and PAE," in *2017 IEEE MTT-S International Microwave Symposium (IMS)*, 2017, pp. 1838–1841.

[11] G. Lasser, M. R. Duffy, and Z. Popović, "Dynamic dual-gate bias modulation for linearization of a high-efficiency multistage PA," *IEEE Trans. Microw. Theory Techn.*, vol. 67, no. 7, pp. 2483–2494, 2019.

[12] S. Laurent, J. P. Teyssier, R. Quere, J. Sombrin, and M. Prigent, "Linearity characterization of RF circuits through an unequally spaced multitone signal," in *2016 88th ARFTG Microwave Measurement Conference (ARFTG)*, 2016, pp. 1–4.

[13] V. Gillet, M. Bouslama, J. Teyssier, M. Prigent, J. Nallatamby, and R. Quéré, "An unequally spaced multi-tone load–pull characterization technique for simultaneous linearity and efficiency assessment of RF power devices," *IEEE Trans. Microw. Theory Techn.*, vol. 67, no. 7, pp. 2505–2513, 2019.

[14] V. Gillet, J. P. Teyssier, A. Al Hajjar, A. Gasmi, C. E. Kacou, M. Prigent, and R. Quéré, "Millimeter-wave power amplifier linearity characterization using unequally spaced multi-tone stimulus," in *2020 IEEE/MTT-S International Microwave Symposium (IMS)*, 2020, pp. 755–758.

[15] J. Teyssier, J. Dunsmore, J. Verspecht, and J. Kerr, "Coherent multi-tone stimulus-response measurements with a VNA," in *2017 89th ARFTG Microwave Measurement Conference (ARFTG)*, 2017, pp. 1–3.

[16] A. Geens, Y. Rolain, W. Van Moer, K. Vanhoenacker, and J. Schoukens, "Discussion on fundamental issues of NPR measurements," *IEEE Trans. Instrum. Meas.*, vol. 52, no. 1, pp. 197–202, 2003.

[17] J. C. Pedro and N. B. Carvalho, *Intermodulation distortion in microwave and wireless circuits*. Artech House, 2003.

[18] N. B. De Carvalho and J. C. Pedro, "A comprehensive explanation of distortion sideband asymmetries," *IEEE Trans. Microw. Theory Techn.*, vol. 50, no. 9, pp. 2090–2101, 2002.

[19] J. P. Martins, N. B. Carvalho, and J. C. Pedro, "Intermodulation distortion of third-order nonlinear systems with memory under multisine excitations," *IEEE Trans. Microw. Theory Techn.*, vol. 55, no. 6, pp. 1264–1271, 2007.

[20] S. Farsi, P. Draxler, H. Gheidi, B. K. Nauwelaers, P. Asbeck, and D. Schreurs, "Characterization of intermodulation and memory effects using offset multisine excitation," *IEEE Trans. Microw. Theory Techn.*, vol. 62, no. 3, pp. 645–657, 2014.

[21] R. Figueiredo, A. Piacibello, V. Camarchia, and N. B. Carvalho, "Swept notch NPR for linearity assessment of systems presenting long-term memory effects," in *2020 95th ARFTG Microwave Measurement Conference (ARFTG)*, 2020, pp. 1–4.

[22] J. C. Pedro and N. B. de Carvalho, "Characterizing nonlinear RF circuits for their in-band signal distortion," *IEEE Trans. Instrum. Meas.*, vol. 51, no. 3, pp. 420–426, 2002.

[23] J. C. Pedro and N. B. De Carvalho, "On the use of multitone techniques for assessing RF components' intermodulation distortion," *IEEE Trans. Microw. Theory Techn.*, vol. 47, no. 12, pp. 2393–2402, 1999.

[24] A. Walker, M. Steer, K. Gard, and K. Gharaibeh, "Multi-slice behavioral model of RF systems and devices," in *Proceedings. 2004 IEEE Radio and Wireless Conference (IEEE Cat. No. 04TH8746)*, 2004, pp. 71–74.

[25] J. P. Martins, P. M. Cabral, N. Borges Carvalho, and J. C. Pedro, "A metric for the quantification of memory effects in power amplifiers," *IEEE Trans. Microw. Theory Techn.*, vol. 54, no. 12, pp. 4432–4439, 2006.

[26] N. B. Carvalho and D. Schreurs, *Microwave and wireless measurement techniques*. Cambridge University Press, 2013.

[27] N. B. Carvalho, K. A. Remley, D. Schreurs, and K. G. Gard, "Multisine signals for wireless system test and design [application notes]," *IEEE Microw. Mag.*, vol. 9, no. 3, pp. 122–138, 2008.

[28] Mini-Circuits. (2020) Drop-in monolithic amplifier. [Online]. Available: https://www.minicircuits.com/pdfs/ERA-2+.pdf

[29] ——. (2020) Super ultra wideband amplifier. [Online]. Available: https://www.minicircuits.com/pdfs/ZVA-213-S+.pdf

Ricardo Figueiredo (Graduate Student Member, IEEE) was born in Viseu, Portugal, in 1995. He received the M.Sc. degree in electronics and telecommunications engineering from the Universidade de Aveiro, Aveiro, Portugal, in 2018, where he is currently pursuing the Ph.D. degree in electrical engineering.

He is currently a Researcher at the Instituto de Telecomumicações, Aveiro. His main research interests include nonlinear instrumentation and nonlinear characterization of microwave systems.

Mr. Figueiredo a is member of the IEEE MTT-S Student Branch Chapter at Universidade de Aveiro.

Nuno Carvalho (Fellow, IEEE) was born in Luanda, Angola, in 1972. He received the Diploma and Doctoral degrees in electronics and telecommunications engineering from the University of Aveiro, Aveiro, Portugal, in 1995 and 2000, respectively.

He is currently a Full Professor and a Senior Research Scientist with the Institute of Telecommunications, University of Aveiro and an IEEE Fellow. He coauthored Intermodulation in Microwave and Wireless Circuits (Artech House, 2003), Microwave and Wireless Measurement Techniques (Cambridge University Press, 2013), White Space Communication Technologies (Cambridge University Press, 2014) and Wireless Power Transmission for Sustainable Electronics (Wiley, 2020). He has been a reviewer and author of over 200 papers in magazines and conferences. He is the Editor in Chief of the Cambridge Wireless Power Transfer Journal, an associate editor of the IEEE Microwave Magazine and former associate editor of the IEEE Transactions on Microwave Theory and Techniques and IET Microwaves Antennas and Propagation Journal. He is the co-inventor of six patents. His main research interests include software-defined radio front-ends, wireless power transmission, nonlinear distortion analysis in microwave/wireless circuits and systems, and measurement of nonlinear phenomena. He has recently been involved in the design of dedicated radios and systems for newly emerging wireless technologies.

Dr. Borges Carvalho is a member of the IEEE MTT ADCOM, the past-chair of the IEEE Portuguese Section, MTT-20 and MTT-11 and also belong to the technical committees, MTT-24 and MTT-26. He is also the vice-chair of the URSI Commission A (Metrology Group). He was the recipient of the 1995 University of Aveiro and the Portuguese Engineering Association Prize for the best 1995 student at the University of Aveiro, the 1998 Student Paper Competition (Third Place) of the IEEE Microwave Theory and Techniques Society (IEEE MTT-S) International Microwave Symposium (IMS), and the 2000 IEE Measurement Prize. He is a Distinguished Lecturer for the RFID-Council and was a Distinguished Microwave Lecturer for the IEEE Microwave Theory and Techniques Society.

Anna Piacibello (Member, IEEE) was born in Chivasso, Italy, in 1991. She received the Bachelor and Master degrees in Electronic Engineering from the Politecnico di Torino in 2013 and 2015, respectively.

In 2017, she was a visiting researcher at the Centre for High Frequency Engineering (CHFE) of Cardiff University. She received the PhD degree cum laude in Electric, Electronic and Communication Engineering from the Politecnico di Torino in 2019. Her current research interests include broadband and highly efficient microwave power amplifiers. Dr. Piacibello is currently a postdoctoral research associate with the Department of Electronics and Telecommunications, Politecnico di Torino, Italy, and with the Microwave Engineering Center for Space Applications, Rome, Italy.

She was a recipient of the 2018 Young Engineer Prize awarded by the EuMA association.

Vittorio Camarchia (Senior Member, IEEE) was born in Turin, Italy, in 1972. He received the Laurea degree and Ph.D. degree in Electronic Engineering from the Politecnico di Torino, Turin, Italy, in 2000 and 2003, respectively.

He was in 2001-2003 a Visiting Researcher with the Electrical and Computer Engineering Department, Boston University. Since 2004 he joined the Department of Electronics and Telecommunications of the Politecnico di Torino where he is presently an Associate Professor. His research is focused on modeling, design and characterization of RF and microwave modules and systems. He is the p.i. of projects for the European Space Agency (ESA), reviewer of the Research Executive Agency of the European Commission for space-related topics and of the major journal of the field. He has published 180 peer-reviewed papers, two books and several book chapters.

Prof. Camarchia is member of the IEEE MTT-S Subcommittees 12 on power amplifiers and 23 on Wireless Communications and serves as member of the International Microwave Symposium Technical Program Review Committee on power amplifiers. He is associate editor of the IEEE Transactions on Microwave Theory and Techniques and of IEEE Access, and has been the Guest editor of the 2020 Special Issue on Broadband Millimeter-wave Power Amplifiers of the IEEE Transactions on Microwave Theory and Techniques. He was a recipient of the 2002 Young Graduated Research Fellowship presented by the GAAS Association.

Chapter 3

A framework to assess and compare linearity metrics

Two major broadband linearity metric limitations impede the establishment of a universal framework to measure and compare RF system linearity performance: measurement inconsistency, and test signal dependence.

In microwaves, Gaussian noise loading is the cornerstone of linearity assessment [9, 46, 53], but a standard test signal has never been postulated because in theory specifying Gaussian signals is straightforward. In practice, linearity metric measurements performed with Gaussian signals are inconsistent [12, 20, 37]. This makes it hard to compare metrics measured with different equipment, different automated toolboxes, and by different users.

Measurements performed with different test signals produce different linearity metrics. Unfortunately, the knowledge to interpret and compare these metrics was missing, and the practical need to assess linearity in real system operation made test signal dependence a critical problem, it forced modern characterization approaches to abandon noise loading techniques, and to move towards the use of modulated test signals. Now, there are virtually infinite application dependent linearity metrics.

This chapter presents test signal standards that guarantee consistent linearity metric measurements, and proposes a solution to overcome linearity metric application dependence.

3.1 Linearity Test Signal Standards

Linearity metrics are test signal dependent. Without specifying relevant signal characteristics, the choices made by automated toolboxes, and by users culminate in inconsistent measurements. This section discusses how test signal standards can guarantee consistency.

3.1.1 How are Gaussian linearity metric measurements inconsistent?

Gaussian noise loading is the foundation of broadband linearity characterization. How come that measurements performed with these signals lead to inconsistent linearity metrics?

Lets revisit the Gaussian distribution PDF:

$$f_X(x) = \frac{1}{\sqrt{2\pi}\sigma} e^{\frac{-(x-\mu)^2}{2\sigma^2}} \tag{3.1}$$

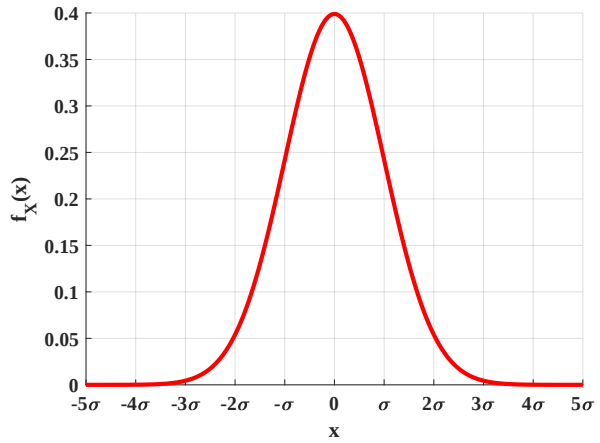

Figure 3.1: Theoretical Gaussian PDF.

In theory, Gaussian signals are fully specified by the average amplitude, μ, and by the standard deviation, σ. In microwaves, μ is zero, and σ^2 is the average power. In practice, measurement inconsistency mostly comes from two overlooked signal characteristics: amplitude range, and high-power amplitude coverage.

The amplitude range is infinite: $x \in (-\infty, +\infty)$. The ideal Gaussian signal is not reproducible in the lab, its tail is cropped. Without rules for cropping, the test signal distribution varies depending on measurement choices. Beyond this, Gaussian signals have low probability of high-power amplitudes that inform about linearity. The net result is that some test signals probe the nonlinear region better than others, which produces linearity metric variability.

Thankfully, the root causes of inconsistency can be minimized. Amplitude range variability can be overcome by specifying a crop factor that balances tail length. A possible solution is to define the crop factor in terms of σ:

$$P_{\text{peak}_{\text{crop}}} = (n\sigma)^2, \tag{3.2}$$

this is equivalent to specifying a fixed finite PAPR for the test signal:

$$\text{PAPR}_{\text{crop}} = \frac{P_{\text{peak}}}{P_{\text{avg}}} = \frac{(n\sigma)^2}{\sigma^2} = n^2. \tag{3.3}$$

The tail should not be so short that it affects the distribution, nor so long that the DAC looses resolution near the average signal power, where most of the signal samples are. Fig. 3.2 depicts this trade-off.

The small probability of observing the nonlinear region can be circumvented by the use of longer test signals, but this can create memory constraints.

Nonetheless, these inconsistency improvements are just halfway towards a standard, and the use of non-repeatable real communication signals only aggravates the problem. Instrumentation grade standards require the same test conditions in every realization. The next section explains what is required to define a robust linearity test signal standard.

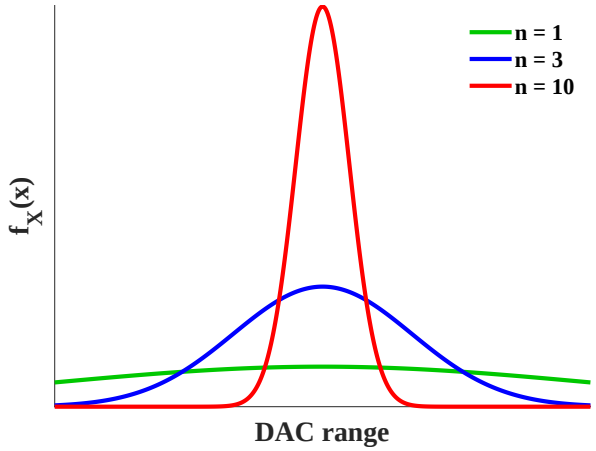

Figure 3.2: Trade-off between crop factor and DAC range coverage when the cropped Gaussian distribution fits the full DAC range.

3.1.2 How to define a robust linearity test signal standard?

Robust linearity test signal standards apply a key principle of system identification to linearity characterization [54, 55], they excite the relevant system states: memory and power.

Exciting all memory states means energizing simultaneously the full system instantaneous bandwidth with sufficient resolution frequency. In Fig. 3.3, the RF carrier excites fast memory effects, the instantaneous bandwidth probes memory that spans the envelope period, and the resolution frequency imposes the slowest long-term memory effect excitation required.

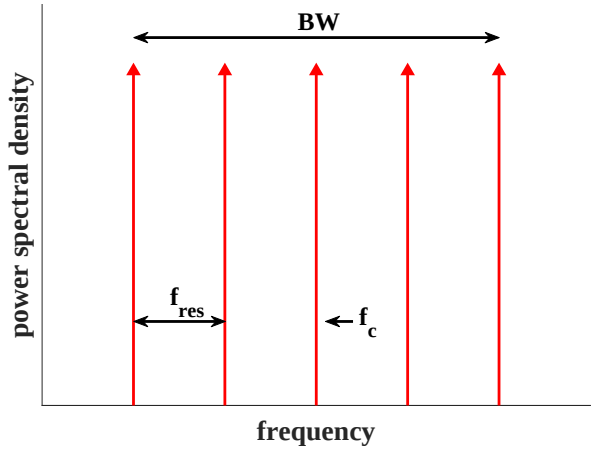

Figure 3.3: Nonlinear dynamic time constants: $\tau_{fast} \approx \frac{1}{f_c}$; $\tau_{env} \approx \frac{1}{BW}$; $\tau_{slow} \approx \frac{1}{f_{res}}$.

Exciting all relevant power states means that the test signal covers the system power range, from zero up to the maximum input instantaneous power allowed. Fig. 3.4 depicts the concept. Each amplitude within this power range is probed according to the test signal PDF.

With multi-tones, memory excitation is asserted by adjusting the number of tones within the system instantaneous bandwidth to guarantee the required resolution frequency. Power excitation is asserted by fitting the signal range to the system range.

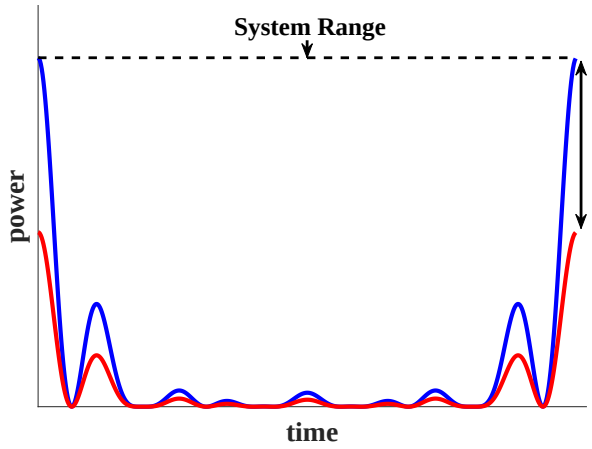

Figure 3.4: The blue test signal range meets the system range, the red one does not.

Beyond requirement compliance, there are several reasons to use multi-tone signals[1]: they preserve time-frequency information during domain conversions; they allow flexible temporal amplitude statistical design; they provide the same waveform consistently; they can be generated with basic equipment; and they are license free.

In summary, any signal that fully excites memory and power states is a candidate for the microwave linearity test signal standard. In practice it makes sense to use signals that are robust, easy to generate, accessible to everyone, with amplitude statistics that probe the nonlinear region well, and that can be consistently reproduced. This makes the uniform multi-tone a suitable choice for the linearity test signal standard.

3.1.3 The uniform multi-tone test signal standard

A standard linearity test signal requires appropriate memory and power excitation. Any properly designed multi-tone can excite the memory states and cover the full power range, but the nonlinear region coverage is dependent on the selected amplitude statistics.

A uniformly distributed multi-tone excites all amplitudes within the power range equally:

$$f_{\mathrm{X}}(x) = \frac{1}{2a}, \tag{3.4}$$

where a is the maximum amplitude allowed, and $x \in [-a, a]$. This asserts a similar excitation of small and large-signal dynamics, which optimizes the nonlinear region coverage. It also means that the signal PAPR is finite:

$$\mathrm{PAPR} = \frac{P_{\mathrm{peak}}}{P_{\mathrm{avg}}} = \frac{a^2}{\frac{a^2}{3}} = 3. \tag{3.5}$$

therefore, the uniform signal does not need to be cropped to fit the DAC range, which avoids quantization and resolution problems.

[1] Other signals can be used, but that study is outside the scope of this work.

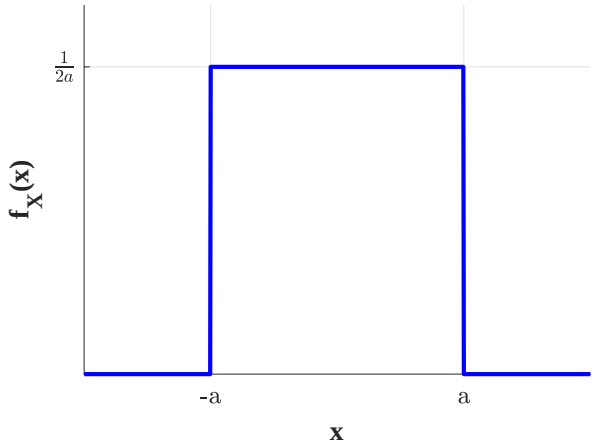

Figure 3.5: Theoretical uniform PDF.

3.1.4 Uniform vs Gaussian Linearity Metrics

The presented linearity test signal standards impose frequency domain and power range requirements on the input signal, but linearity metrics are influenced by how the selected statistics probe the power range. How can linearity metrics measured with different signal statistics be compared fairly? The influence of statistics on the system response must be isolated. This is achieved by fixing the spectrum and power range, and changing amplitude statistics. Fixing the power range means comparing linearity metrics at the same peak power. Fig. 3.6 shows, for uniform and Gaussian distributions, the difference in amplitude range between having signals with the same average power, or with the same peak power.

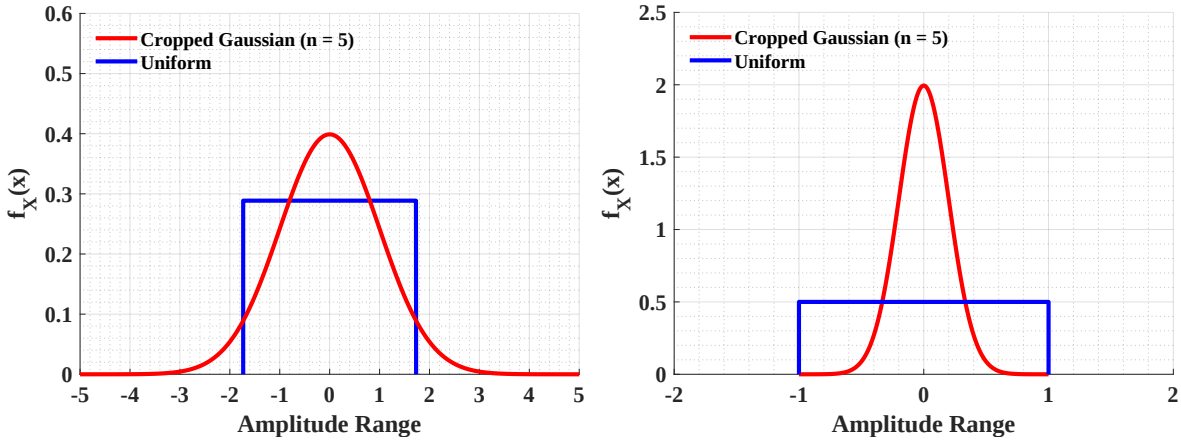

(a) Normalized average power.

(b) Normalized peak power.

Figure 3.6: Uniform vs Gaussian distribution amplitude range.

Fig. 3.7 plots linearity metrics measured at the output of the same RF system when excited with uniform and Gaussian multi-tone test signal standards that occupy the same power range [2]. The superior sensitivity to nonlinear power of the uniform multi-tone manifests in

[2]For characterization details, refer to [elmJ1, Sec. IV.], attached at the end of this chapter.

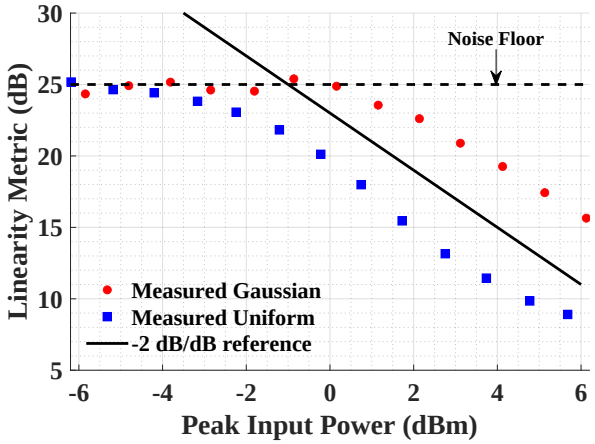

Figure 3.7: Uniform vs Gaussian linearity metrics same power range.

three ways: observable power range; metric value; and metric trend. The uniform linearity metric is observable at a lower power range, it only requires -2 dBm of peak power with the experimental setup used, whereas the Gaussian test signal requires 1 dBm. Also, the uniform metric is lower, meaning that it accumulates more nonlinear power. Finally, up to the maximum peak power measured, the Gaussian linearity metric trend only detects 3rd-order behaviors, evidenced by the 2 dB metric decrease per dB of input power, whereas the uniform metric can discern higher order behaviors as peak power goes beyond 1 dBm.

In short, the uniform multi-tone is better than the Gaussian for linearity characterization.

3.2 Expected Linearity Metric

Overcoming linearity metric test signal dependence means being able to predict and compare the linearity performance of a system under different test signal excitation without having to measure the system in those test conditions. In other words, being able to establish identities between metrics obtained with different test signals. ELM enables that.

3.2.1 The ELM definition

The response, y(t), of any nonlinear system can be divided into a linear, and a nonlinear response to the input signal, x(t):

$$y(t) = f[x(t)] = f_{\text{lin}}[x(t)] + f_{\text{nlin}}[x(t)] \tag{3.6}$$

A linearity metric aims to convey the average power ratio between the nonlinear response, and the linear response of a system over time. Therefore, the Expected Linearity Metric (ELM) is a principled way to define a linearity metric:

$$\text{ELM} = \frac{E[f_{\text{lin}}[x(t)]^2]}{E[f_{\text{nlin}}[x(t)]^2]}. \tag{3.7}$$

The expected values, $\text{E}[(\cdot)^2]$, can be computed as:

$$E[f[x(t)]^2] = \int_{-\infty}^{\infty} f[x(t)]^2 f_X(x)dx, \tag{3.8}$$

where $f_X(x)$ is the PDF of the test signal, x(t).

3.2.2 Measuring ELM

In the frequency domain [3], ELM is given by:

$$\text{ELM} = \frac{\int_{-\infty}^{\infty} S_{f_{\text{lin}}[x(t)]}(f)df}{\int_{-\infty}^{\infty} S_{f_{\text{nlin}}[x(t)]}(f)df}. \tag{3.9}$$

It is a CCPR like metric that also accounts for adjacent-channel distortion power, so, it can be measured using the feed-forward characterization technique depicted in Fig. 3.8.

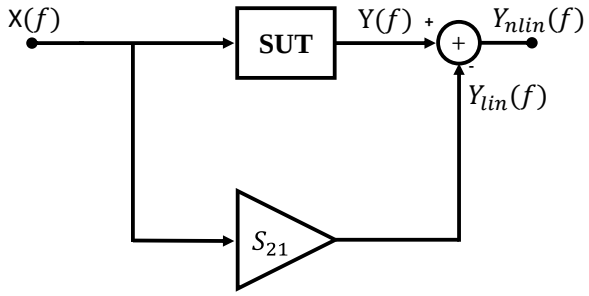

Figure 3.8: ELM feed-forward characterization technique.

The ELM measurement steps are the following:

- excite the System Under Test (SUT) with the test signal, X(f).
- observe the SUT response, Y(f);
- feed-forward $Y_{\text{lin}}(f)$ to extract $Y_{\text{nlin}}(f)$ from Y(f);
- compute ELM.

$Y_{\text{lin}}(f)$ is X(f) amplified by the small-signal S_{21} of the SUT. Input/output signals are generated/captured using the typical VSG/VSA setup presented in section 1.1.2.

The linearity metrics in Fig. 3.7 are ELM curves, obtained using this method.

3.2.3 Establishing ELM metric identities

According to (3.7), the ELM computation steps are:

- apply x(t) to $f_{lin}(\cdot)$, and compute the average power of the linear response;
- apply x(t) to $f_{nlin}(\cdot)$, and compute the average power of the nonlinear response;
- compute ELM.

[3] Note that $E[f[x(t)]] = \int_{-\infty}^{\infty} S_{f[x(t)]}(f)df$.

This link between the system, the input signal, and ELM is the key to establish linearity metric identities. With the system model, $f_{lin}(\cdot)$ and $f_{nlin}(\cdot)$, and the test signal waveform, $x(t)$, ELM is computable for any system, for any signal. For computation, the model must appropriately describe the nonlinear and dynamic behaviors of the system, and the waveform must be a numerical replica of the real test signal. With this, it is possible to relate and compare ELM for different test signals using simple and general math. Since $E[f_{nlin}[x(t)]^2]$ varies nonlinearly with input signal statistics, the ELM identities are, in general, nonlinear relations, not scalar factors.

Fig. 3.9 overlaps computed and measured ELM of the same RF system under uniform, and Gaussian multi-tone linearity test signal standard excitation[4]. The measurement and computed ELM are in agreement within 1 dB of error up to the measurement noise floor. This proves that ELM enables users to predict and relate linearity metrics obtained with different signal excitation without having to measure them in those test conditions.

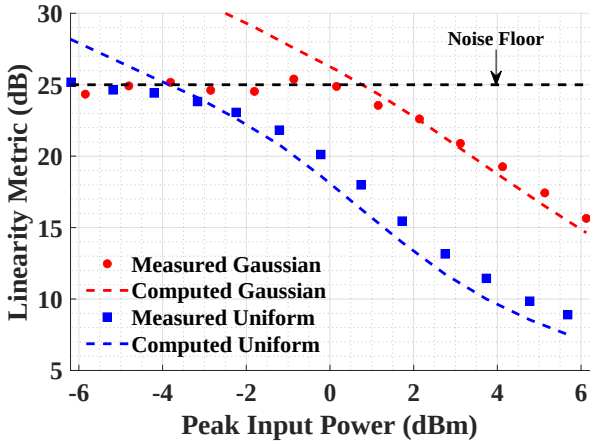

Figure 3.9: Measured and computed ELM curves.

The ELM approach is simple and effective. It solves the test signal dependence problem with the use system models, test signal waveforms, and average power computations. This simplification speeds up linearity characterization, and intermediate design stages. In some cases, a single measurement is enough; no need for power sweeps, nor to test for every signal [5].

3.2.4 ELM and communication signals

The argument for using communication signals in linearity characterization has been that they excite RF systems in real operation conditions. Without identities between linearity metrics, communication signals provide the desired application specific metric value.

Now, the ELM framework is capable of predicting linearity metrics under real modulated signals. Fig. 3.10 evidences that. Computed and measured ELM agree when the same RF system is under LTE signal excitation with different modulation schemes[6].

[4]For computation details, refer to [elmJ1, Sec. IV.], attached at the end of this chapter.

[5]In [elmJ1], one high-power measurement performed with the uniform multi-tone linearity test signal standard was enough to extract a model capable of correctly predicting linearity in all measured scenarios.

[6]The test signal is a R.7 reference channel LTE downlink frame, generated with MATLAB lteRMCDLTool. For more details, refer to [elmJ1, Sec. IV.], attached at the end of this chapter.

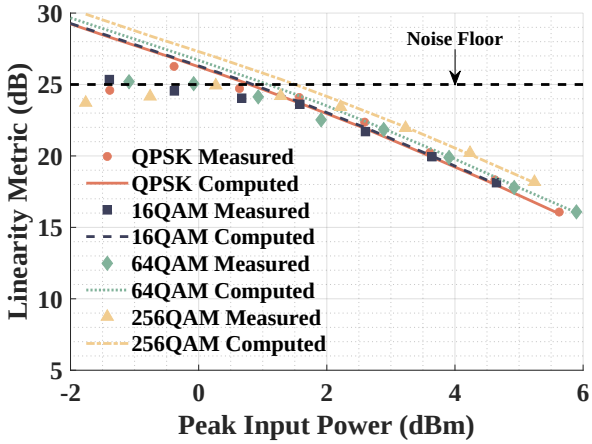

Figure 3.10: ELM metric evaluated under LTE excitation with different modulation schemes.

Note that when the modulation scheme changes, the linearity metric does not change significantly. As shown in Fig. 3.11, this happens because as modulation changes, the LTE signal maintains similar baseband amplitude statistics, the same frequency domain, and encodes information in the temporal-frequency grid. To retrieve the modulation scheme, the signal must be decoded, it is not observable at RF. Therefore, it is hard to relate RF linearity metrics with EVM without decoding.

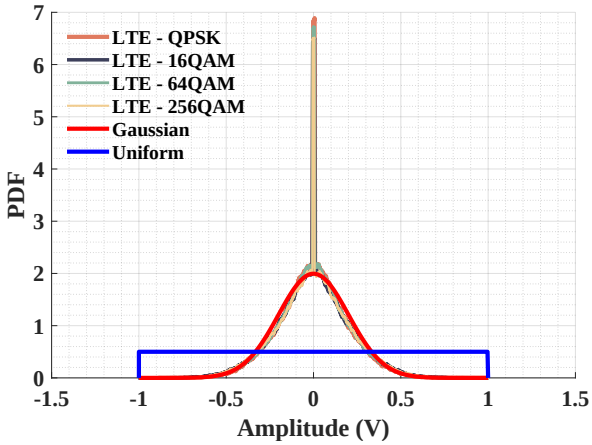

Figure 3.11: PDF of LTE signals with different modulation, and normalized peak power.

Furthermore, ELM effectively overcomes the past inability to relate linearity under multi-tone excitation with linearity in real communication scenarios. All the computed ELM results presented were obtained from a single high-power measurement of the RF system, excited with the uniform multi-tone test signal standard. With this measurement it was possible to accurately model the system and predict ELM under LTE excitation.

The takeaway is: to improve ELM predictive ability it is now more important to probe nonlinear behavior appropriately, than to mimic real communication signals. The combined used of ELM and the uniform multi-tone linearity test signal standard is a step towards a universal framework to measure and compare RF system linearity performance.

Support Articles

“Linearity Metrics and Signal Statistics - The Need for Standards”

Figueiredo and Carvalho

2022 IEEE/MTT-S International Microwave Symposium - IMS 2022

Linearity Metrics and Signal Statistics - The Need for Standards

Ricardo Figueiredo[#$1], Nuno Carvalho[#$2]
[#]DETI, Universidade de Aveiro, Portugal
[$]Instituto de Telecomunicações - Aveiro, Portugal
[1]ricardofigueiredo@ua.pt, [2]nbcarvalho@ua.pt

***Abstract*— Linearity metric dependence on signal statistics makes linearity requirements application specific, and hard to interpret and specify. This work presents and validates a simple method to relate linearity metrics obtained from signals with different statistical distributions, and evidences why specifying standard linearity test signals is so important to get universally traceable linearity metrics in microwave.**

***Keywords*— linearity, metrics, nonlinear distortion, statistics.**

I. Introduction

In microwave, it is consensual that system linearity must be tested close to real operation [1]. What is not well understood is how to make traceable measurements, that yield comparable linearity metrics, when different test signals are used.

Classically, noise loading techniques were used to test all possible system states. Solid theoretical foundation exists for Gaussian noise loading, which supports linearity metrics like noise power ratio, and co-channel power ratio (CCPR) [2], [3]. Alternatively, real communication test signals have the advantage of measuring linearity in real operation. Some works already developed methods to correctly characterize signal distortion under modulated signal conditions [4], but real communication signals are non-repeatable, therefore not suitable for a standard, and there is a lack theoretical support to interpret linearity metrics measured with non-Gaussian signals. Different statistical distributions produce different linearity metrics [5], [6], [7], [8], [9], [10], and there is no simple method to relate them.

So, how can we make traceable linearity measurements that provide comparable metrics? For that, we need standards to design linearity test signals, and we must establish identities between metrics obtained from different signals. To the authors' knowledge, no one has yet presented an easy method to achieve this. This work presents and validates a theoretical framework to compute linearity metrics at the output of any nonlinear static system for any test signal, that can relate metrics obtained from different signals, and makes important considerations about standards for linearity test signals.

II. Theoretical Framework

The response, $\mathrm{y(t)}$, of a general static nonlinear system to any excitation signal, $\mathrm{x(t)}$, can be given by [11]

$$y(t) = \sum_{n=1}^{\infty} a_n x(t)^n, \tag{1}$$

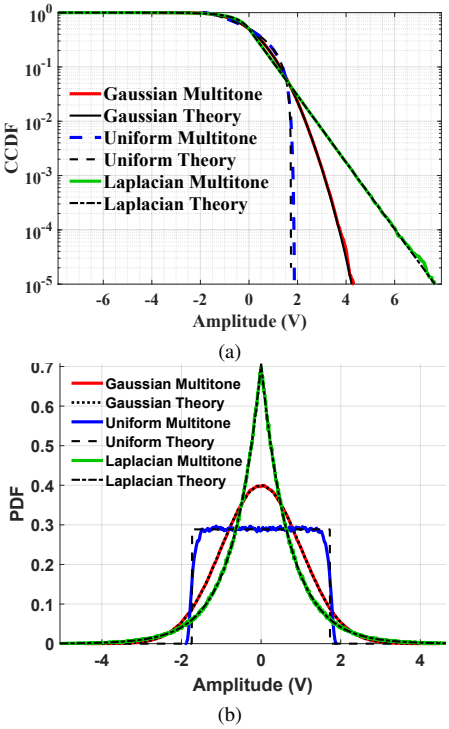

Fig. 1. Statistical distributions normalized to unitary average power: (a) complementary cumulative distribution function (CCDF); (b) PDF.

where $\mathrm{a_n}$ is the nth-order kernel. This response can be divided in linear and nonlinear responses, as described in (2) and (3).

$$y_{\mathrm{lin}}(t) = a_1 x(t) \tag{2}$$

$$y_{\mathrm{nlin}}(t) = \sum_{n=2}^{\infty} a_n x(t)^n \tag{3}$$

From (1) to (3), a baseband equivalent signal representation is assumed, so, only inband terms are contemplated.

Linearity metrics are power ratios computed from measurements of the system response over time. These depend on excitation signal statistics on an average sense [1].

From the average power of the moments of $x(t)$ [12]

$$E[(x(t)^n)^2] = \int_{-\infty}^{\infty} (x(t)^n)^2 f_X(x(t))\, dx, \tag{4}$$

where $f_X(x)$ is the probability density function (PDF) of $x(t)$, it is possible to define the expected linearity metric (ELM) as

the ratio of the average power of the linear response over the average power of the nonlinear response, as expressed in (5).

$$ELM = \frac{E[(a_1 x(t))^2]}{E[(\sum_{n=2k+1}^{\infty}(a_n x(t)^n))^2]}. \quad (5)$$

Likewise, average moment power can be computed from its power spectral density (PSD) [12], as follows:

$$E[(x(t)^n)^2] = \int_{-\infty}^{\infty} S_{x^n}(f)\ df. \quad (6)$$

So, in the presented formulation, that only contemplates the inband response, ELM is also given by (7).

$$ELM = \frac{\int_{min(f_{lin})}^{max(f_{lin})} S_{y_{lin}}(f)\ df}{\int_{min(f_{nlin})}^{max(f_{nlin})} S_{y_{nlin}}(f)\ df} \quad (7)$$

Equation (7) evidences that ELM is a CCPR like metric that also contemplates adjacent-channel distortion power.

By knowing the system kernels and the excitation distribution, (5) can be used to compute the ELM for any signal, and to compare metrics obtained from different signals in any desired conditions (e.g. same average/peak power). With (7) it is possible to validate experimentally the theoretical ELM by performing a CCPR like characterization [3].

Note that the presented formulation can be adapted to nonlinear dynamic system models, and that the use of CCPR characterization for ELM assessment, as presented here, is also valid for nonlinear dynamic systems.

III. Experimental Procedure

The ELM theory is valid if the ELM obtained from CCPR like characterization equals the theoretical ELM given by (5).

The experimental ELM is obtained by exiting the device under test (DUT) with $\mathrm{x(t)}$, and observing its response, $\mathrm{y(t)}$. Then, $\mathrm{y_{lin}(t)}$ and $\mathrm{y_{nlin}(t)}$ are obtained by subtracting from $\mathrm{y(t)}$ a replica of $\mathrm{x(t)}$ linearly amplified by the measured small-signal s-parameters of the DUT. Finally, ELM is obtained from (7). This is measured at several power levels.

The theoretical ELM is computed from (5) using a DUT model, which is extracted in a least-squares sense from a high-power input-output observation of $\mathrm{x(t)}$, and $\mathrm{y(t)}$.

Three statistical distribution excitations are used: Gaussian, uniform, and Laplacian. Each distribution is realized by a 2001 multitone with 10 MHz bandwidth. Thus, all signals are bandlimited and white. The multitone design follows the guidelines in [13]. It is assumed that the multitone sample is large enough to approximate the desired statistical PSD, which is reasonable, since its statistics agree with the theoretical definition, presented in [12], up to 10^{-5}, as shown in Fig. 1a.

The DUT is an ERA2+ power amplifier board from mini-circuits. It is biased with 7.3 V and $40\mathrm{mA}$. It is excited at 5.67 GHz. Its input 3 dB compression point is 3 dBm, and the measured $\mathbf{s_{21}}$ parameter is $10\angle 245°$.

The experimental setup, depicted in Fig. 2, consists of: a Keysight M8190A to generate the baseband signal; a

(a) (b)

Fig. 2. Measurement Setup: (a) Schematic; (b) Photo.

Keysight E8267D to up-convert the baseband signal to the desired carrier frequency; a Keysight N9041B for synchronous input/output baseband signal measurement; a TTI PL320QMD for DUT bias; and a computer for measurement automation.

IV. Experimental Result Analysis

Fig. 3 shows the input/output PSD for each distribution at an average input power of -9 dBm. Note that the same input PSD produces different output PSDs for each excitation. This evidences the importance of signal excitation, namely phase information, in intermodulation distortion profiles [14].

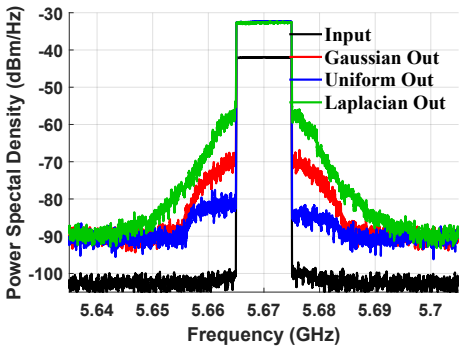

Fig. 3. Input and output PSD for each excitation distribution at -9 dBm average input power.

Fig. 4a and Fig. 4b show the theoretical and measured ELM versus average and peak power, respectively. The theoretical ELM is computed from a DUT model extracted with a high power uniform excitation measurement. Table 1 lists the model normalized mean squared error (NMSE) performance for each distribution. NMSE is given by (8).

$$NMSE_{dB} = 10\ \log\left(\frac{\sum |y_{meas}(t) - y_{model}(t)|^2}{\sum |y_{meas}(t)|^2}\right). \quad (8)$$

Table 1. NMSE @6dBm peak power of polynomial model extracted from uniform signal when tested with different signals.

Test Signal		
Gaussian	Uniform	Laplacian
-26 dB	-30 dB	-27 dB

Measured and theoretical ELM agree well until the experimental setup noise floor (25 dB metric range for Laplacian and Gaussian, 30 dB for uniform). The uniform

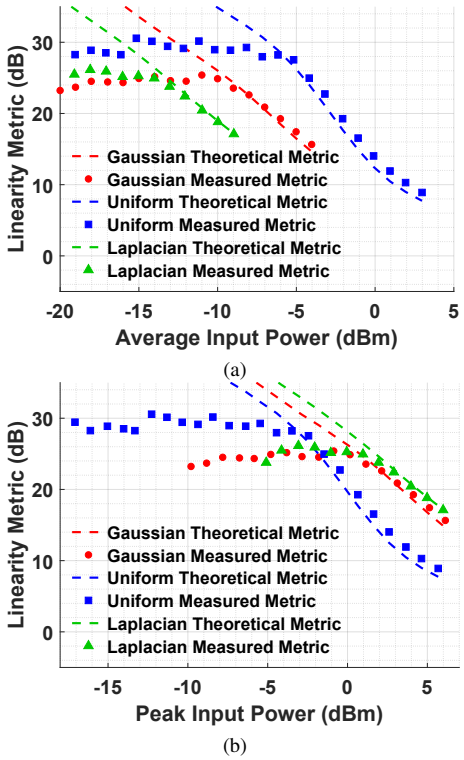

Fig. 4. Experimental and theoretical ELM for each tested distribution: (a) ELM vs average power; (b) ELM vs peak power.

distribution allows for a larger metric range because all power levels are equiprobable. Also, the uniform distribution allows for a greater dynamic power range for ELM assessment, both in terms of average power, and peak power. The peak power level was limited to 6 dBm to avoid damaging the DUT.

Lets interpret the metrics in light of the distributions used.

For equal average power, the uniform metric is better, because in that case it has much lower peak power than the Gaussian, and Laplacian distributions. The Laplacian metric is the worst since it has higher probability of high peak powers than the Gaussian. This is clearly depicted in Fig. 1b.

For equal peak power, the Laplacian metric is better because its instantaneous amplitude values are the most narrowly concentrated around zero. The uniform metric is the worst because it has the highest probability of high-power amplitudes. This can also be understood from Fig. 1b.

These metrics are easily relatable through (5). The proof is that theoretical ELM curves can correctly estimate the measured ELM up to the noise floor for any of the tested distributions, despite being computed from a model extracted from a single high-power uniform excitation measurement.

V. Final Discussion

This work provided tools to assess linearity under different signal excitation, and evidenced the issues of interpreting metrics without test signal standards. Similar distributions, like the Gaussian and Laplacian, have 1 dB ELM differences when assessed at the same peak power, but these can reach 6 dB when compared at the same average power. Direct comparisons are harder to make between unlike distributions. With the presented tool, this is now much easier, but for traceable linearity metrics, a standard test signal is still required! What distribution is most suited for this?

This initial work points towards the uniform distribution. It operates in a wider power range, it is easy to clearly define its peak power and generate it without clipping. Furthermore, it is hard to specify universal standards for Gaussian and Laplacian distributions. The theoretical amplitude ranges are infinite, where should they be truncated? How to avoid further generator clipping? Beyond this, these distributions have low probability of high power amplitudes, meaning that the nonlinear region is less probed when compared to a uniform distribution when the signals occupy the full DUT dynamic range, which is particularly problematic in dynamic scenarios.

Future art developments should aim to answer these questions, so that a standard linearity test signal can be defined, and so that we finally get traceable linearity metrics.

Acknowledgment

This work is funded by FCT/MCTES through national funds and when applicable co-funded EU funds under the project UIDB/50008/2020-UIDP/50008/2020. The work of Ricardo Figueiredo was supported by FCT and EU through FSE and Programa Operacional Regional Centro under Ph.D. Grant SFRH/BD/146935/2019.

References

[1] N. B. Carvalho, K. A. Remley, D. Schreurs, and K. G. Gard, "Multisine signals for wireless system test and design," *IEEE Microw. Mag.*, vol. 9, no. 3, pp. 122–138, 2008.

[2] R. W. Koch, "Random signal method of nonlinear amplitude distortion measurement," *IEEE Trans. Instrum. Meas.*, vol. IM-20, no. 2, pp. 95–99, 1971.

[3] J. C. Pedro and N. B. de Carvalho, "Characterizing nonlinear RF circuits for their in-band signal distortion," *IEEE Trans. Instrum. Meas.*, vol. 51, no. 3, pp. 420–426, 2002.

[4] J. Verspecht, A. Stav, J.-P. Teyssier, and S. Kusano, "Characterizing amplifier modulation distortion using a vector network analyzer," in *2019 93rd ARFTG Microwave Measurement Conference (ARFTG)*, 2019, pp. 1–4.

[5] V. Aparin, "Analysis of CDMA signal spectral regrowth and waveform quality," *IEEE Trans. Microw. Theory Techn.*, vol. 49, no. 12, pp. 2306–2314, 2001.

[6] J. Pedro and N. Carvalho, "Statistics of microwave signals and their impact on the response of nonlinear dynamic systems," in *Conference, 2003. Fall 2003. 62nd ARFTG Microwave Measurements*, 2003, pp. 143–153.

[7] K. Remley, "Multisine excitation for ACPR measurements," in *IEEE MTT-S International Microwave Symposium Digest, 2003*, vol. 3, 2003, pp. 2141–2144 vol.3.

[8] D. Schreurs, M. Myslinski, and K. Remley, "RF behavioural modelling from multisine measurements: influence of excitation type," in *33rd European Microwave Conference Proceedings*, vol. 3, 2003, pp. 1011–1014 Vol.3.

[9] K. M. Gharaibeh, K. G. Gard, and M. B. Steer, "The applicability of noise power ratio (NPR) in real communication signals," in *2006 67th ARFTG Conference*, 2006, pp. 251–253.

[10] G. Lasser, M. R. Duffy, and Z. Popović, "Dynamic dual-gate bias modulation for linearization of a high-efficiency multistage PA," *IEEE Trans. Microw. Theory Techn.*, vol. 67, no. 7, pp. 2483–2494, 2019.

[11] J. Pedro and S. Maas, "A comparative overview of microwave and wireless power-amplifier behavioral modeling approaches," *IEEE Trans. Microw. Theory Techn.*, vol. 53, no. 4, pp. 1150–1163, 2005.

[12] A. Leon-Garcia, *Probability, Statistics, and Random Processes for Electrical Engineering*. Pearson Education, 2008.
[13] J. Pedro and N. Carvalho, "Designing multisine excitations for nonlinear model testing," *IEEE Trans. Microw. Theory Techn.*, vol. 53, no. 1, pp. 45–54, 2005.
[14] R. Figueiredo, N. B. Carvalho, A. Piacibello, and V. Camarchia, "Nonlinear dynamic RF system characterization: Envelope intermodulation distortion profiles—a noise power ratio-based approach," *IEEE Trans. Microw. Theory Techn.*, vol. 69, no. 9, pp. 4256–4271, 2021.

"Linearity Metrics: Signal Statistics and Metric Identities"

Figueiredo, Pereira, Oliveira, and Carvalho

IEEE Transactions on Microwave Theory and Techniques

(under review)

Linearity Metrics: Signal Statistics and Metric Identities

Ricardo Figueiredo, *Graduate Student Member, IEEE*, Samuel S. Pereira, Arnaldo S. R. Oliveira, Nuno Carvalho, *Fellow, IEEE*

***Abstract*—This work proposes a uniformly distributed multi-tone linearity test signal standard to overcome the inconsistency problem of broadband linearity metric measurements that has impeded the establishment of a universally accepted framework to assess and compare RF system linearity. Beyond this, a novel linearity metric is proposed to solve the problem of linearity metric application dependence: the expected linearity metric (ELM). The ELM formulation allows it to be computed using simple and general math from the RF system behavioral model, and the test signal waveform. The experimental results show that by exciting an RF system with the proposed linearity test signal standard it is possible to use the input/output data from a single high power measurement to accurately predict the linearity performance of that system under different signal excitation. This is verified for LTE signals, which shows that the proposed approach effectively eliminates linearity metric application dependence. Our method provides consistent measurements, and enables a fair comparison of linearity performance between different systems, and relates linearity metrics between different test signals. In this document several guidelines are provided on how to best use ELM for different applications, being among the relevant remarks the use of ELM to objectively determine the input backoff required to meet desired linearity performance when using different signals.**

***Index Terms*—linearity, metrics, nonlinear distortion, statistics.**

I. Introduction

System linearity is key in modern wireless telecommunication technologies and standards [1]. They require robust linearity metrics capable of providing insightful requirements about the true limits of co-channel and adjacent channel distortion for correct system operation. Without this capability, linearity metrics become just blind marks that must be met to comply with the requirement list, but do not necessarily translate into tangible practical implications. A debilitating weakness of modern linearity characterization in this regard is the existent difficulty in making traceable measurements, that yield comparable linearity metrics, especially when different test signals are used. Two important reasons for this are the fact that there is no standard linearity characterization test signal, and that it is not easy to establish identities between linearity metrics obtained using different test signals.

The closest thing resembling a standard multi-tone linearity test signal in microwave applications is the use of Gaussian noise loading techniques. They are the base that supports linearity metrics like adjacent channel power ratio, noise power ratio, and co-channel power ratio [2], [3], [4]. In theory, it is easy to specify a Gaussian test signal, it only requires the specification of the average amplitude, which is zero in microwave applications, and the specification of the standard deviation, which is the average signal power. In practice, it is hard to guarantee repeatable linearity characterization using a Gaussian test signal. The work reported in [5], that presented a widely used linearity characterization setup, already mentions the very high metric variability that can be observed in measurements with Gaussian test signals, and the need to use large waveforms to mitigate such variation. Two major factors that difficult laboratory generation of Gaussian signals are their infinite amplitude range, and their low probability of high-power samples. Thus, despite the usefulness of Gaussian signals in microwave applications, it is desirable to have a more robust and repeatable test signal standard to trace linearity metric measurements; a test signal that can be accurately reproduced in any lab in the world, in any test conditions.

The nonexistence of identities to relate linearity metrics obtained with different test signals, allied with the need to assess system linearity close to real operation, lead to linearity characterization performed with modulated signals instead of Gaussian test signals. However, real communication signals are non-repeatable, therefore, they are also not suitable for a linearity test signal standard. Nonetheless, several works have efforted to relate nonlinear distortion with relevant modulated signal metrics like error vector magnitude (EVM) [6], [7], [8], [9], [10], [11], [12], and it is now possible to perform classical distortion characterization and correctly predict its influence on EVM under modulated signal conditions.

But linearity metrics measured with real communication signals are application dependent, they are only meaningful for that specific communication signal. Several studies report this test-signal/metric dependence. In [13], Aparin showed that the Gaussian approximation can be used to accurately predict the cross-modulation distortion of forward link CDMA

Manuscript received Month Day, Year; revised Month Day, Year; accepted Month Day, Year. Date of publication Month Day, Year; date of current version Month Day, Year. This work is funded by FCT/MCTES through national funds and when applicable co-funded EU funds under the project UIDB/50008/2020-UIDP/50008/2020. The work of Ricardo Figueiredo was supported by FCT and EU through FSE and Programa Operacional Regional Centro under Ph.D. Grant SFRH/BD/146935/2019. The work of Samuel S. Pereira was supported by FCT and EU through FSE and Programa Operacional Regional Centro under Ph.D. Grant SFRH/BD/14758/2019. *(Corresponding author: Ricardo Figueiredo.)*

Ricardo Figueiredo, Samuel S. Pereira, Arnaldo S. R. Oliverira, and Nuno Carvalho are with the Departamento de Eletrónica, Telecomunicações e Informática, Instituto de Telecomunicações, Universidade de Aveiro, Campus Universitário de Santiago, 3810-193 Aveiro, Portugal (e-mail: ricardofigueiredo@ua.pt; ; ; nbcarvalho@ua.pt).

Color versions of one or more of the figures in this article are available online at https://ieeexplore.ieee.org.

Digital Object Identifier

signals with a large number of channels, but that it is not accurate for reverse link CDMA signals. This has to do with differences in signal high-order statistical moments, that in the reverse link can produce differences in linearity just by alternating between OQPSK or QPSK modulation schemes. To be able to accurately predict linearity, the author had to specifically develop the theoretical statistical analysis of the CDMA signal. The study reported in [14] compared ACPR metrics measured with different multitone signals with ACPR metrics measured with real communication signals. The authors observed that multitone signals with similar PAPR to the real communication signal obtained better ACPR metrics, but none of the multitones was capable of reproducing the metric obtained with the real communication signal. In [15] it was shown that, for the same device, the NPR measured with an IS-95 signal differs more than 5 dB from the NPR measured using a Gaussian signal.

The influence of test signal on linearity metrics is now well-known, but it is not very well understood or studied. In [3] it is recognized that it is very complex to accurately describe real modulated signals mathematically, so this work proposes the use of a statistical representation of the signal to study linearity. This way, with the aid of a behavioral model it is possible to compute the auto-correlation function at the output of a nonlinear system, given the input signal statistics. This allows for the computation of linearity metrics at the system output. But the proposed approach, besides being mathematically complex, requires specific theoretical development for each input signal statistics that we might want to consider, making it hard to use. This is also the limitation of the statistical analysis presented in [13], it is specific to CDMA signals. The work reported in [16] laid out the initial steps on how to interpret linearity metrics in light of the amplitude statistics of the test signal used for measurement, evidencing the limitations of supporting the linearity analysis on simple statistical metrics like PAPR. In [17] it was added that to understand the linearity metrics imposed by a given test signal, it is not enough to look into the signal spectrum and the amplitude statistics, it is necessary to consider the temporal waveform as a whole, meaning that it is necessary to have in mind both the amplitude and phase of the test signal spectrum. Despite these relevant developments, there is still not enough insight to clearly interpret linearity metrics measured with different test signals, or to relate them.

All these linearity characterization limitations create critical overarching problems. Designers do not have a universal metric to reference their linearity improved designs. Manufacturers cannot provide complete linearity characterization of their products, as it is impracticable to test them with all communication signals. And application engineers cannot know a priori if a given device they purchase will comply to the linearity specifications of their application if that signal is not contemplated on the manufacturer's datasheet. Therefore, the specification of a robust standard linearity characterization test signal, and the establishment of identities between standard metrics and metrics obtained from modulated signals, is a fundamental step towards traceable linearity characterization.

In [18], we presented a simple theoretical framework to compute and relate linearity metrics at the output of any nonlinear static system for any test signal. Here, we expand our initial contribution in greater detail by:

- Providing a formulation that can contemplate dynamics;
- Addressing the specification of standard linearity characterization test signals, focusing on Gaussian, Laplacian, and uniform statistical distributions;
- Validating our approach using LTE signals;
- And providing guidelines to help designers, manufacturers, and application engineers to measure, provide, use, and interpret linearity metrics in practical scenarios.

This article is organized as follows. Section II expands on the theoretical formulation of signal statistics and linearity metric identities presented in [18]. Section III addresses the details of explicitly specifying linearity characterization test signals. Section IV presents the experimental validation of the article hypothesis with generic test signals, and modulated signals. Section V provides guidelines to use linearity metrics in an effective manner, according to user goals. At last, Section VI presents the final conclusion.

II. Linearity Metrics: Definition and Identities

The output signal, $\mathrm{y(t)}$, of a nonlinear system is a function of the input signal, $\mathrm{x(t)}$. This function can be divided into a linear, and a nonlinear response [19]:

$$y(t) = f[x(t)] = f_{\mathrm{lin}}[x(t)] + f_{\mathrm{nlin}}[x(t)] \tag{1}$$

Linearity metrics are defined as some kind of average power ratio between the linear response and the nonlinear response over time [20]. Knowing this, it is useful to define the expected linearity metric (ELM) as:

$$\mathrm{ELM} = \frac{E[f_{\mathrm{lin}}[x(t)]^2]}{E[f_{\mathrm{nlin}}[x(t)]^2]} = \frac{\int_{-\infty}^{\infty} S_{f_{\mathrm{lin}}[x(t)]}(f)df}{\int_{-\infty}^{\infty} S_{f_{\mathrm{nlin}}[x(t)]}(f)df}. \tag{2}$$

This definition uses the relation between average power, $\mathrm{E}[(\cdot)^2]$, and power spectral density (PSD) [21], $\mathrm{S(f)}$, to define ELM as a metric that can be interchangeably evaluated in the time-domain or in the frequency domain with ease. Recall that $\mathrm{E}[(\cdot)^2]$ can be computed as follows:

$$E[f[x(t)]^2] = \int_{-\infty}^{\infty} f[x(t)]^2 f_X(x)dx, \tag{3}$$

where $\mathrm{f_X(x)}$ is the probability density function PDF of $\mathrm{x(t)}$.

The ELM time-domain definition evidences the link between input-signal statistics, the system, and the linearity metric, independently of the signal or system used. This link is the key to understand how to compute and establish identities between linearity metrics obtained from different test signals.

Using a Volterra series representation of a general nonlinear dynamic system [22], $\mathrm{f_{lin}[x(t)]}$ and $\mathrm{f_{nlin}[x(t)]}$ are given by (4) and (5), respectively, where $\mathrm{y_{nlin}(t)}$ is given by (6).

$$f_{\mathrm{lin}}[x(t)] = \int_{-\infty}^{\infty} h_1(\tau)x(t-\tau)d\tau \tag{4}$$

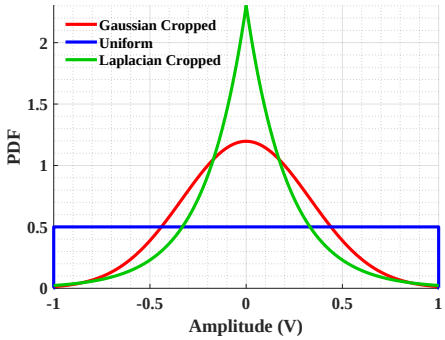

Fig. 1. Statistical distributions PDFs normalized to the same peak power.

$$f_{\mathrm{nlin}}[x(t)] = \sum_{n=2}^{\infty} y_{\mathrm{nlin}}(t) \tag{5}$$

$$\begin{aligned} y_{\mathrm{nlin}}(t) = \int_{-\infty}^{\infty} \cdots \int_{-\infty}^{\infty} h_n(\tau_1, \ldots, \tau_n) \cdot \\ \cdot x(t-\tau_1) \cdot \ \ldots \ \cdot x(t-\tau_n) \cdot d\tau_1 \cdot \ \ldots \ \cdot d\tau_n \end{aligned} \tag{6}$$

In the Volterra series, $\mathrm{h_n}$ is the nth-order system kernel, and τ_n is a temporal delay that spans the system memory. If the system is memoryless, ELM resorts to the formulation in [18].

By knowing the system kernels it is possible to compute the ELM for any signal. In other words, it is possible to predict and compare linearity metrics obtained from different test signals. But note that linearity metric identities are not scalar factors, they are nonlinear relations that vary with power. Using the presented formulation, if different input signals have the same average power and occupy the same spectrum, they have the same $\mathrm{E[f_{lin}[x(t)]^2]}$, but different $\mathrm{E[f_{nlin}[x(t)]^2]}$. The latter can only be the same if the signals are statistically identical [22]. Otherwise, the denominator in (2) varies nonlinearly according to the input signal statistics.

The frequency domain formulation resembles well-known metric definitions like ACPR, CCPR, and NPR. Thus, notched, feed-forward, or correlation based characterization techniques can be used to evaluate ELM experimentally [23], [24], [12]. In fact, when using a bandpass representation, ELM only contemplates in-band distortion components that are relevant for microwave applications, and becomes a CCPR like metric that also accounts for adjacent-channel distortion power.

In summary, for any test signal, ELM can be computed from the system model, and measured using well-known characterization procedures. But have in mind that ELM, as any other linearity metric, depends nonlinearly on the system under test and on the test signal. Therefore, direct ELM comparisons between different systems and signals are conveyed by the nonlinear relation in (2), not just by simple scalar factors.

III. Specifying Standard Linearity Test Signals

From system identification, we know that test signals must excite all relevant system states. Applying this principle to linearity characterization means guaranteeing an appropriate excitation of memory, and amplitude states [25]. To probe all relevant memory states, the test signal must cover the system spectral domain with sufficient resolution [23]. Covering the amplitude domain implies that the test signal must swing across the system full dynamic range. This is guaranteed by exciting the system at the average power that matches the signal peak power with the maximum instantaneous excitation power allowed by the system. But note that different amplitudes are probed differently according to the test signal PDF, $\mathrm{f_X(x)}$. Therefore, when specifying a linearity characterization standard, it is critical to have in mind signal characteristics like the PDF, dynamic range, and peak-to-average power ratio (PAPR), as well as their reproducibility in the laboratory.

Table. I presents the theoretical value of these signal characteristics for the well-known Gaussian, Laplacian, and uniform statistical distributions. The average power, peak power, and PAPR are respectively computed as follows:

$$\mathrm{P_{avg}} = \int_{-\infty}^{+\infty} x^2 f_X(x) dx, \tag{7}$$

$$\mathrm{P_{peak}} = max(|x|^2), \tag{8}$$

$$\mathrm{PAPR} = \frac{\mathrm{P_{peak}}}{\mathrm{P_{avg}}}. \tag{9}$$

In the Gaussian distribution, m stands for the average amplitude, and σ is the standard deviation. In the Laplacian distribution, λ is the decay factor. In the uniform distribution, a is the maximum amplitude allowed.

TABLE I
Distribution Statistical Characteristics.

	Gaussian	Laplacian	Uniform
$\mathrm{f_X(x)}$	$\frac{1}{\sqrt{2\pi}\sigma}\mathrm{e}^{\frac{-(\mathrm{x}-\mathrm{m})^2}{2\sigma^2}}$	$\frac{\lambda}{2}\mathrm{e}^{-\lambda\|\mathrm{x}\|},\ \lambda>0$	$\frac{1}{2\mathrm{a}}$
range	$\mathrm{x}\in(-\infty,\infty)$	$\mathrm{x}\in(-\infty,\infty)$	$\mathrm{x}\in[-\mathrm{a},\mathrm{a}]$
$\mathrm{P_{avg}}$	σ^2	$\frac{2}{\lambda^2}$	$\frac{\mathrm{a}^2}{3}$
$\mathrm{P_{peak}}$	∞	∞	a^2
PAPR	∞	∞	3

TABLE II
Criteria for Cropping Distributions

	Gaussian	Laplacian
$\mathrm{P_{peak_c}}$	$(\mathrm{n}\sigma)^2$	$\left(\frac{\ln(\mathrm{pct})}{\lambda}\right)^2$
$\mathrm{PAPR_c}$	n^2	$\frac{\ln(\mathrm{pct})^2}{2}$

At first glance, there is a clear difference between the uniform distribution and the reminder distributions in Table. I, it has a well-bound range, whereas the Gaussian and Laplacian distributions have an infinite dynamic range. The infinite amplitude range implies that it is impossible to generate a theoretical Gaussian/Laplacian signal. In practice its tail must be cropped. This raises questions about where to truncate the signal. For instrumentation grade standards, it must be guaranteed that the distribution is cropped at the same amplitude, in every realization. Otherwise, each realization is performed with a slightly different distribution. In theory, this

can be overcome by specifying a well-defined crop factor for each distribution, as suggested in the $\mathrm{P}_{\mathrm{peak_c}}$ column of Table. II. $\mathrm{P}_{\mathrm{peak_c}}$ specifies the cropped peak power at which $\mathrm{PAPR_c}$ is evaluated, n is the Gaussian distribution crop factor, defined in terms of σ, and pct is the Laplacian distribution crop factor, defined as a percentage of $\frac{\lambda}{2}$. But guaranteeing these crop conditions in the lab is not trivial at all! First, the cropped distribution must fit the DAC range, meaning that the longer the tail, the lower the resolution near the average power, where most of the signal samples are. Furthermore, if the average power is swept to assess the linearity metric, the generator will saturate differently at the high-power samples as power increases, leading to a further truncation of the tail, which cannot be precisely controlled, and that depends on the average signal power. The uniform distribution avoids all these problems, because it allows the maximum distribution amplitude to be set to the maximum instantaneous excitation power allowed by the system while providing a uniform quantization of all amplitude states. This makes PAPR a well-defined metric in practical uniform distributions, which is not the case for Gaussian/Laplacian distributions.

The low probability of high-power samples is another important limiting factor to consider when using Gaussian/Laplacian signals as linearity characterization test signal standards, because the high-power samples are the ones that inform about the system linearity. This means that Gaussian/Laplacian waveforms must be very large to contemplate all relevant high power amplitudes, which can create memory constraints in waveform generation and reception. This problem makes it hard to guarantee coverage of all relevant high power states of a nonlinear dynamic system. Once again, the uniform distribution overcomes this problem. It covers the system dynamic range with a uniform amplitude quantization that asserts that both small and large-signal dynamics are excited in a similar manner [26]. To evidence the better coverage of the uniform distribution of the high-power amplitude range, Fig. 1 plots the Gaussian, Laplacian, and uniform distribution PDFs for the same peak power, i.e. when the distributions cover the full system dynamic range.

In conclusion, any signal that complies with the aforementioned frequency domain, and temporal amplitude statistics requirements can be used as a test signal. When using distributions with infinite domains it is required to specify well-defined crop factors. Nonetheless, from a linearity characterization test-signal standard point of view, it makes sense to use amplitude statistics that adequately probe the large amplitude range that informs on the system nonlinear behavior. From the presented analysis, the uniform distribution is suited for such a standard. It samples all relevant amplitude and dynamic states equally, and its definition is sufficiently robust to allow repeatable and traceable linearity measurements. Note that uniform statistics differ from real communication signal statistics, but with the ELM, and its ability to relate metrics obtained from different signals, this is no longer as important as it was in the past. Now it is more important to probe nonlinear behavior appropriately, which improves the ELM predictive ability, than to mimic real communication signals.

Let's now discuss the standard linearity characterization signal type. Multi-tones are a good candidate for this standard. They are easily generated in any RF lab without the need for a license. They don't loose information in time-frequency domain conversions. And they can easily comply to the test signal requirements here stated. When using multi-tones, the memory state excitation can be asserted by assigning a number of equal magnitude tones that guarantees the required resolution frequency within the system pass-band. The desired amplitude statistics can be obtained following the multi-tone generation technique presented in [22]. The use of equal magnitude multitones is preferred, because it has been shown to make a better coverage of the amplitude states [25]. And, as will be shown in the following section, when properly designed, multi-tone test signals can be used with ELM to predict linearity under real communication scenarios.

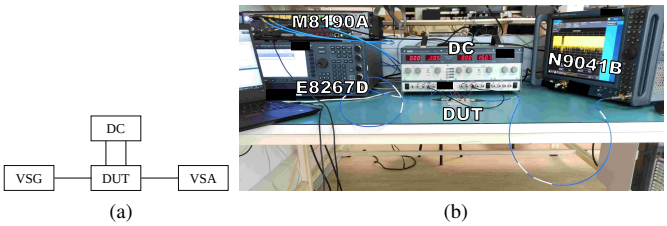

Fig. 2. Measurement Setup: (a) Schematic; (b) Photo.

IV. Experimental Validation

The goal of this experimental section is to validate that the measured ELM can be predicted/computed from an appropriate system model, and that this model can predict the measured ELM under different excitation signals, evidencing that the technique presented in this work is not only useful for multi-tone linearity test-signal standards, but also useful in real communication scenarios. Furthermore, this section expands on the impact that different linearity test signal standards have on the measured ELM with empirical evidence.

A. Device under test and experimental setup

All the system output response measurements presented in this work are measured at the output of an ERA2+ power amplifier board from mini-circuits. It is biased with 7.3 V and 40 mA, as recommended in the datasheet. It is excited at 5.67 GHz. Its input 3 dB compression point is 3 dBm, and the measured $\mathbf{s_{21}}$ parameter is $10\angle 245°$.

The s-paramenter measurements are obtained using a Keysight PNA-X N5242A, calibrated using a Keysight N7555A electronic calibration module.

The experimental setup used for linearity characterization is depicted in Fig. 2. It is a standard vector signal analysis bench which consists of: a Keysight M8190A to generate the baseband signal; a Keysight E8267D to up-convert the baseband signal to the desired carrier frequency; a Keysight N9041B for synchronous input/output baseband signal measurement; a TTI PL320QMD for device under test (DUT) bias; and a computer for measurement automation.

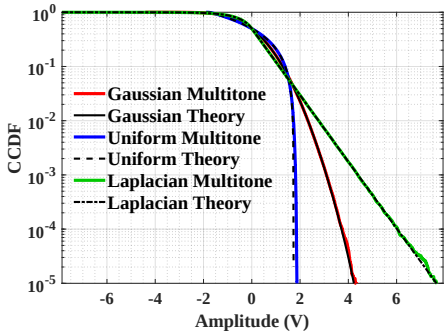

(a)

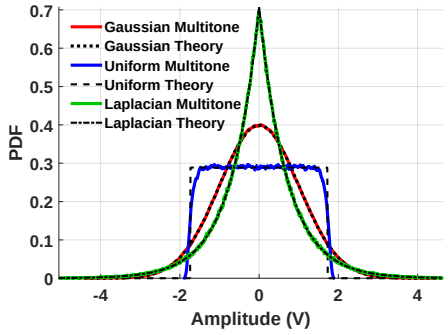

(b)

Fig. 3. Statistical distributions normalized to unitary average power: (a) complementary cumulative distribution function (CCDF); (b) PDF.

B. Linearity characterization test signals

The experimental validation is performed with two different signal types: multitone signals to study the impact of different linearity test signal standards in linearity metric measurements, and LTE signals to study ELM measurements in real communication scenarios.

1) Multitone test signals: A multitone test signal standard is designed for each of the statistical distributions studied in Section III: the Gaussian, the uniform, and the Laplacian distribution. Each distribution is realized by a 2001 multitone with 10 MHz bandwidth. Thus, all signals are bandlimited and white. The multitone design follows the guidelines in [22]. It is assumed that the multitone sample is large enough to approximate the desired statistical PSD, which is reasonable, since its statistics agree with the theoretical definition, presented in [21], up to 10^{-5}, as shown in Fig. 3a. Test signal input power is swept from -20 dBm of average power up to 6 dBm of peak power, which is assumed to be the maximum input peak power allowed before damaging the DUT. Note that this input peak power is near the 3 dB compression point when the device is operated at CW.

2) LTE test signals: The signal used is the LTE downlink reference measurement waveform. It is generated with the MATLAB lteRMCDLTool. The reference channel used is the R.7, which generates a baseband signal with 10 MHz bandwidth, covering the same frequency domain as the multitone test signals from the previous section. The LTE waveform used contains a full LTE frame with 10 ms duration. Different LTE signals are generated with the following modulation schemes: QPSK, 16QAM, 64QAM, and 256QAM. Fig. 4 shows the 16QAM example LTE waveform with normalized average power. For all LTE signals, input power is swept from -15 dBm of average power up to 6 dBm of peak power.

TABLE III
NMSE @6DBM PEAK POWER OF POLYNOMIAL MODEL EXTRACTED FROM UNIFORM SIGNAL WHEN TESTED WITH DIFFERENT SIGNALS.

Test Signal		
Gaussian	Uniform	Laplacian
-26 dB	-30 dB	-27 dB

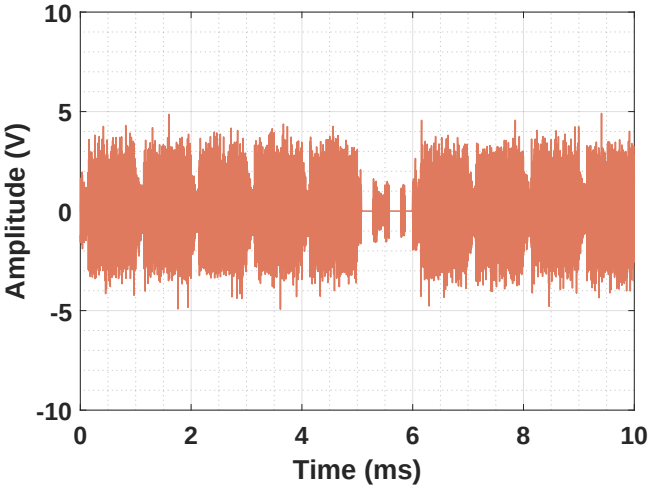

Fig. 4. Temporal sample of a LTE 16QAM frame with normalized average power.

C. ELM validation and predictive ability

To validate the proposed hypothesis, we defined specific and independent procedures to measure and compute the ELM.

The measured ELM is obtained using a feed-forward based linearity characterization technique as follows: first, using the experimental setup depicted in Fig. 2, we excite the DUT with the test signal, $\mathrm{x(t)}$, and observe its response, $\mathrm{y(t)}$; then, $\mathrm{y_{nlin}(t)}$ is obtained by subtracting $\mathrm{y_{lin}(t)}$ from $\mathrm{y(t)}$; finally, the ELM is obtained using (2). Note that $\mathrm{y_{lin}(t)}$ is a linearly amplified replica of $\mathrm{x(t)}$, and that the amplification factor is given by the measured small-signal $\mathrm{s_{21}}$ parameter of the DUT. This measurement procedure is repeated for each power level, for each test signal.

The theoretical ELM is computed using a model of the DUT. First, we excite the DUT with a uniform multi-tone linearity test signal standard that occupies the full system dynamic range, meaning that the signal peak power matches the DUT maximum input peak power, as suggested in Section III. Next, from a single input/output observation of the uniform multitone test signal we extract the DUT model in a least squares sense. A polynomial model in our example. Table III lists the model normalized mean squared error (NMSE) performance for each multitone test signal distribution used at the maximum input peak power. NMSE is given by (10).

$$NMSE_{dB} = 10\ \log\left(\frac{\sum |y_{meas}(t) - y_{model}(t)|^2}{\sum |y_{meas}(t)|^2}\right). \quad (10)$$

The aforementioned experimental steps are performed with Fig. 2 bench. Then, for each power level and test signal, a simulated replica of the experimental RF test signal is applied to the DUT model. The linear response is given by applying the test signal to the linear kernels, expressed in (4), and the nonlinear response is given by applying the test signal to the nonlinear kernels, expressed in (5). This guarantees that the ELM takes into account the temporal waveform as a whole - test signal spectrum amplitude and phase - as suggested in [17]. Finally, the theoretical ELM is computed using (2).

Fig. 6a and Fig. 6b show the theoretical and measured ELM for different multitone linearity test signal standards versus test signal average and peak power. And Fig. 7a and Fig. 7b show the theoretical and measured ELM for LTE test signals with different modulation schemes versus test signal average and peak power. The markers correspond to experimental measurement points, and the dashed lines to the theoretical predictions. For both signal types, the measured and theoretical ELM are in agreement within 1 dB of error up to the experimental setup noise floor. These results validate both our hypothesis, as well as the ELM predictive ability. Our hypothesis is validated because the computed ELM for the uniform multitone test signal with 6 dBm of input peak power agrees with the measured ELM for that signal, at that power level. Basically, we can correctly compute the ELM measured in the same conditions that the DUT is modeled. The ELM predictive ability is also validated because from the model extracted from a single high-power uniform multitone measurement it is possible to predict the ELM for uniform multitone test signals with lower power levels, and for different multitone and LTE test signals within the same power range. This proves that if the system model is sufficiently good within the excitation domain, it is possible to predict and relate ELMs for different test signals.

To the authors knowledge, this is the first time metric identities are successfully established between linearity metrics obtained with different test signals since the problem of linearity metric dependence on test signal was first mentioned in works like [13], [14], [15]. Note that contrarily to some previous state of the art works [3], [13], the presented approach does not require dedicated theoretical development for each test signal, and does not require complex mathematics like autocorrelation functions. Our approach just introduces system models, already extensively used in design and linearization applications, to aid linearity characterization, and performs average power measurements, that can be done with standard RF equipment such as power meters or VSAs.

Furthermore, these results are achieved with a simple DUT model, with lower performance than can be achieved by state of the art modeling strategies, as evidenced by Table. III. This means that the proposed strategy is sufficiently robust to make correct ELM predictions using simple models, and that it is likely possible to obtain even better results if state of the art models are used. But we must reinforce: our proposal is not model dependent. The ELM is always measured using the same well-defined experimental procedure presented above. This procedure does not depend on the system, nor on any model we may use to describe it. But to predict ELM in non-measured scenarios we obviously need a model that can appropriately describe the system. That can be any kind of model. Here, a simple polynomial model obtained from a single input/output measurement of the uniform multitone linearity test signal standard was enough to predict linearity for all the presented test scenarios. To the best of our knowledge, this has not been achieved before. This achievement allows us to speed up linearity characterization, and this may also speed up intermediate design stages. In some scenarios, like the one presented, a single measurement is enough. No need for power sweeps, nor to test for every signal.

A final note, the 25 dB ELM range observed in the experimental results is imposed by the feedforward setup used. ELM range can be increased by improving instrumentation.

D. Linearity test signal standards - experimental analysis

Before interpreting the experimental results plotted in Fig. 6 in light of the test signal distribution, first, take a look at Fig. 5, and realize the importance of the test signal in linearity assessment. Fig. 5 evidences that signals with the same input PSD, but different amplitude statistics produce different intermodulation distortion profiles [23]. It is important to remember that when assessing linearity. Not only average signal power matters, phase information is also very important.

Fig. 6a plots ELM against average input power. This is how linearity metrics are typically plotted, but have in mind that uniform, Gaussian, and Laplacian test signals cover different power ranges in this scenario, as evidenced by Fig. 3b. Also, Fig. 6a depicts that distributions with lower PAPR enable larger average input power observation domains. They can reach higher average powers without exceeding the maximum input power allowed by the system under test. This is obvious, but important. It justifies why the uniform distribution can reach higher average input powers.

By analyzing the individual ELM trend with average input power for each distribution we observe that ELM, like IMR and NPR [27], [28], can identify dominant nonlinear behaviors. Note that ELM decreases at a $2\ \mathrm{dB/dB}$ rate for the whole measurement range for the Gaussian and Laplacian signals. This indicates a dominant 3rd-order nonlinearity. For the uniform signal this is only observed up to $0\ \mathrm{dBm}$, beyond which ELM starts decreasing at a lower rate, which implies interference between 3rd and 5th order nonlinearities.

Let's now analyze the influence of signal statistics on the linearity metric. If we draw a vertical line in Fig. 6a to compare metrics at the same average power level, we obtain different values, and that difference is explained by the signal statistics. The uniform metric is the most linear, because, for the same average power, the uniform multitone signal has a much lower peak power than the Gaussian, and Laplacian signals. As previously stated, and as depicted in Fig. 3b, the power range of each signal is not the same. The Laplacian metric is the most nonlinear because the Laplacian signal has higher PAPR

and higher probability of occurrence of high power samples than the Gaussian signal, as shown in Fig. 3a.

If we now draw an horizontal line to know the average input excitation power level required to have the same linearity metric, we observe that ELM can help us predict the backoff level required when the system excitation signal is changed according to the application. Signals with higher PAPR require more backoff to have similar linearity requirements. But note that the backoff required is not equal to the signal PAPR, it depends on the dominant nonlinear behavior. For ELM values between 15-22 dB (i.e. the 3rd-order dominant region) the Gaussian signal, which has 10 dB PAPR, requires 3 dB backoff from the uniform test signal to have the same ELM. And the Laplacian signal, which has 15 dB PAPR, requires 7 dB of backoff. For example, to meet a 20 dB ELM linearity criterion, the uniform test signal can be excited up to -3.5 dBm of average input power, the Gaussian signal can only go up to -6.5 dBm, and the Laplacian signal up to -10.5 dBm. But in regions dominated by other nonlinear behaviors, the backoff levels required can differ. For instance, if we trust the model in the 25-30 dB ELM region, which is empirically bellow the noise floor, the theoretical curves indicate that in this region the required backoff levels are smaller.

Fig. 6b plots ELM against peak input power. In this unusual graph, linearity metrics along the same vertical line are given by test signals that cover the same system power range, as shown in Fig. 1. A brief analysis of Fig. 6b based on signal statistics tells us that in this scenario the uniform linearity metric is the least linear, because it has the highest probability of high power amplitudes, whereas the Laplacian metric is the most linear, because it has its amplitude samples most narrowly concentrated around zero.

Actually, Fig. 6b provides us a fair comparison of test signal standard sensitivity to nonlinear distortion power exactly because test signals along the same vertical line cover the same power range. The plotted curves evidence three reasons why the uniform test signal has the highest sensitivity to nonlinear power among the measured test signals: observable power range; metric value; and metric trend. The uniform linearity metric is observable (i.e. it is above the noise floor) at a lower power range. With our setup, it is possible to observe the uniform linearity metric with -2 dBm of peak power, whereas the Gaussian test signal requires 2 dBm, and the Laplacian 3 dBm. Also, at the same power range, (i.e. along the same vertical line), the uniform metric is lower, meaning that it accumulates more nonlinear power according to (2). Finally, up to the maximum peak power measured, the Gaussian and Laplacian linearity metric trends exhibit a 3rd-order behavior, 2 dB/dB, whereas the uniform metric, within the same power range, can discern higher order behaviors as peak power goes beyond 1 dBm. Furthermore, the uniform test signal PAPR is closer to CW and 2-tone signal PAPR [29], therefore, the use of the uniform signals can make narrowband and broadband linearity metrics easier to compare, because even though they do not cover the same frequency domain, they cover the power range in a more similar way than the Gaussian test signal.

Overall, these results and their analysis convey a very clear need: the need to specify a linearity test signal standard in order to consistently measure the same linearity metric when measuring the same device. Without such a standard, metrics can easily vary up to 6 dB for the same device, at the same input average or peak power values. And this is just from the small sample of signals analyzed in this work. How can we seriously specify and meet linearity requirements if there is room for such metric variation with slight statistical amplitude manipulation? This linearity test signal standard must be clearly definable in amplitude range and frequency domain, must probe the nonlinear region appropriately, and must be easy to generate in any RF lab. As experimentally validated here, the uniform multitone is a good candidate that meets the aforementioned criteria.

A final and important note regarding ELM and its predictive ability. Observe that the theoretical ELM curve remains true to the measured results even when higher-order effects enter into play. This is a major improvement on previous identities established between linearity metrics [30], [31], which were not only limited to Gaussian multitone signals, but also limited to 3rd-order nonlinearities.

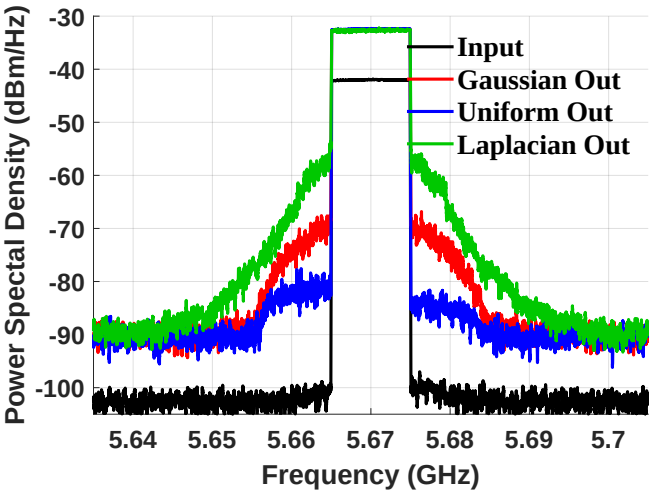

Fig. 5. Input and output PSD for each excitation distribution at -9 dBm average input power.

E. ELM in real communication scenarios

Finally, let's analyze ELM performance in real communication scenarios using LTE test signals.

The most important thing about Fig. 7 results, as already mentioned, is that the theoretical ELM agrees with the measured ELM. In other words, the ELM approach based on multitone signals is capable of predicting linearity metrics under real modulated signals. Meaning that with the ELM framework we have overcome the limitations found in the past to relate linearity under multitone excitation with linearity in real communication scenarios [14], [20].

The most surprising thing about Fig. 7 results, is that when the modulation scheme changes, the RF linearity metric does not change. To understand why that happens we must look into the baseband signal statistics. As shown in Fig. 8, despite the fact that signal modulation changes, the amplitude

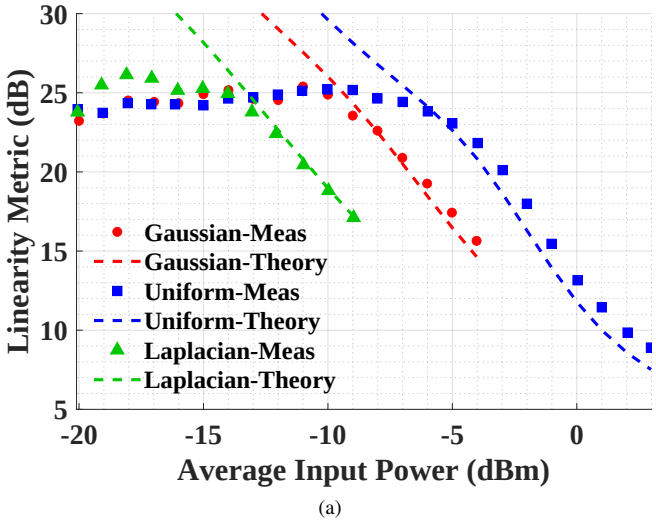

(a)

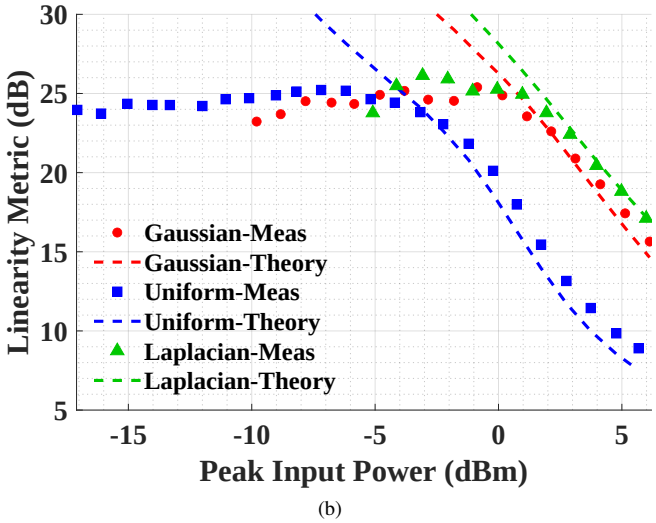

(b)

Fig. 6. Experimental and theoretical ELM for each tested distribution: (a) ELM vs average power; (b) ELM vs peak power.

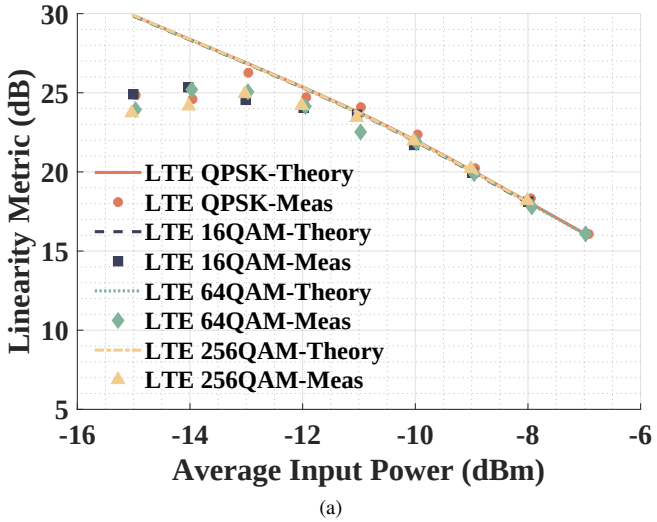

(a)

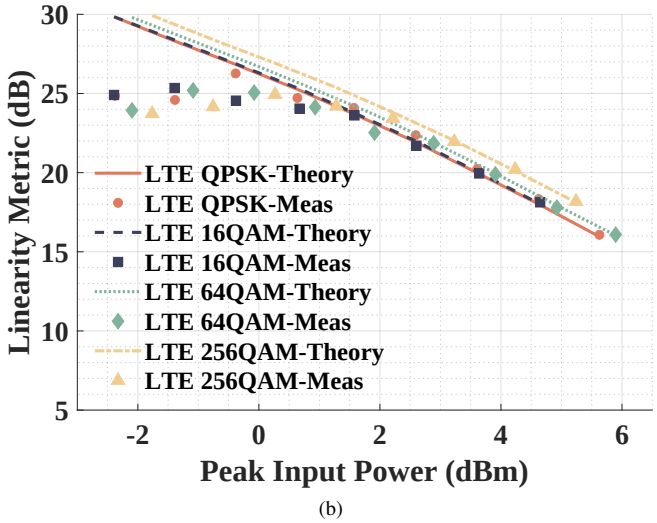

(b)

Fig. 7. Experimental and theoretical ELM for LTE signals with different modulation schemes (a) ELM vs average power; (b) ELM vs peak power.

statistics of the baseband LTE waveform remain the same. This has to do with the way LTE signals are generated. When modulation changes, the LTE signal maintains similar baseband amplitude statistics, the same frequency domain, and encodes information in the temporal-frequency grid. To retrieve the modulation scheme, the signal must be decoded, it is not directly observable at RF. This means that in some communication scenarios, that use OFDM, such as LTE applications, it is hard to relate RF linearity metrics with EVM without decoding.

After understanding this, the experimental results make sense. The LTE ELM manifests an intermediate linearity performance between Laplacian and Gaussian test signals, which is expected from the LTE signal statistics, whose distribution is in-between the Laplacian and the Gaussian distribution. The ELM trend also manifests dominant 3rd-order nonlinear behavior, as ELM decreases 2 dB/dB. The slight metric change with modulation scheme versus peak input power in Fig. 7b (less than 1 dB) has to do with the slight change in distribution near the maximum amplitude observed in Fig. 8a.

V. Guidelines for Broadband Linearity Metric Use

As mentioned in Section I, the lack of broadband linearity test signal standards to measure linearity metrics, and the lack of knowledge to establish identities between metrics obtained with different test signals, or the lack of knowledge to even compare and interpret such metrics, was a critical limitation of the broadband linearity characterization art. It hindered the fair assessment of system linearity performance, and it created overarching problems to designers, manufacturers, and application engineers who must make informed decisions and provide technical answers based on linearity metrics. Here we compile the most significant contributions of this work into guidelines to help linearity metric users make fair decisions.

A. Guidelines for designers

The job of RF system designers is to balance design parameters to meet performance requirements, like linearity.

Broadband linearity assessment has always been a challenge for designers. Without linearity test signal standards it is

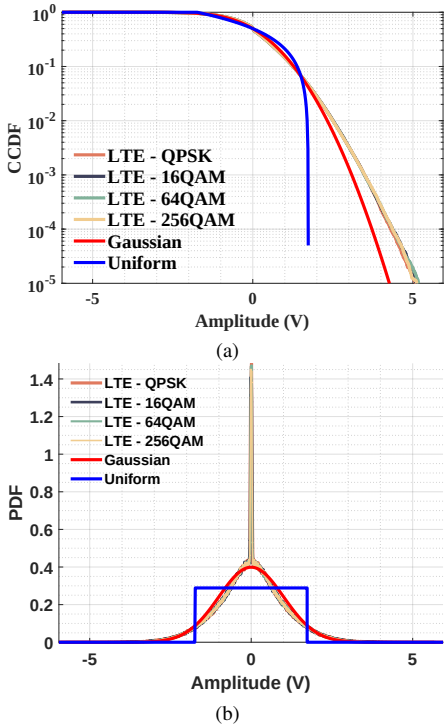

Fig. 8. LTE signal statistics normalized to unitary average power: (a) CCDF; (b) PDF.

hard to obtain consistent metric results, and to make fair linearity performance comparisons. Without metric identities, broadband linearity metrics become application specific, and there is no easy way to assert the absolute linearity performance of systems designed for different applications. In short, contrarily to narrowband linearity metrics, broadband linearity metrics were inconsistent. Therefore, the reluctance to abandon narrowband linearity optimization design strategies is understandable. But this work provides designers with some better answers, which can motivate the development of novel design strategies supported by broadband linearity metrics.

First, lets address metric consistency. As proved in Section IV, uniformly distributed signals are highly sensitive to nonlinearity. And, as suggested in Section III, a fair assessment of system linearity requires the excitation of all power and frequency states. Therefore, the ELM measured from the system response to a uniform test signal that forces the maximum limits of operation of the system - i.e. that excites the full power range and the full frequency band - is a consistent linearity performance indicator that can be used to guide design optimization. For example, the DUT measured in this work has a 9 dB ELM when excited with a uniform multitone test signal that forces its maximum limits of operation (6 dBm of peak input power). Devices with higher ELM at their limit of operation are more linear than the DUT here tested. By opposition, devices with lower ELM are less linear. As you can see, this metric provides an objective way to compare system linearity. But, of course, it must be considered in the context of other relevant system performance parameters, such as power, carrier frequency, and bandwidth.

The linearity metric application independence is achieved by the ELM formulation. Using (2) it is possible to easily predict and compare linearity performance for specific application scenarios. For that, we only require appropriate system models, and appropriate test signal descriptions. For instance, from the results presented in this work, it is possible to predict that the system under test, when excited with -9 dBm of average input power, has a 17 dB ELM for the Laplacian signal, a 24 dB ELM for the Gaussian signal, and a 21 dB ELM for the LTE signal. This solves the linearity performance comparison problem between systems designed for different applications. Also, it enables designers to understand, in intermediate design stages, the impact their decisions have on linearity performance for certain applications. This allows them to make design decisions that optimize linearity for specific applications, or to make compromises that provide the best overall linearity, regardless of the signal.

The aforementioned insights should be straightforward to incorporate in modern RF system design flows, and their usage will enable designers to understand better the broadband linearity dependence on design parameters, and their trade-offs with other performance requirements, which will ultimately potentiate better broadband RF system designs.

B. Guidelines for Manufacturers

Manufacturers must provide their customers with the linearity specification of their products, and in modern applications the broadband linearity performance is increasingly relevant.

Without ways to relate linearity metrics obtained with different test signals, manufacturers had no choice but to refrain to measuring linearity metrics with real communication signals. But this made the linearity performance specific to the selected application, which narrows the number of potential interest users. Manufacturers could try to circumvent this by performing linearity measurements with several interest signals, but this is cumbersome, time consuming, and impracticable, particularly if we have in mind the number of all possible interest communication signals.

Now, with the ELM and its ability to relate linearity metrics measured with different test signals, manufacturers only have to provide linearity metrics measured with a consistent linearity test signal standard, such as the uniformly distributed multitone, and a good behavioral model of their product. With this it is possible to predict the ELM for any signal using (2). Evidently, manufacturers should also complement their information with ELM measurements using some interest application test signals, as well as the theoretical predictions using (2). Therefore, the manufacturer datasheet data about linearity could include curves like the ones plotted in Fig. 6a

By using ELM, the number of potential users grows, because now users are equipped with an additional tool that helps them understand if a given product fits their linearity needs.

C. Guidelines for Application Engineers

The broadband linearity characterization limitations found by application engineers relate with the manufacturer guidelines from the previous section: in the past, if the manufacturer

datasheet did not specify broadband linearity for the application engineers are working on, they could not know if a given device met their linearity requirements before buying it. With ELM there are ways to circumvent this problem.

If the linearity metric for the desired application is provided by the manufacturer in a graph like Fig. 6a, application engineers only have to verify if the input level of backoff that meets the linearity requirement is complaint with all other application requirements. Lets say we need a 20 dB ELM, and that we are using a Gaussian signal in our application. Fig. 6a immediately tells the application engineer that this DUT can be used up to -7 dBm of average input power, which might, or might not, comply with other requirements, such as output power or efficiency.

On the other hand, if the linearity metric for the desired application is not provided in the manufacturer datasheet, application engineers can now input their signal into the manufacturer model, and simply compute ELM using (2). For instance, lets say we have the same 20 dB ELM specification, but that we are using LTE signals. By computing ELM from the DUT model, the application engineer would get the dashed lines in Fig. 7a, and would realize that he needs an additional 2 dB of input power backoff to meet the linearity requirement with this device, and would have tools to study how this impacts other application requirements.

ELM can make the life of application engineers easier in respect to broadband linearity performance interpretation.

VI. Conclusion

This work addressed the problem of broadband linearity metric consistency by detailing how to specify robust standard linearity test signals. This standard enables traceable and repeatable linearity measurements in the RF laboratory. This work also addressed the problem of linearity metric application dependence, by proposing the ELM formulation. ELM allows simple linearity metric computation from the system behavioral model and the test signal waveform.

Among the most relevant contributions of this work are:

- ELM as a linearity metric that can be interchangeably evaluated in the time and frequency domains, and that allows the comparison of linearity metrics obtained with different test signals through simple and general math.
- The insights on how test signal statistics affect linearity metrics, and on why the uniform test signal is more sensitive than the Gaussian test signal to nonlinear power.
- The proof and clarification that multitone test signal linearity measurements can be used to effectively predict linearity performance in real communication scenarios.
- ELM as a tool to objectively predict the required input power backoff to meet a desired linearity metric level.
- The guidelines for the best use of broadband linearity metrics by designers, manufacturers, and RF engineers.

The important takeaway from the study is that for linearity characterization purposes, and to support modeling, it is better to use uniformly distributed multitone linearity characterization test signals that fully excite all relevant system states, than to use Gaussian test signals, or real communication signals. The linearity performance in real operation can be predicted using ELM, or can also be complementary measured, but the guiding measurement to assess and compare linearity metrics should be performed with the uniform linearity characterization standard signal.

After stating this, the hope is that ELM becomes widely used as a broadband linearity characterization metric, and that the developments presented in this work can help motivate future research to effectively incorporate ELM as a design goal in the broadband RF system design flow.

References

[1] C. Fager, T. Eriksson, F. Barradas, K. Hausmair, T. Cunha, and J. C. Pedro, "Linearity and efficiency in 5g transmitters: New techniques for analyzing efficiency, linearity, and linearization in a 5g active antenna transmitter context," *IEEE Microw. Mag.*, vol. 20, no. 5, pp. 35–49, 2019.

[2] R. W. Koch, "Random signal method of nonlinear amplitude distortion measurement," *IEEE Transactions on Instrumentation and Measurement*, vol. IM-20, no. 2, pp. 95–99, 1971.

[3] K. Gard, H. Gutierrez, and M. Steer, "Characterization of spectral regrowth in microwave amplifiers based on the nonlinear transformation of a complex gaussian process," *IEEE Trans. Microw. Theory Techn.*, vol. 47, no. 7, pp. 1059–1069, 1999.

[4] J. C. Pedro and N. B. de Carvalho, "Characterizing nonlinear RF circuits for their in-band signal distortion," *IEEE Trans. Instrum. Meas.*, vol. 51, no. 3, pp. 420–426, 2002.

[5] T. Reveyrand, D. Barataud, J. Lajoinie, M. Campovecchio, J.-M. Nebus, E. Ngoya, J. Sombrin, and D. Roques, "A novel experimental noise power ratio characterization method for multicarrier microwave power amplifiers," in *55th ARFTG Conference Digest*, vol. 37, 2000, pp. 1–5.

[6] S.-W. Chen, W. Panton, and R. Gilmore, "Effects of nonlinear distortion on cdma communication systems," *IEEE Trans. Microw. Theory Techn.*, vol. 44, no. 12, pp. 2743–2750, 1996.

[7] K. M. Gharaibeh, K. G. Gard, and M. B. Steer, "Accurate estimation of digital communication system metrics-SNR, EVM and /spl rho/in a nonlinear amplifier environment," in *64th ARFTG Microwave Measurements Conference, Fall 2004.*, 2004, pp. 41–44.

[8] J. B. Sombrin, "On the formal identity of evm and npr measurement methods: Conditions for identity of error vector magnitude and noise power ratio," in *2011 41st European Microwave Conference*, 2011, pp. 337–340.

[9] P. Medrel, T. Reveyrand, A. Martin, P. Bouysse, J.-M. Nébus, and J. Sombrin, "Time domain envelope characterization of power amplifiers for linear and high efficiency design solutions," in *WAMICON 2013*, 2013, pp. 1–6.

[10] K. Freiberger, H. Enzinger, and C. Vogel, "A noise power ratio measurement method for accurate estimation of the error vector magnitude," *IEEE Trans. Microw. Theory Techn.*, vol. 65, no. 5, pp. 1632–1645, 2017.

[11] Y. Rolain, M. Zyari, E. Van Nechel, and G. Vandersteen, "A measurement-based error-vector-magnitude model to assess non linearity at the system level," in *2017 IEEE MTT-S International Microwave Symposium (IMS)*, 2017, pp. 1429–1432.

[12] J. Verspecht, A. Stav, J.-P. Teyssier, and S. Kusano, "Characterizing amplifier modulation distortion using a vector network analyzer," in *2019 93rd ARFTG Microwave Measurement Conference (ARFTG)*, 2019, pp. 1–4.

[13] V. Aparin, "Analysis of CDMA signal spectral regrowth and waveform quality," *IEEE Trans. Microw. Theory Techn.*, vol. 49, no. 12, pp. 2306–2314, 2001.

[14] K. Remley, "Multisine excitation for ACPR measurements," in *IEEE MTT-S International Microwave Symposium Digest, 2003*, vol. 3, 2003, pp. 2141–2144 vol.3.

[15] K. M. Gharaibeh, K. G. Gard, and M. B. Steer, "The applicability of noise power ratio (NPR) in real communication signals," in *2006 67th ARFTG Conference*, 2006, pp. 251–253.

[16] J. Sevic and M. Steer, "On the significance of envelope peak-to-average ratio for estimating the spectral regrowth of an rf/microwave power amplifier," *IEEE Trans. Microw. Theory Techn.*, vol. 48, no. 6, pp. 1068–1071, 2000.

[17] J. Pedro and N. Carvalho, "Statistics of microwave signals and their impact on the response of nonlinear dynamic systems," in *Conference, 2003. Fall 2003. 62nd ARFTG Microwave Measurements*, 2003, pp. 143–153.
[18] R. Figueiredo and N. Carvalho, "Linearity metrics and signal statistics - the need for standards," in *2022 IEEE MTT-S International Microwave Symposium (IMS)*, 2022.
[19] J. Pedro and S. Maas, "A comparative overview of microwave and wireless power-amplifier behavioral modeling approaches," *IEEE Trans. Microw. Theory Techn.*, vol. 53, no. 4, pp. 1150–1163, 2005.
[20] N. B. Carvalho, K. A. Remley, D. Schreurs, and K. G. Gard, "Multisine signals for wireless system test and design," *IEEE Microw. Mag.*, vol. 9, no. 3, pp. 122–138, 2008.
[21] A. Leon-Garcia, *Probability, Statistics, and Random Processes for Electrical Engineering*. Pearson Education, 2008.
[22] J. Pedro and N. Carvalho, "Designing multisine excitations for nonlinear model testing," *IEEE Trans. Microw. Theory Techn.*, vol. 53, no. 1, pp. 45–54, 2005.
[23] R. Figueiredo, N. B. Carvalho, A. Piacibello, and V. Camarchia, "Nonlinear dynamic RF system characterization: Envelope intermodulation distortion profiles—a noise power ratio-based approach," *IEEE Trans. Microw. Theory Techn.*, vol. 69, no. 9, pp. 4256–4271, 2021.
[24] J. Pedro and N. Carvalho, "A novel set-up for co-channel distortion ratio evaluation," in *2000 IEEE MTT-S International Microwave Symposium Digest (Cat. No.00CH37017)*, vol. 3, 2000, pp. 1851–1854 vol.3.
[25] D. Schreurs, M. Myslinski, and K. Remley, "RF behavioural modelling from multisine measurements: influence of excitation type," in *33rd European Microwave Conference Proceedings*, vol. 3, 2003, pp. 1011–1014 Vol.3.
[26] N. De Carvalho and J. Pedro, "Large- and small-signal imd behavior of microwave power amplifiers," *IEEE Trans. Microw. Theory Techn.*, vol. 47, no. 12, pp. 2364–2374, 1999.
[27] J. C. Pedro and N. B. Carvalho, *Intermodulation distortion in microwave and wireless circuits*. Artech House, 2003.
[28] R. W. Koch, "Random signal method of nonlinear amplitude distortion measurement," *IEEE Trans. Instrum. Meas.*, vol. IM-20, no. 2, pp. 95–99, 1971.
[29] R. Figueiredo and N. Carvalho, "Two-tone signals harmonic conditions for papr variation," in *2022 International Workshop on Integrated Nonlinear Microwave and Millimetre-Wave Circuits (INMMiC)*, 2022, pp. 1–3.
[30] J. C. Pedro and N. B. De Carvalho, "On the use of multitone techniques for assessing RF components' intermodulation distortion," *IEEE Trans. Microw. Theory Techn.*, vol. 47, no. 12, pp. 2393–2402, 1999.
[31] N. B. De Carvalho and J. C. Pedro, "Compact formulas to relate acpr and npr to two-tone imr and ip3," *Microwave Journal*, vol. 42, no. 12, pp. 70–70, 1999.

Ricardo Figueiredo (Graduate Student Member, IEEE) was born in Viseu, Portugal, in 1995. He received the M.Sc. degree in electronics and telecommunications engineering from the Universidade de Aveiro, Aveiro, Portugal, in 2018, where he is currently pursuing the Ph.D. degree in electrical engineering.

He is currently a Researcher at the Instituto de Telecomumicações, Aveiro. His main research interests include nonlinear instrumentation and nonlinear characterization of microwave systems.

Mr. Figueiredo a is member of the IEEE MTT-S Student Branch Chapter at Universidade de Aveiro.

Samuel S. Pereira (Graduate Student Member, IEEE) was born in 1995 in the city of Albergaria-a-Velha. In 2018 he finished his MSc degree in Electrical and Telecommunications Engineering from the University of Aveiro, Aveiro, Portugal. Since then, he is working for his PhD in Electrical Engineering at the same university. His main research interests include reconfigurable systems and communication systems and he is currently working on the development of delta-sigma based transmitters. He also worked with C-RAN applications for 5G, radio-over-Fiber systems and optical upconversion.

Nuno Carvalho (Fellow, IEEE) was born in Luanda, Angola, in 1972. He received the Diploma and Doctoral degrees in electronics and telecommunications engineering from the University of Aveiro, Aveiro, Portugal, in 1995 and 2000, respectively.

He is currently a Full Professor and a Senior Research Scientist with the Institute of Telecommunications, University of Aveiro and an IEEE Fellow. He coauthored Intermodulation in Microwave and Wireless Circuits (Artech House, 2003), Microwave and Wireless Measurement Techniques (Cambridge University Press, 2013), White Space Communication Technologies (Cambridge University Press, 2014) and Wireless Power Transmission for Sustainable Electronics (Wiley, 2020). He has been a reviewer and author of over 200 papers in magazines and conferences. He is the Editor in Chief of the Cambridge Wireless Power Transfer Journal, an associate editor of the IEEE Microwave Magazine and former associate editor of the IEEE Transactions on Microwave Theory and Techniques and IET Microwaves Antennas and Propagation Journal. He is the co-inventor of six patents. His main research interests include software-defined radio front-ends, wireless power transmission, nonlinear distortion analysis in microwave/wireless circuits and systems, and measurement of nonlinear phenomena. He has recently been involved in the design of dedicated radios and systems for newly emerging wireless technologies.

Dr. Borges Carvalho is a member of the IEEE MTT ADCOM, the past-chair of the IEEE Portuguese Section, MTT-20 and MTT-11 and also belong to the technical committees, MTT-24 and MTT-26. He is also the vice-chair of the URSI Commission A (Metrology Group). He was the recipient of the 1995 University of Aveiro and the Portuguese Engineering Association Prize for the best 1995 student at the University of Aveiro, the 1998 Student Paper Competition (Third Place) of the IEEE Microwave Theory and Techniques Society (IEEE MTT-S) International Microwave Symposium (IMS), and the 2000 IEE Measurement Prize. He is a Distinguished Lecturer for the RFID-Council and was a Distinguished Microwave Lecturer for the IEEE Microwave Theory and Techniques Society.

Chapter 4

Conclusion

To wrap up, lets make a brief critical overview of the presented work, focusing on its major state of the art contributions, its limitations, and potential future work directions.

4.1 Major Contributions

This work contributed to NPR, nonlinear dynamic characterization, and linearity metrics[1]. The major contributions to each topic are succinctly summarized in the following bullet points.

NPR contributions:

- Evidenced the limitations of using classical NPR, and multi-notch NPR to characterize linearity in nonlinear dynamic scenarios with theory, simulation, and experiments.
- Provided theoretical support to the use of multi-tones with different statistics, and different number of tones to assess NPR.
- Developed swept NPR to measure nonlinear dynamics and linearity simultaneously in nonlinear dynamic scenarios.

Nonlinear dynamic characterization contributions:

- Demonstrated theoretically the limitation of classical mechanism based approaches to nonlinear dynamic characterization in broadband excitation scenarios.
- Developed a tool to detect nonlinear dynamics under broadband excitation: the static IMD reference profile. Nonlinear dynamics are detected by computing the dynamic error between the measured system nonlinear response, and the static IMD profile.

Linearity metric contributions:

- Laid out procedures to define linearity test signal standards that guarantee consistent linearity metric measurements.
- Defined two linearity metrics: SNDR and ELM.

[1] All published works, properly grouped in research topics, are listed in the Published Works chapter.

- Enabled, with ELM, the comparison of linearity metrics measured with different test signals, regardless of the test signal, and regardless of the system under test.

In hindsight, the contributions of this work have improved multi-tone linearity characterization techniques, and metrics. It is now possible to detect nonlinear dynamics under broadband excitation, and linearity test signal standards, allied with ELM, are a step towards a universal framework to assess and compare RF system linearity.

4.2 Limitations

This work, as any, has technical and scope limitations.

The technical limitations are mostly related with the practical implementation of the proposed solutions. The most relevant technical limitations are:

- The swept NPR procedure requires a large number of measurements. This is complex and time consuming, and might not be feasible in some practical scenarios.
- It is not obvious how to correctly define a static IMD reference profile in practice.
- It is hard to implement linearity test signal standards in practice, because it is hard to convince everyone to follow the proposed methodology.

The scope limitations are imposed by the assumptions made in this work. They limit the use of the presented techniques in the context of some relevant RF systems and applications. The most limiting assumption is the single input, single output analysis of RF system linearity. This excludes Multiple Input Multiple Output (MIMO) systems, which are increasingly relevant [30]. Beyond this, the bias and loading conditions, neglected in this work, are also relevant in MIMO RF systems.

But note that these limitations do not subtract the value added by the aforementioned contributions, that solved existing RF system linearity characterization problems. They merely frame the range of applicability of this work, and obviate how its impact can be further amplified by leaving open and clear future work opportunities.

4.3 Future Work

Many future RF systems will be massive MIMO systems with large active antenna arrays [30]. Therefore, future work should aim to expand the contributions here presented to MIMO RF system linearity characterization, which implies the following developments:

- appropriately define multiple input linearity test signals;
- define linear, and nonlinear responses per each output port;
- assess linearity per channel;
- understand how to assess system linearity globally.

However, real MIMO RF systems are not ideal. The lack of port isolation, imposed by the practical implementation need for high integration, introduces coupling/crosstalk effects between the system ports. Coupling effects affect linearity by introducing both loading and bias drift [58, 59]. These inputs must be considered in future developments. Furthermore, system integration also implies loss of access to individual input/output ports. MIMO RF system linearity characterization must be performed Over the Air. This adds enormous complexity to linearity characterization because, now, the linear and nonlinear responses are radiated differently into space, following distributions that are not well understood [60–62]. This means that a spatial dimension must be added to linearity characterization.

Another relevant pathway for future work is to improve RF system design. Many modern RF systems continue to be designed using CW and two-tone signals [63–65]. Multi-tones are mostly used for the final experimental validation. This happens because designers lack insight on how multi-tone linearity metrics can be used to guide and improve their designs. Some worked to understand the important system design trade-offs between linearity, efficiency, and output power under multi-tone excitation [20, 66, 67]. Now, to enable first pass design for modern RF applications, it is necessary to incorporate the nonlinear dynamic analysis here presented, and develop a framework to perform RF system design informed by multi-tone RF system linearity in a seamless way to designers.

References

[1] Anna Piacibello et al. “A 5-W GaN Doherty Amplifier for Ka-Band Satellite Downlink With 4-GHz Bandwidth and 17-dB NPR”. In: *IEEE Microwave and Wireless Components Letters* 32.8 (2022), pp. 964–967. DOI: 10.1109/LMWC.2022.3160227.

[2] Anna Piacibello et al. “Linearity-aware design of Doherty power amplifiers”. In: *2019 IEEE MTT-S International Microwave Conference on Hardware and Systems for 5G and Beyond (IMC-5G)*. 2019, pp. 1–3. DOI: 10.1109/IMC-5G47857.2019.9160390.

[3] Patrícia Bouça et al. “Intermodulation Distortion Analysis of Microwave Tunable Filters Using Barium Strontium Titanate Capacitor and Varactor Diode”. In: *2020 15th European Microwave Integrated Circuits Conference (EuMIC)*. 2021, pp. 205–208.

[4] Patrícia Bouça et al. “Barium Strontium Titanate Thick Films for Tunable Software-Defined Radio Front-Ends”. In: *2021 IEEE MTT-S International Microwave Symposium (IMS)*. 2021, pp. 258–261. DOI: 10.1109/IMS19712.2021.9574935.

[5] Patrícia Bouça et al. “Design and Characterization of Novel Barium Strontium Titanate Thick Films for Sub-6 GHz RF Applications”. In: *IEEE Transactions on Microwave Theory and Techniques* 70.1 (2022), pp. 611–621. DOI: 10.1109/TMTT.2021.3125030.

[6] Patrícia Bouça et al. “Reconfigurable Three Functional Dimension Single and Dual-Band SDR Front-Ends Using Thin Film BST-Based Varactors”. In: *IEEE Access* 10 (2022), pp. 4125–4136. DOI: 10.1109/ACCESS.2022.3140686.

[7] JI Upshur et al. “Evaluation of linearity characterization techniques for multicarrier solid-state power amplifiers”. In: *1999 IEEE MTT-S International Topical Symposium on Technologies for Wireless Applications (Cat. No. 99TH8390)*. IEEE. 1999, pp. 47–52. DOI: 10.1109/MTTTWA.1999.755127.

[8] J.C. Pedro and N.B. Carvalho. “A novel set-up for co-channel distortion ratio evaluation”. In: *2000 IEEE MTT-S International Microwave Symposium Digest (Cat. No.00CH37017)*. Vol. 3. 2000, 1851–1854 vol.3. DOI: 10.1109/MWSYM.2000.862341.

[9] Roland W. Koch. “Random Signal Method of Nonlinear Amplitude Distortion Measurement”. In: *IEEE Transactions on Instrumentation and Measurement* IM-20.2 (1971), pp. 95–99. DOI: 10.1109/TIM.1971.5570700.

[10] G.L. Heiter. "Characterization of Nonlinearities in Microwave Devices and Systems". In: *IEEE Transactions on Microwave Theory and Techniques* 21.12 (1973), pp. 797–805. DOI: 10.1109/TMTT.1973.1128134.

[11] J.C. Pedro and N.B. De Carvalho. "On the use of multitone techniques for assessing RF components' intermodulation distortion". In: *IEEE Transactions on Microwave Theory and Techniques* 47.12 (1999), pp. 2393–2402. DOI: 10.1109/22.808986.

[12] A. Geens et al. "Discussion on fundamental issues of NPR measurements". In: *IEEE Transactions on Instrumentation and Measurement* 52.1 (2003), pp. 197–202. DOI: 10.1109/TIM.2002.808034.

[13] S.-W. Chen, W. Panton, and R. Gilmore. "Effects of nonlinear distortion on CDMA communication systems". In: *IEEE Transactions on Microwave Theory and Techniques* 44.12 (1996), pp. 2743–2750. DOI: 10.1109/22.554660.

[14] Yves Rolain et al. "A measurement-based error-vector-magnitude model to assess non linearity at the system level". In: *2017 IEEE MTT-S International Microwave Symposium (IMS)*. 2017, pp. 1429–1432. DOI: 10.1109/MWSYM.2017.8058887.

[15] Jacques Sombrin and Pierre Medrel. "Cross-correlation method measurement of error vector magnitude and application to power amplifier non-linearity performances". In: *2016 88th ARFTG Microwave Measurement Conference (ARFTG)*. 2016, pp. 1–4. DOI: 10.1109/ARFTG.2016.7839726.

[16] Jan Verspecht et al. "Characterizing Amplifier Modulation Distortion Using a Vector Network Analyzer". In: *2019 93rd ARFTG Microwave Measurement Conference (ARFTG)*. 2019, pp. 1–4. DOI: 10.1109/ARFTG.2019.8739226.

[17] Jose Carlos Pedro and Nuno Borges Carvalho. "A novel nonlinear distortion characterisation standard for RF and microwave communication systems". In: *Engineering Science & Education Journal* 10.3 (2001), pp. 113–119.

[18] José Carlos Pedro and Nuno Borges Carvalho. *Intermodulation distortion in microwave and wireless circuits*. Artech House microwave library. Artech House, 2003. ISBN: 9781580533560.

[19] Nuno Borges Carvalho and Dominique Schreurs. *Microwave and wireless measurement techniques*. Cambridge University Press, 2013. ISBN: 9781107004610.

[20] T. Reveyrand et al. "A Novel Experimental Noise Power Ratio Characterization Method for Multicarrier Microwave Power Amplifiers". In: *55th ARFTG Conference Digest*. Vol. 37. 2000, pp. 1–5. DOI: 10.1109/ARFTG.2000.327395.

[21] Nuno B. Carvalho et al. "Multisine signals for wireless system test and design [Application Notes]". In: *IEEE Microwave Magazine* 9.3 (2008), pp. 122–138. DOI: 10.1109/MMM.2008.919938.

[22] P. Medrel et al. "Time domain envelope characterization of power amplifiers for linear and high efficiency design solutions". In: *WAMICON 2013*. 2013, pp. 1–6. DOI: 10.1109/WAMICON.2013.6572774.

[23] Saeed Farsi et al. “Characterization of Intermodulation and Memory Effects Using Offset Multisine Excitation”. In: *IEEE Transactions on Microwave Theory and Techniques* 62.3 (2014), pp. 645–657. DOI: 10.1109/TMTT.2014.2302745.

[24] J. Schoukens and T. Dobrowiecki. “Design of broadband excitation signals with a user imposed power spectrum and amplitude distribution”. In: *IMTC/98 Conference Proceedings. IEEE Instrumentation and Measurement Technology Conference. Where Instrumentation is Going (Cat. No.98CH36222)*. Vol. 2. 1998, 1002–1005 vol.2. DOI: 10.1109/IMTC.1998.676874.

[25] J.C. Pedro and N.B. Carvalho. “Designing band-pass multisine excitations for microwave behavioral model identification”. In: *2004 IEEE MTT-S International Microwave Symposium Digest (IEEE Cat. No.04CH37535)*. Vol. 2. 2004, 791–794 Vol.2. DOI: 10.1109/MWSYM.2004.1339082.

[26] Su Jiangtao, J. Benedikt, and P. J. Tasker. “A new method for the design of multi-sine excitations for the assessment of non-linear devices”. In: *2008 IEEE MTT-S International Microwave Symposium Digest*. 2008, pp. 265–268. DOI: 10.1109/MWSYM.2008.4633154.

[27] Minsheng Li et al. “Accurate multisine representation of digital communication signals for characterization of nonlinear circuits”. In: *2006 IEEE Radio and Wireless Symposium*. 2006, pp. 527–530. DOI: 10.1109/RWS.2006.1615210.

[28] J.C. Pedro and N.B. Carvalho. “Designing multisine excitations for nonlinear model testing”. In: *IEEE Transactions on Microwave Theory and Techniques* 53.1 (2005), pp. 45–54. DOI: 10.1109/TMTT.2004.839340.

[29] Ulf Gustavsson et al. “Implementation Challenges and Opportunities in Beyond-5G and 6G Communication”. In: *IEEE Journal of Microwaves* 1.1 (2021), pp. 86–100. DOI: 10.1109/JMW.2020.3034648.

[30] Christian Fager et al. “Linearity and Efficiency in 5G Transmitters: New Techniques for Analyzing Efficiency, Linearity, and Linearization in a 5G Active Antenna Transmitter Context”. In: *IEEE Microwave Magazine* 20.5 (2019), pp. 35–49. DOI: 10.1109/MMM.2019.2898020.

[31] Kate A. Remley et al. “Measurement Challenges for 5G and Beyond: An Update from the National Institute of Standards and Technology”. In: *IEEE Microwave Magazine* 18.5 (2017), pp. 41–56. DOI: 10.1109/MMM.2017.2690882.

[32] Nuno Borges Carvalho. *GANDALF: Single Chip KaBand*. URL: https://www.it.pt/Projects/Index/4593.

[33] C Boulanger et al. “A new criterion for power amplifier comparison and optimisation”. In: *IEE Seminar on Microwave and RF Power Amplifiers (Ref. No. 2000/118)*. IET. 2000, pp. 1/1–1/6. DOI: 10.1049/ic:20000656.

[34] A. Mallet et al. “A new satellite repeater amplifier characterization system for large bandwidth NPR and modulated signals measurements”. In: *2002 IEEE MTT-S International Microwave Symposium Digest (Cat. No.02CH37278)*. Vol. 3. 2002, 2245–2248 vol.3. DOI: 10.1109/MWSYM.2002.1012320.

[35] K.M. Gharaibeh, K.G. Gard, and M.B. Steer. "Accurate estimation of digital communication system metrics - SNR, EVM and ρ in a nonlinear amplifier environment". In: *64th ARFTG Microwave Measurements Conference, Fall 2004.* 2004, pp. 41–44. DOI: 10.1109/ARFTGF.2004.1427570.

[36] Jacques B. Sombrin. "On the formal identity of EVM and NPR measurement methods: Conditions for identity of error vector magnitude and noise power ratio". In: *2011 41st European Microwave Conference.* 2011, pp. 337–340. DOI: 10.23919/EuMC.2011.6101738.

[37] E. Van Nechel, Y. Rolain, and J. Lataire. "Extracting Improved Figures of Merit for Characterizing Nonlinear Devices using Multisine Excitation Signals". In: *2018 91st ARFTG Microwave Measurement Conference (ARFTG).* 2018, pp. 1–4. DOI: 10.1109/ARFTG.2018.8423813.

[38] N. Borges de Carvalho and J.C. Pedro. "A comprehensive explanation of distortion sideband asymmetries". In: *IEEE Transactions on Microwave Theory and Techniques* 50.9 (2002), pp. 2090–2101. DOI: 10.1109/TMTT.2002.802321.

[39] João Paulo Martins et al. "A Metric for the Quantification of Memory Effects in Power Amplifiers". In: *IEEE Transactions on Microwave Theory and Techniques* 54.12 (2006), pp. 4432–4439. DOI: 10.1109/TMTT.2006.882871.

[40] João Paulo Martins, Nuno Borges Carvalho, and José Carlos Pedro. "Intermodulation Distortion of Third-Order Nonlinear Systems With Memory Under Multisine Excitations". In: *IEEE Transactions on Microwave Theory and Techniques* 55.6 (2007), pp. 1264–1271. DOI: 10.1109/TMTT.2007.896794.

[41] Nuno Borges De Carvalho and José Carlos Pedro. "Compact formulas to relate ACPR and NPR to two-tone IMR and IP3". In: *Microwave Journal* 42.12 (1999), pp. 70–70.

[42] Karl Freiberger, Harald Enzinger, and Christian Vogel. "A Noise Power Ratio Measurement Method for Accurate Estimation of the Error Vector Magnitude". In: *IEEE Transactions on Microwave Theory and Techniques* 65.5 (2017), pp. 1632–1645. DOI: 10.1109/TMTT.2017.2654221.

[43] V. Aparin. "Analysis of CDMA signal spectral regrowth and waveform quality". In: 49.12 (2001), pp. 2306–2314. DOI: 10.1109/22.971614.

[44] K.A. Remley. "Multisine excitation for ACPR measurements". In: *IEEE MTT-S International Microwave Symposium Digest, 2003.* Vol. 3. 2003, 2141–2144 vol.3. DOI: 10.1109/MWSYM.2003.1210586.

[45] Khaled M. Gharaibeh, Kevin G. Gard, and Michael B. Steer. "The applicability of Noise Power Ratio (NPR) in real communication signals". In: *2006 67th ARFTG Conference.* 2006, pp. 251–253. DOI: 10.1109/ARFTG.2006.4734397.

[46] K.G. Gard, H.M. Gutierrez, and M.B. Steer. "Characterization of spectral regrowth in microwave amplifiers based on the nonlinear transformation of a complex Gaussian process". In: 47.7 (1999), pp. 1059–1069. DOI: 10.1109/22.775437.

[47] J.F. Sevic and M.B. Steer. "On the significance of envelope peak-to-average ratio for estimating the spectral regrowth of an RF/microwave power amplifier". In: 48.6 (2000), pp. 1068–1071. DOI: 10.1109/22.904747.

[48] J.C. Pedro and N.B. Carvalho. "Statistics of microwave signals and their impact on the response of nonlinear dynamic systems". In: *Conference, 2003. Fall 2003. 62nd ARFTG Microwave Measurements.* 2003, pp. 143–153. DOI: 10.1109/ARFTGF.2003.1459765.

[49] Ricardo Figueiredo et al. "Nonlinear Dynamic RF System Characterization: Envelope Intermodulation Distortion Profiles—A Noise Power Ratio-Based Approach". In: *IEEE Transactions on Microwave Theory and Techniques* 69.9 (2021), pp. 4256–4271. DOI: 10.1109/TMTT.2021.3092398.

[50] Rohde & Schwarz. *Noise Power Ratio Signal Generation and Measurement.* 2016. URL: https://www.rohde-schwarz.com/us/applications/npr-application-note_56280-15651.html.

[51] Ricardo Figueiredo and Nuno Borges Carvalho. "Issues of Multi-Notch NPR Characterization Procedures". In: *2021 97th ARFTG Microwave Measurement Conference (ARFTG).* 2021. DOI: 10.1109/ARFTG52261.2021.9639973.

[52] Ricardo Figueiredo et al. "Swept Notch NPR for Linearity Assessment of Systems Presenting Long-Term Memory Effects". In: *2020 95th ARFTG Microwave Measurement Conference (ARFTG).* 2020, pp. 1–4. DOI: 10.1109/ARFTG47271.2020.9241380.

[53] J.C. Pedro and N.B. de Carvalho. "Characterizing nonlinear RF circuits for their in-band signal distortion". In: *IEEE Transactions on Instrumentation and Measurement* 51.3 (2002), pp. 420–426. DOI: 10.1109/TIM.2002.1017710.

[54] Rik Pintelon and Johan Schoukens. *System identification: a frequency domain approach.* John Wiley & Sons, 2012.

[55] Oliver Nelles. *Nonlinear system identification: from classical approaches to neural networks and fuzzy models.* Springer Science & Business Media, 2013.

[56] Ricardo Figueiredo et al. "Linearity Metrics: Signal Statistics and Metric Identities". In: *IEEE Transactions on Microwave Theory and Techniques* (under review).

[57] Ricardo Figueiredo and Nuno Carvalho. "Linearity Metrics and Signal Statistics - The Need for Standards". In: *2022 IEEE/MTT-S International Microwave Symposium - IMS 2022.* 2022, pp. 868–871. DOI: 10.1109/IMS37962.2022.9865648.

[58] Katharina Hausmair et al. "Prediction of Nonlinear Distortion in Wideband Active Antenna Arrays". In: *IEEE Transactions on Microwave Theory and Techniques* 65.11 (2017), pp. 4550–4563. DOI: 10.1109/TMTT.2017.2699962.

[59] Filipe M. Barradas et al. "Power, Linearity, and Efficiency Prediction for MIMO Arrays With Antenna Coupling". In: *IEEE Transactions on Microwave Theory and Techniques* 65.12 (2017), pp. 5284–5297. DOI: 10.1109/TMTT.2017.2766067.

[60] Bhaskara Rupakula and Gabriel M. Rebeiz. "Third-Order Intermodulation Effects and System Sensitivity Degradation in Receive-Mode 5G Phased Arrays in the Presence of Multiple Interferers". In: *IEEE Transactions on Microwave Theory and Techniques* 66.12 (2018), pp. 5780–5795. DOI: 10.1109/TMTT.2018.2854194.

[61] Nuutti Tervo et al. "Measurement Method for Characterizing Nonlinearity Under Near-Field and Far-Field Interferers in 5G mmW Phased Arrays". In: *2019 49th European Microwave Conference (EuMC)*. 2019, pp. 420–423. DOI: 10.23919/EuMC.2019.8910825.

[62] Christopher Mollén et al. "Spatial Characteristics of Distortion Radiated From Antenna Arrays With Transceiver Nonlinearities". In: *IEEE Transactions on Wireless Communications* 17.10 (2018), pp. 6663–6679. DOI: 10.1109/TWC.2018.2861872.

[63] Matthew Cullen et al. "Noise Power Ratio Prediction and Measurement of a Ku band GaN Power Amplifier". In: *2019 93rd ARFTG Microwave Measurement Conference (ARFTG)*. 2019, pp. 1–4. DOI: 10.1109/ARFTG.2019.8739219.

[64] Salah Din et al. "High-power K-band GaN PA MMICs and module for NPR and PAE". In: *2017 IEEE MTT-S International Microwave Symposium (IMS)*. 2017, pp. 1838–1841. DOI: 10.1109/MWSYM.2017.8059010.

[65] Clément Mallet et al. "Analog predistortion for high power amplifier over the Ku-band (13,75–14,5 GHz)". In: *2017 47th European Microwave Conference (EuMC)*. 2017, pp. 848–851. DOI: 10.23919/EuMC.2017.8230977.

[66] Vincent Gillet et al. "An Unequally Spaced Multi-Tone Passive Load-Pull (USMT-PLP) to simultaneously characterize Linearity and Efficiency of RF Power Devices". In: *2018 International Workshop on Integrated Nonlinear Microwave and Millimetre-wave Circuits (INMMIC)*. 2018, pp. 1–3. DOI: 10.1109/INMMIC.2018.8429983.

[67] Vincent Gillet et al. "An Unequally Spaced Multi-Tone Load–Pull Characterization Technique for Simultaneous Linearity and Efficiency Assessment of RF Power Devices". In: *IEEE Transactions on Microwave Theory and Techniques* 67.7 (2019), pp. 2505–2513. DOI: 10.1109/TMTT.2019.2918799.

Published Works

Own Works

NPR Contributions

International Conference

[nprC1] Ricardo Figueiredo et al. "Swept Notch NPR for Linearity Assessment of Systems Presenting Long-Term Memory Effects". In: *2020 95th ARFTG Microwave Measurement Conference (ARFTG)*. 2020, pp. 1–4. DOI: 10.1109/ARFTG47271.2020.9241380.

[nprC2] Ricardo Figueiredo and Nuno Borges Carvalho. "Issues of Multi-Notch NPR Characterization Procedures". In: *2021 97th ARFTG Microwave Measurement Conference (ARFTG)*. 2021. DOI: 10.1109/ARFTG52261.2021.9639973.

Journal

[nprJ1] Ricardo Figueiredo et al. "Nonlinear Dynamic RF System Characterization: Envelope Intermodulation Distortion Profiles—A Noise Power Ratio-Based Approach". In: *IEEE Transactions on Microwave Theory and Techniques* 69.9 (2021), pp. 4256–4271. DOI: 10.1109/TMTT.2021.3092398.

ELM Contributions

International Conference

[elmC1] Ricardo Figueiredo and Nuno Carvalho. "Linearity Metrics and Signal Statistics - The Need for Standards". In: *2022 IEEE/MTT-S International Microwave Symposium - IMS 2022*. 2022, pp. 868–871. DOI: 10.1109/IMS37962.2022.9865648.

Journal

[elmJ1] Ricardo Figueiredo et al. "Linearity Metrics: Signal Statistics and Metric Identities". In: *IEEE Transactions on Microwave Theory and Techniques* (under review).

Two-Tone Characterization Contributions

International Conference

[2toneC1] Ricardo Figueiredo and Nuno Carvalho. "Two-Tone Signals Harmonic Conditions for PAPR Variation". In: *2022 International Workshop on Integrated Nonlinear Microwave and Millimetre-Wave Circuits (INMMiC)*. 2022, pp. 1–3. DOI: 10.1109/INMMiC54248.2022.9762178.

Nonlinear Array Characterization Contributions

International Conference

[nlarrayC1] Ricardo Figueiredo and Nuno Borges Carvalho. "Co-Channel Radiation Pattern Distortion in Transmitting 5G Antenna Arrays due to 3rd Order Intermodulation Products". In: *2019 49th European Microwave Conference (EuMC)*. 2019, pp. 626–629. DOI: 10.23919/EuMC.2019.8910766.

Co-Authored Works

PA Linearity Characterization Contributions

International Conference

[paC1] Anna Piacibello et al. "Linearity-aware design of Doherty power amplifiers". In: *2019 IEEE MTT-S International Microwave Conference on Hardware and Systems for 5G and Beyond (IMC-5G)*. 2019, pp. 1–3. DOI: 10.1109/IMC-5G47857.2019.9160390.

Journal

[paJ1] Anna Piacibello et al. "A 5-W GaN Doherty Amplifier for Ka-Band Satellite Downlink With 4-GHz Bandwidth and 17-dB NPR". In: *IEEE Microwave and Wireless Components Letters* 32.8 (2022), pp. 964–967. DOI: 10.1109/LMWC.2022.3160227.

BST Linearity Characterization Contributions

International Conference

[bstC1] Patrícia Bouça et al. "Barium Strontium Titanate Thick Films for Tunable Software-Defined Radio Front-Ends". In: *2021 IEEE MTT-S International Microwave Symposium (IMS)*. 2021, pp. 258–261. DOI: 10.1109/IMS19712.2021.9574935.

[bstC2] Patrícia Bouça et al. "Intermodulation Distortion Analysis of Microwave Tunable Filters Using Barium Strontium Titanate Capacitor and Varactor Diode". In: *2020 15th European Microwave Integrated Circuits Conference (EuMIC)*. 2021, pp. 205–208.

Journal

[bstJ1] Patrícia Bouça et al. "Design and Characterization of Novel Barium Strontium Titanate Thick Films for Sub-6 GHz RF Applications". In: *IEEE Transactions on Microwave Theory and Techniques* 70.1 (2022), pp. 611–621. DOI: 10.1109/TMTT.2021.3125030.

[bstJ2] Patrícia Bouça et al. "Reconfigurable Three Functional Dimension Single and Dual-Band SDR Front-Ends Using Thin Film BST-Based Varactors". In: *IEEE Access* 10 (2022), pp. 4125–4136. DOI: 10.1109/ACCESS.2022.3140686.